

HT-SERIES FINAL DESIGN REPORT

by

Team Hotel

**Team Members: Ethan Clemmitt, Alec Cepeda, Logan Brodhead, Zongxu Dong, Vito
Pratomo, Joe Lullo**

AE 443 Aircraft Systems Design



May 10, 2018



Group Member Contributions

Name	Signature	Responsibility	AIAA Number
Logan Brodhead		Aerodynamics, Performance, Stability & Control	922622
Alec Cepeda		Configuration, CAD	922620
Ethan Clemmitt		Structures & Loads, Weights & Balances	688033
Zongxu Dong		Propulsion, CONOPS	922623
Joseph Lullo		Propulsion, Costs	922625
Arvinto Pratomo		CAD	922621

Faculty Adviser	Signature
Dr. Huy Tran	

Contents

LIST OF FIGURES	vi
LIST OF TABLES	viii
COMPLIANCE CHECKLIST	x
EXECUTIVE SUMMARY	xi
1 CONCEPT OF OPERATIONS	1
1.1 Goal	1
1.2 Requirements and Constraints	1
1.3 Mission Design	2
1.4 Fielding and Maintenance	3
2 SIZING ANALYSIS	4
2.1 Initial Sizing	4
2.2 Constraint Analysis	6
2.3 Comparison to Competitive Aircraft	6
3 PERFORMANCE	7
3.1 Cruise Conditions, Max Velocity, & Stall Speeds	7
3.2 Drag Per Mission Segment	8
3.3 Takeoff & Landing Performance	8
3.4 Climb Performance & Flight Envelope	9
3.5 Fuel Estimations	11
3.6 Loiter & Range Performance	11
3.7 Emergency Divert	13
3.8 Trade Study: Cruise Velocity	14
4 CONFIGURATION	15
4.1 Design Morphology	15
4.2 External Layout	17
4.2.1 General Sizing	17
4.2.2 Engines	17
4.2.3 Landing Gear	17
4.2.4 Wing & Empennage	18
4.2.5 Windows	18
4.2.6 Doors	18
4.2.7 3-View	19
4.3 Internal Layout	21
4.3.1 Fuel Tanks	21
4.3.2 Avionics	21
4.3.3 Battery System	22
4.3.4 Oxygen and Cabin Systems	22
4.3.5 Seats	22

4.3.6	Storage	23
4.3.7	Consumer Appeal	23
5	AERODYNAMICS	24
5.1	Airfoil Selection	24
5.2	Wing Geometry	26
5.3	Flap Design	26
5.4	Lift & Drag Models	28
6	PROPULSION	30
6.1	Engine Requirements	31
6.2	Engine Safety Considerations	32
6.3	Engine Selection Process	32
6.3.1	Number of Engines	32
6.3.2	Piston Engine vs. Turboprop Engine	32
6.3.3	Candidate Engine Specifications	33
6.3.4	Rolls Royce M250-B17-F Turboprop Performance	34
6.3.5	Propeller Selection	34
6.4	Inlet & Nacelle Design	35
6.5	Propulsion Architecture Selection	36
6.6	Batteries Selection Trade Study	37
6.7	Electric Motor Selection	40
6.8	Fuel System	41
7	STABILITY & CONTROL	42
7.1	Empennage	42
7.1.1	Tail Configuration	42
7.1.2	Airfoil	42
7.1.3	Sizing	43
7.2	Control Surface Sizing	45
7.3	Stability Derivatives	46
7.4	Trim Configurations	46
7.5	Longitudinal Stability	47
7.6	Lateral Stability	51
7.7	Directional Stability	54
8	STRUCTURES & LOADS	55
8.1	Materials Selection	55
8.1.1	Trade Study: Fuel Cost Savings of Composite Materials	58
8.2	Internal Structural Element Layout	59
8.2.1	Wing Structure	59
8.2.2	Fuselage Structure	63
8.2.3	Empennage Structure	65
8.3	Landing Gear	66
8.4	Aircraft Loads	70

8.4.1	Ground Loads	70
8.4.2	Landing Loads	71
8.4.3	Flight Loads	71
8.4.4	V-n Diagram	72
8.5	Pressurization	72
8.6	Fuselage Manufacturing & Weight Commonality	73
9	WEIGHTS & BALANCE	74
9.1	Major Component Weights & Locations	74
9.2	Center of Gravity Envelope	77
10	AUXILIARY AIRCRAFT SYSTEMS	77
10.1	Engine Controls	77
10.2	Hydraulics System and Flight Controls	78
10.3	Electric and Emergency System	78
10.4	Pneumatic System and Environmental Control System	79
10.5	Avionics	79
11	COST ANALYSIS	80
11.1	Initial Cost Estimate & Breakdown	80
11.1.1	Implication of Family Aircraft Development Cost	80
11.1.2	Research, Development, Testing, & Evaluation Costs	81
11.1.3	Flyaway Cost	83
11.1.4	Sell Price for 15% Profit	83
11.2	Operations & Maintenance Cost Considerations	84
11.2.1	Fuel & Oil Costs	84
11.2.2	Crew Salaries	84
11.2.3	Maintenance Expenses	84
11.2.4	Yearly Maintenance & Operation Costs	85
11.3	Cost Saving Options	85
11.3.1	Maximum Production Quantity	85
11.3.2	Alternate Manufacturing Materials	86
11.3.3	Weight and Speed Reduction	86
11.4	Model Uncertainties and Inaccuracies	86
12	CONCLUSIONS	86

LIST OF FIGURES

0.1	HT-LIT and HT-LITTLE aircraft.	xi
1.1	Mission profile diagram.	2
2.1	Results of aircraft constraint analysis.	6
3.1	Stall speed across every altitude in operating window.	8
3.2	Determination of rate of climb across altitudes.	10
3.3	Flight envelope of a) HT-LIT b) HT-LITTLE.	10
3.4	Performance parameters for both aircraft.	12
3.5	Payload range a) HT-LIT b) HT-LITTLE.	13
3.6	Effects of cruise speed on maximum cruise range.	14
4.1	First stage of design iterations for wing and tail configuration.	15
4.2	VSP models of multiple design iterations.	17
4.3	3-View of HT-LIT and HT-LITTLE.	19
4.4	Interior layout of the HT-LITTLE.	21
4.5	Interior layout of the HT-LIT.	21
4.6	View from the cockpit of the aircraft.	22
4.7	View of the cabin of the HT-LIT and HT-LITTLE.	23
5.1	Airfoil parameter comparisons.	24
5.2	Cm curves of airfoils considered for main wing.	25
5.3	NACA 2415 airfoil used for the wing.	25
5.4	Flaps at take off and landing deflections.	28
5.5	Lift curve for mission segments of both HT-LIT and HT-LITTLE.	29
5.6	Drag polar of a) HT-LIT and b) HT-LITTLE.	29
6.1	Nacelle layout diagram.	31
6.2	Available power output as a function of altitude.	34
6.3	Views of the nacelle and inlet design.	35
6.4	Parallel HEP system layout.	37
6.5	Siemens 170 kW electric motor.	40
6.6	Fuel system schematic diagram.	41
7.1	Overview of the tail configuration.	42
7.2	NACA 0009 airfoil used for the horizontal and vertical stabilizers.	43
7.3	Stability envelopes of HT-LIT and HT-LITTLE.	43
7.4	Trade study of vertical tail size.	45
7.5	Trim diagrams of HT-LIT and HT-LITTLE.	47
7.6	Desirable flying qualities for dynamic longitudinal stability [1].	49
7.7	Simulink block diagram of longitudinal controller.	50
7.8	HT-LIT and HT-LITTLE short-period flying qualities shown before and after feedback control.	51
7.9	Simulink block diagram of lateral/directional controller.	54
8.1	Structural layout of HT-LIT aircraft.	55
8.2	Internal structure of right HT-LIT aircraft wing.	59
8.3	Internal structure of HT-LIT/HT-LITTLE wing FEM model.	61
8.4	Trefftz plot for a) HT-LIT and b) HT-LITTLE at cruise.	61
8.5	Lift pressure distribution along HT-LIT/HT-LITTLE wing FEM model.	61

8.6	Deflection along HT-LIT/HT-LITTLE wing FEM model.	62
8.7	Lower-order method results for a) shear load, b) bending moment, c) deflection angle, and d) deflection along wing.	63
8.8	Diagrams of internal structural layouts of a) fuselage and b) empennage.	65
8.9	Nose landing gear retraction system design.	68
8.10	Main landing gear retraction system constraint design.	69
8.11	Lateral and Longitudinal tip-over relevant dimensions for the HT-LIT aircraft with decompressed nose gear.	70
8.12	Diagrams of internal structural layouts of a) fuselage and b) empennage.	72
9.1	Component weight layout for HT-LIT aircraft.	75
9.2	Component weight layout for HT-LITTLE aircraft.	76
9.3	CG envelopes for HT-LIT and HT-LITTLE aircraft.	77
10.1	Diagrams of the engine control systems and hydraulic systems.	78
10.2	Diagrams of the electrical and pneumatic systems.	79

LIST OF TABLES

1.1	Summary table for mission requirements	1
1.2	Summary table for mission requirements (continued)	2
1.3	Mission parameter and specifications	3
2.1	Initial sizing design parameters	5
2.2	Calculated fuel data from initial sizing	5
2.3	Calculated weights from initial sizing	5
2.4	Comparison to competitive aircraft	7
3.1	Drag of the aircraft at every mission leg	8
3.2	Takeoff & landing under various conditions for HT-LIT	9
3.3	Takeoff & landing under various conditions for HT-LITTLE	9
3.4	Fuel weight estimations	11
3.5	Range and loiter performance for HT-LIT	12
3.6	Range and loiter performance for HT-LITTLE	12
3.7	Divert capabilities at different altitudes	13
5.1	NACA 2415 airfoil parameters	25
5.2	Wing geometric parameters	26
5.3	QFD of high-lift devices	27
5.4	Flap dimensions and parameters	27
5.5	Drag buildup of HT-LIT and HT-LITTLE	30
5.6	Aerodynamic Coefficients for various mission legs	30
6.1	Overview of main powerplant components	31
6.2	Required vs. available thrust and power for cruise	32
6.3	Turboprop/piston engines weights & maximum power output	33
6.4	Candidate turboprop engine specifications	33
6.5	Rolls Royce M250-B17F performance and specifications [2]	34
6.6	Propeller system specifications	35
6.7	Summary table for series HEP	36
6.8	Summary table for parallel HEP	36
6.9	Summary table for series-parallel HEP	37
6.10	Comparison of different lithium ion batteries	38
6.11	Parameter priority table for battery trade study	38
6.12	Ranking table for battery trade study	39
6.13	Final score of battery trade study	39
6.14	Performance of the electric propulsion section	41
7.1	Horizontal stabilizer geometric parameters	44
7.2	Vertical stabilizer geometric parameters	45
7.3	Deflection ranges of the control surfaces	46
7.4	Stability derivatives	46
7.5	Stability derivatives (continued)	46
7.6	Tabulated trim deflections	47
7.7	Longitudinal static stability parameters	48
7.8	Requirements for various levels of dynamic longitudinal stability [1]	48

7.9	Natural flying qualities of HT-LIT and HT-LITTLE aircraft	50
7.10	Final gains for longitudinal control design	51
7.11	Eigenvalues for Dutch roll, roll, and spiral roll modes	52
7.12	Lateral mode eigenvalues for state-feedback control	53
7.13	HT-LIT lateral mode performance vs. requirements	53
7.14	HT-LITTLE lateral mode performance vs. requirements	53
7.15	Directional static stability derivatives	54
7.16	Engine-out rudder deflection	54
8.1	Properties of various composite materials compared with aluminum 6061-T6	57
8.2	Cruise performance for composite vs aluminum manufacturing materials	58
8.3	Manufacturing cost differences for aluminum vs composite materials (in millions of dollars)	59
8.4	Tire Specifications for HT-LIT and HT-LITTLE aircraft	67
9.1	Weights and balance table for the HT-LIT	75
9.2	Weights and balance table for the HT-LITTLE	76
10.1	Avionics components of HT-LIT aircraft	80
11.1	Wrap rates adjusted for inflation	81
11.2	DAPCA estimates for labor costs for HT-LIT and HT-LITTLE (in millions of dollars)	81
11.3	DAPCA estimates for RDT&E costs for HT-LIT and HT-LITTLE(in millions of dollars)	82
11.4	Avionics components cost per aircraft (in thousands of dollars)	83
11.5	Flyaway cost estimates for varying production quantities of 6-seater and 4-seater Aircraft (in millions of dollars)	83
11.6	Aircraft price to make 15% profit for 6-seater Aircraft (in millions of dollars)	84
11.7	Cost comparisons for similar aircraft (in millions of dollars)	84
11.8	Maintenance & operations cost per year and per flight hour (in thousands of dollars)	85

COMPLIANCE CHECKLIST

Description	Requirements (HT-LIT/HT-LITTLE)	Compliance (HT-LIT/HT-LITTLE)	Section
Target Cruise Speed	200 kts	270 kts / 260 kts	4.1
Minimum Cruise Speed	174 kts	174 kts	4.1
Climb/rate	1300 ft/m 1500 ft/m	3100 ft/min 3400 ft/min	4.4
Passenger Capacity	5 / 3 passengers	Accommodate 5 / 3 passengers	5.3.5
Cargo Capacity	luggage space for 6 / 4 people.	Accommodate luggage space for 6 / 4 people.	5.3.6
Range	750 nmi / 1000 nmi	750 nmi / 1000 nmi	4.6
Takeoff & Landing Length	1800 ft / 1500 ft over 50 ft obstacle in dry pavement above sea level and 5000 ft above sea level	1800 ft / 1500 ft over 50 ft obstacle in dry pavement above sea level and 5000 ft above sea level	4.3
Engine in use by 2018	Engine must be available by 2028	Future engine will be available by 2028 with data.	7.3
Electric Motor	Motor must be available by 2028	Motor is available by 2028 with data.	7.7
Emergency divert	Must be capable of reaching alternate airport due to engine failure	Aircraft will successfully land due to engine failure.	4.7
Crew Capacity	Aircraft must contain 1 pilot	can accommodate 1 pilot.	5.3.5
VFR and IFR capable with an autopilot	Aircraft is capable of an autonomous flight	Aircraft can fly in an autonomous flight.	11.5
Icing conditions	Capable of flight in known icing conditions	Aircraft able to fly in icing conditions.	11.4
Aircraft Unit Cost	The unit cost per aircraft will be minimizes by production cost	The unit cost per aircraft will be around 4 / 3 million dollars.	13
One engine Inoperative Requirements	Aircraft must meet 14 CFR 23.67 requirements	Aircraft does meet the 14 CFR 23.67 requirements.	4.7

EXECUTIVE SUMMARY (AP)

Team Hotel Inc. proudly presents the HT-series hybrid-electric general aviation aircraft family in response to the Request for Proposal posed to the Spring 2018 AE 443 - Senior Design II class at the University of Illinois. This team consists of six senior students in the Aerospace Engineering department at the University of Illinois. The need for long-range hybrid-electric aircraft is increasing as research into battery technology is ramping up; companies such as Nissan and Tesla have had success in the automotive industry using electric concept designs, and the natural next step is to apply this idea to practical applications in the aviation industry. The goal of this project was to design a clean alternative solution to fill this impending industry gap, while also providing a luxurious product at a competitive price.

The HT-series family of aircraft is made up of two variants, the HT-LIT and the HT-LITTLE. Both are powered by twin Rolls Royce M250 engines, each providing 420 shaft horsepower. Both variants also carry two electric motors which are powered by one 500-pound lithium-ion battery. The HT-LIT is a 6-seat aircraft with a gross takeoff weight of 7,276 pounds. The primarily-composite is 32 feet long, housing a spacious, pressurized cabin. The HT-LITTLE is a 4-seat aircraft with a gross takeoff weight of 6,703 pounds, a fuselage length of 26.5 feet, and a luxurious cabin of the same cross-sectional area as the larger variant. The HT-series of aircraft share the same wing and tail dimensions. The planform area of the main wing is 200 square feet and the planform areas of the horizontal and vertical tail are 54.2 square feet and 28.6 square feet, respectively.

Both aircraft close on all of the requirements in the RFI. The HT-LIT and HT-LITTLE aircraft have cruise speeds of 270 knots and 260 knots, respectively, and each exceeds the climb requirement of 1300 feet/minute. Each aircraft meets the required takeoff and landing field lengths of 1800 feet and 1500 feet, respectively, while additionally being able to clear a 50-foot obstacle at sea level. Both aircraft meet the required ranges: 750 nautical miles for the HT-LIT and 1000 nautical miles for the HT-LITTLE. The aircraft family can accommodate the required minimum cargo capacity for both the passengers and pilot. The aircraft family has the required autopilot capabilities and deicing systems, and both aircraft meet the one engine inoperative requirement from the 14 CFR 23.67.

As it stands, the sale price for this family of aircraft to maintain a 15% profit is between \$3 and \$6 million, depending on the amount of aircraft produced. These aircraft utilize technology that will be disruptive to the present aviation environment for high-end general aviation aircraft and will certainly be a stepping stone towards a greener and more sustainable hybrid-electric market.



Figure 0.1: HT-LIT and HT-LITTLE aircraft.

1 CONCEPT OF OPERATIONS

1.1 Goal

The aim of designing this new family of hybrid-electric general aviation aircraft was introducing a better choice to the market, offering an option with higher fuel efficiency, lower operation cost, and better flight performance to the customer. With the increasing advocacy for environmental protection and pollution reduction, electrically-powered aircraft seem to be the clear direction the aerospace industry will be moving towards during the upcoming few decades. In this aircraft family, the four-seat model aims to enter the market by 2028 and the six-seat model aims to enter the market by 2030, both featuring a propulsion system that will be ready for service by 2028. In order to be competitive in the market, it was necessary to constrain the production costs and maintenance costs to a reasonable range. Also, both aircraft needed to be able to be fully functional under varying circumstances, including extreme climates, to show their reliability and flexibility.

1.2 Requirements and Constraints

The RFI [3] clearly stated the mission requirements desired of this family of hybrid-electric general aviation aircraft. Summary tables for the requirements are shown in Table 1.1 and continued in Table 1.2.

Table 1.1: Summary table for mission requirements

Requirements	6-seater	4-seater
Capacity	6 people with luggage (1 pilot, 5 passengers)	4 people with luggage (1 pilot, 3 passengers)
Cruise Speed	Desired: 200 knots Minimum: 174 knots	Desired: 200 knots Minimum: 174 knots
Cruise Range	750 nmi	1000 nmi
Maximum Takeoff and landing Length	1800 ft over a 50ft obstacle at dry pavement runway at sea level; also show performance at 5000 ft above sea level as well as for grass and concrete fields at sea level (ISA + 18°F)	1500 ft over a 50ft obstacle dry pavement runway at sea level; also show performance at 5000 ft above sea level as well as for grass and concrete fields at sea level (ISA + 18°F)
VFR and IFR	Capable for both with autopilot	Capable for both with autopilot
Flight in Icing Conditions	Equipped with de-icing equipment	Equipped with de-icing equipment
Regulation	Meets applicable certification rules in FAA 14 CFR Part 23	Meets applicable certification rules in FAA 14 CFR Part 23
Climb Rate	1300 feet per minute at sea level	1500 feet per minute at sea level

Table 1.2: Summary table for mission requirements (continued)

Requirements	6-seater	4-seater
One Engine Inoperative Situation	Meet 14 CFR 23.67 Climb with an emergency range at the maximum feasible Weight from an engine failure at 5000 ft AGL (ISA + 18°F) both with electric power from batteries alone and with electric power plus the other functional engine.	Meet 14 CFR 23.67 Climb with an emergency range at the maximum feasible Weight from an engine failure at 5000 ft AGL (ISA + 18°F) both with electric power from batteries alone and with electric power plus the other functional engine

In order to make the design more efficient and competitive to comparable models, the cruise altitude for both aircraft was set to 17,000ft with the cruise speed of 270 knots and 260 knots for the 4-seater and 6-seater respectively.

1.3 Mission Design

The mission profile for this family of hybrid-electric general aviation aircraft is presented in Fig. 1.1 and Table 1.3 below. The primary section of the mission consists of 7 segments: legs 0 to 7 correspond to a regular mission where the aircraft takes off, climbs to cruising altitude, flies to its destination, waits clearance for landing (loitering), does a divergence if needed, and then lands. With the ability to divert, the aircraft will be prepared to land safely around the country under unexpected situations.

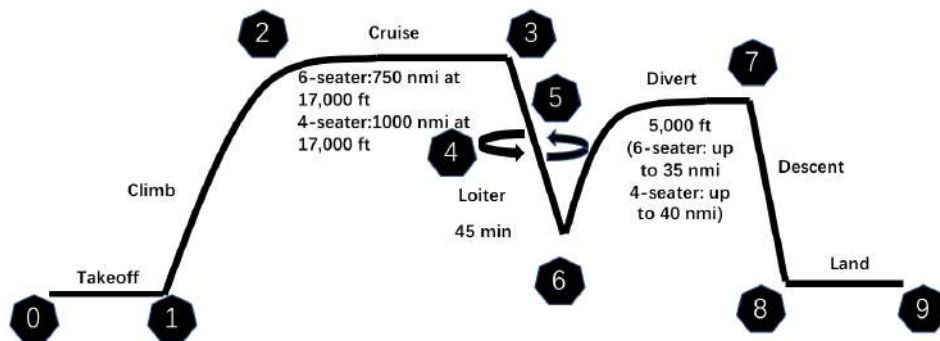


Figure 1.1: Mission profile diagram.

Table 1.3: Mission parameter and specifications

Mission Leg	Description	Altitude	Rate of Climb	Speed	Distance	Endurance	Propulsion Mode
0 - 1	Takeoff	-	-	-	6-seater: 1102 ft 4-seater: 887 ft	-	Electric & ICE
1 - 2	Climb	-	6-seater: 1,300 ft/min 4-seater: 1500 ft/min	-	-	-	Electric & ICE
2 - 3	Cruise	17,000 ft	-	6-seater: 270 knots 4-seater: 260 knots	6-seater: 750 nmi 4-seater: 1000 nmi	-	Electric & ICE
4 - 5	Loiter	17,000 ft	-	-	-	45 min	ICE
5 - 6	Descent	-	-	-	-	-	ICE
6 - 7	Divert	5,000 ft	-	150 knots	6-seater: 35nmi 4-seater 40nmi	-	Electric & ICE
7 - 8	Descent	-	-	-	-	-	ICE
8 - 9	Land	-	-	-	6-seater: 1669 ft 4-seater: 1465ft	-	ICE

This mission profile was chosen because it is widely implemented by similar types of aircraft: it includes a point to point flight that satisfies most needs for costumers (etc. New York - Chicago or San Francisco - Seattle) with enough loitering time to get landing clearance. The divert ability can provide extra safety to the passengers.

1.4 Fielding and Maintenance

The reliability of an aircraft is an important factor when customers are considering a purchase. Moreover, the more destinations it can reach, the larger a potential market it will have. Consequently, this family of hybrid-electric general aviation aircraft was designed to be able to not only land on runways with dry pavement, but also to land on grass and concrete fields. This allows them to be able to reach remote destinations where the runway conditions might not be ideal. Both aircraft were additionally designed to be easily maintained using common, existing commercial components, easily accessible parts, and readable fuel, oil, and hydraulic fluid gauges. The battery packs, avionics, and other sub systems are accessible for checking and replacement. Small issues can be easily solved by reading through the manual and using basic tools that are common in most hangars. The aircraft were designed to have a longer operation span between required maintenance and lower mean time between failure compared to other similar type aircraft, therefore reducing the maintenance cost and increasing the reliability. All these benefits will lead to a lower total operation cost to any prospective owner.

For this design, the high commonality between the 6-seater and 4-seater allows similar maintenance process for

both aircraft. Firstly, a quick whole aircraft inspection is required for every 100 flight hours in which will take about 10 man-hours. The propellers will have a time between overhaul of 1,500 hours and the turboprop engines will have a 3,000 hours TBO. Also the battery pack will need replacement after 800 charge/recharge cycles. Moreover, the wing structure will need special inspection for every 6,000 flight hours and the stabilizer structure will have its first inspection at 8,500 flight hours with subsequent repetitive inspections for every 500 flight hours. The safe life limit for the wing structure is about 30,000 flight hours.

Required preventative maintenance includes avionic equipment and battery cooling system checking, landing gear wheel pressure checking, and fuel tank leak inspection every time before flight. Other maintenance procedures such as engine washing, aircraft cleaning, and hanger storage are recommended in order to keep the vehicle in good shape.

2 SIZING ANALYSIS

2.1 Initial Sizing

In order to determine the important preliminary values for the 6 seated aircraft such as takeoff gross weight, empty weight, and fuel weight, the process of initial sizing required several important parameters. The information gained from this exercise would prove valuable to the design of the 6 seat aircraft which would in turn be productive to the design of the 4 seater. The information gained from the 6 seat aircraft was simply scaled to the 4 seat aircraft after looking at market trends in aircraft specifications. These design points would of course be tweaked and moved during the design process but gave a good jumping off point to begin design work. The necessary parameters for completing a sizing analysis were found through a combination of historical aircraft data, statistical data available in Raymer Chapters 3 and 6 [4], or were given as design requirements in the Request for Information [3]. The value of each important parameter that was found is presented in Table 2.1. Traditional aircraft sizing methodologies needed modifications to accommodate hybrid-electric aircraft systems. How the weight of the payload was calculated was one modification that was made. Although the battery directly affects the propulsion system of the aircraft, its mass was considered a part of the payload, since the mass of the battery does not change significantly during flight.

Table 2.1: Initial sizing design parameters

Parameter	Value	Units	Source
$\frac{L}{D}_{max}$	14.3	-	Obtained From Similar Aircraft
c_{bph} Cruise	0.4	$\frac{lb}{hp \cdot h}$	Raymer Table 3.4 [4]
c_{bph} Loiter	0.5	$\frac{lb}{hp \cdot h}$	Raymer Table 3.4 [4]
Velocity	210	Knots	Given by RFI [3]
Cruise Altitude	10,000	Feet	Given by RFI [3]
Loiter Time	2,700	Seconds	Given by RFI [3]
Passengers	5	People	Given by RFI [3]
Pilot	1	Person	Given by RFI [3]
Cruise Distance	750	Nautical Miles	Given by RFI [3]
Battery Estimate	800	Pounds	Estimated

Data about the fuel usage during each flight segment is presented in Table 2.2 (note that these do not represent the final values of the aircraft and were merely used as a starting point in sizing the aircraft systems - values such as cruise altitude and velocity were altered in later design stages in order to achieve better performance and increased consumer appeal), and Table 2.3 contains the key weights that were calculated and used in the constraint analysis.

Table 2.2: Calculated fuel data from initial sizing

Segment	Fuel Weight Fraction	Fuel Weight (lbs)
Takeoff	0.97	178
Climb	0.985	86
Cruise	0.923	439
Loiter	0.979	109
Land	0.995	25

Table 2.3: Calculated weights from initial sizing

Segment	Weight (lbs)
Takeoff Gross Weight	5950
Empty Weight	2940
Total Fuel Weight	891

Given the weight of the HT-LIT being approximately 6000 lbs market research was conducted to determine that the subtraction of 2 seats from the aircraft would put the 4 seated HT-LITTLE at approximately 5000 lbs.

2.2 Constraint Analysis

This initial sizing was a good estimate for Performance, Aerodynamics, Stability & Control, and Propulsion for finding components that would fit the mission requirements, though as more information was gained about the proper sizing of batteries, a more accurate design point was pinned down.

The weights obtained in the Initial Sizing Section were used to find the required thrust and wing area using a constraint analysis. The product of the constraint analysis was the constraint plot shown in Fig. 2.1. This graph was used to find a design point for the concept aircraft, which had to be in the positive design space (the space shaded in pink on the figure). The design point that was chosen is represented with a red star in Fig. 2.1. This choice corresponded to a final design point of 6000 lbs, $27 \frac{W}{S}$, and $.115 \frac{hp}{W}$. Similar values would be used for the HT-LITTLE aircraft but with its respective sizing analysis predicted weight of approximately 5000 lbs.

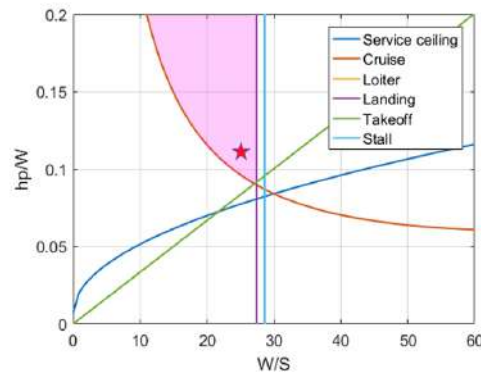


Figure 2.1: Results of aircraft constraint analysis.

2.3 Comparison to Competitive Aircraft

Once a design point was picked and the initial sizing of the aircraft complete it was important to see how the design compared to competitive aircraft already in the market. As show in Table 2.4, the HT-LIT has similar weight to the other 6 seated aircraft though the power of an aircraft of much larger size. This is due to the allotment of battery weight in the aircraft. Because of this extra 500 lb battery weight the aircraft became heavy enough to have power requirements similar to that of a much larger aircraft while remaining as small in weight and size as a traditional 6 seated aircraft. This configuration should allow for superior performance due to the overpowered nature of the aircraft and will allow the aircraft to be marketed as a luxury aircraft which will be helpful due to its already expensive nature of utilizing heavy, expensive batteries in its powerplant.

Table 2.4: Comparison to competitive aircraft

Aircraft	Seats	Takeoff Weight (lb)	Span (ft)	AR	Power (hp)	Length (ft)	Cruise Speed (kt)	Range (nmi)	Wing Area (ft ²)
Beechcraft Bonanza	6	3,650	33' 6"	6.2	300	27' 6"	176	716	181
Piper Seneca	6-7	4,773	38'	7.4	440	28' 7.44"	188	870	195
Beechcraft Baron	6	5,100	37' 10"	7.2	520	28'	180	942	199
Beechcraft King Air	8-9	6,950	50' 3"	9.8	1,100	35' 6"	226	1,321	258
Vulcanair P68	7	4,387	39' 4.5"	7.7	400	31' 4"	161	1,140	200
Vulcanair Canguro	10-11	7,495	49' 2.5"	9.37	840	39' 10.5"	155	850	258
Team Hotel Inc HT-LIT	6	6,000	40'	8.0	840	32'	210	810	200

3 PERFORMANCE

The performance section will evaluate the success of each aircraft in meeting the requirements set by the RFI [3] by using the parameters calculated within sections in aerodynamics, structures, and propulsion. The requirements for the HT-LIT four-seater include: a target cruise speed of 200 kt, a cruise range of 750 nmi, a maximum takeoff and landing balanced field length of 1,800 ft, an initial climb rate of at least 1,300 ft/min, and climb out capability with one engine system inoperative. The requirements for the HT-LITTLE six-seater include: a target cruise speed of 200 kt, a cruise range of 1000 nmi, a maximum takeoff and landing balanced field length of 1,500 ft, an initial climb rate of at least 1,500 ft/min, and climb out capability with one engine system inoperative. All performance parameters specified by the RFI [3] are satisfied in this configuration..

3.1 Cruise Conditions, Max Velocity, & Stall Speeds

The target cruise speed specified in the RFI is 200 kt. A target market was established by analyzing similar aircraft, like the Piper Seneca, Beechcraft Baron, Beechcraft Airking, and Cessna Skycourier. A detailed analysis can be found in Section 3.8. To remain marketable with a not yet fully price efficient propulsion configuration, the cruise velocity of the HT-LIT was chosen to be 270 kts and 260 kts for the HT-LITTLE. Both cruise at an altitude of 17,000 ft. These cruise parameters were chosen to compete with larger, more luxurious turboprops already on the market as a means of justifying the larger price tag while still operating at efficient power outputs for the turboprop engines selected. Due to the higher cruise velocity, the aircraft can operate at a smaller angle of attack and not incur as high of an induced drag value. The ratio of lift over drag at cruise conditions is 15.1 for the HT-LIT and 14.8 for the HT-LITTLE.

By calculating the power available at sea level and at cruise altitude, as described by equations outlined in

Anderson [5], then converting to thrust and comparing to thrust required, maximum velocity at these operation altitudes was found. By sweeping across all operating altitudes the stall velocity was also found for all altitudes, giving the lower velocity limit at every condition, which is shown in Fig. 3.1. These trends were combined to form the flight envelope, showing the operable velocities and altitudes for the HT-LIT and HT-LITTLE.

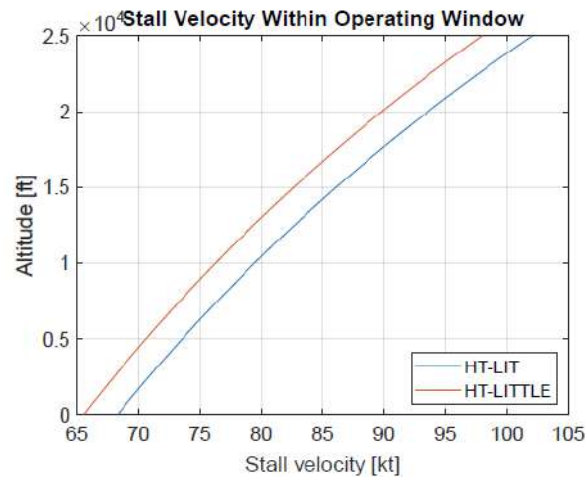


Figure 3.1: Stall speed across every altitude in operating window.

3.2 Drag Per Mission Segment

Drag for every leg of the mission profile was calculated by combining the parasite drag and the drag induced by lift produced at every segment. Takeoff and landing calculations were performed at sea level and climb uses averaged climb velocity and lift values. Drag values are shown in Table 3.1.

Table 3.1: Drag of the aircraft at every mission leg

Mission Leg	Drag Value LIT	Drag Value LITTLE
Takeoff (@ TO)	753 lb	650 lb
Climb (average)	812 lb	691 lb
Cruise	509 lb	504 lb
Loiter (@ 17,000 ft)	452 lb	416 lb
Landing (@ TD)	1153 lb	957 lb

3.3 Takeoff & Landing Performance

The RFI requirements for landing and takeoff are a maximum balanced field length with a 50 ft obstacle of 1,800 ft on dry pavement (sea level ISA +18°F) for the 6-seat configuration and 1,500 ft under the same conditions for the 4-seater. Calculations in this section were performed using equations and Heun's integration methods, described in

Introduction to Flight Mechanics by Thomas Yechout [6], to find forces acting on the aircraft, and the optimal transition and climb paths resulting from the takeoff and landing velocities. The forces that were calculated for takeoff at sea level are shown in Table 3.2, and Table 3.3 shows the resulting takeoff and landing distance and velocity on wet grass and dry concrete at both sea level and an altitude of 5,000 ft for both aircraft configurations.

Table 3.2: Takeoff & landing under various conditions for HT-LIT

Altitude	Runway Material	Takeoff Distance	Landing Distance	Takeoff Velocity	Touchdown Velocity
Sea Level	Dry Concrete	1,102 ft	1,669 ft	96 kt	78 kt
	Wet Grass	1,140 ft	2,182 ft		
5,000 ft	Dry Concrete	1,601 ft	1,704 ft	104 kt	91 kt
	Wet Grass	1,671 ft	2,255 ft		

Table 3.3: Takeoff & landing under various conditions for HT-LITTLE

Altitude	Runway Material	Takeoff Distance	Landing Distance	Takeoff Velocity	Touchdown Velocity
Sea Level	Dry Concrete	995 ft	1,397 ft	92 kt	75 kt
	Wet Grass	1,026 ft	1,888 ft		
5,000 ft	Dry Concrete	1,439 ft	1,466 ft	99 kt	87 kt
	Wet Grass	1,494 ft	1,964 ft		

The takeoff and landing requirements of the RFI were satisfied at both sea level and at 5,000 ft for both configurations. Capabilities on wet grass are still sufficient for takeoff, but, due to the drastic decrease in friction, landing increases to well above the desired 1,800 ft.

Due to this being a twin-engine aircraft, 14 CFR 23.67 climb requirement after obstacle clearance must also be met. Operating purely on the electric motors, the lowest power engine out scenario, the aircraft can surpass the climb requirement of 1.5% velocity and achieve a max climb rate of 195 ft/min at a velocity of 187 ft/s for the HT-LIT and 237 ft/min at 180 ft/s for the HT-LITTLE, exceeding the climb out requirement. Both aircraft are capable of landing on a gravel, metal mat, dirt, and concrete. Justification and reasoning can be found in section 8.3.

3.4 Climb Performance & Flight Envelope

The only requirements for climb performance were an initial rate of climb of 1,300 ft/min for the HT-LIT and 1,500 ft/min for the HT-LITTLE. The climb performances were determined, using equations described in Yechout [6], by calculating the difference between power required and power available at various altitudes, resulting in the corresponding rate of climb. The climb performance across all operating altitudes is shown in Fig. 3.2. Evident by the data presented in Fig. 3.2, both aircraft can easily achieve a rate of climb requirement at sea-level and beyond, satisfying the specified requirement.

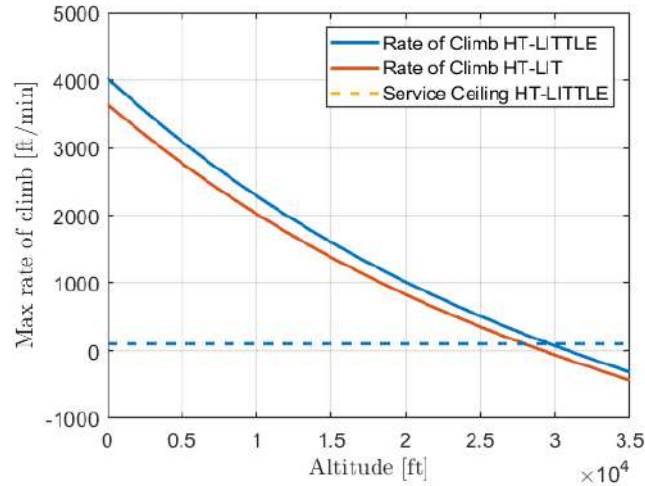
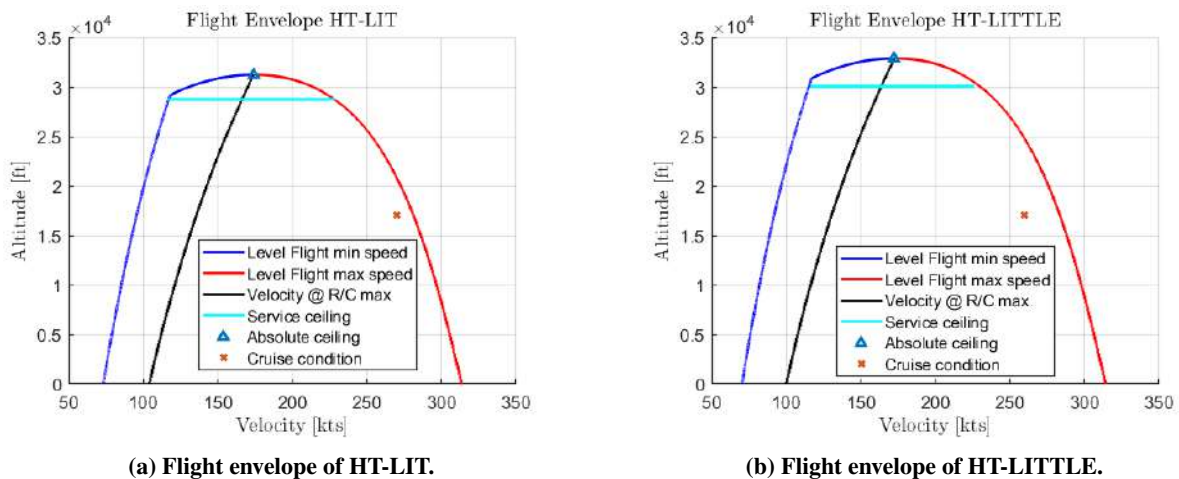


Figure 3.2: Determination of rate of climb across altitudes.

The performance based service ceiling was found by determining the altitude at which maximum rate of climb falls below 100 ft/min. Using this method, the fully loaded service ceiling of the HT-LIT and LITTLE were found to be 28,748 ft and 30,050 ft, respectively. The absolute ceilings, point at which the aircraft cannot fly any higher, as shown by the peaks of the flight envelopes in Fig. 3.3a and Fig. 3.3b, are 31,200 ft for the HT-LIT and 32,900 ft for the HT-LITTLE.



(a) Flight envelope of HT-LIT.

(b) Flight envelope of HT-LITTLE.

Figure 3.3: Flight envelope of a) HT-LIT b) HT-LITTLE.

With a representative maximum climb profile through the entire flight envelope, a time to climb to the 20,000 ft cruise altitude was calculated to be 11.4 minutes for the HT-LITTLE and 13.4 minutes for the HT-LIT. These values are representative of the ideal max climb rate; during normal operation a comfort climb designed for the nature of the flight would likely be used instead, drastically increasing the time to climb.

3.5 Fuel Estimations

In order to accurately calculate the fuel weight for both the HT-LIT and HT-LITTLE when operating a normal cruise mission, a modified version of fuel weight estimation was implemented. This method used the thrust required for each section and the TSFC at every operation altitude, as well as the operation time to find the fuel needed for each segment. A summary of the fuel weight estimation for the HT series aircraft is shown in Table 3.4.

Table 3.4: Fuel weight estimations

Mission Segment	HT-LIT	Fuel Fraction (%)	HT-LITTLE	Fuel Fraction (%)
Takeoff	101.7 lb	1.40	97.9 lb	1.46
Climb	138.4 lb	1.90	122.75 lb	1.83
Cruise	716.3 lb	9.84	903.6 lb	13.48
Loiter	139.7 lb	1.92	133.3 lb	1.99
Divert	37.2 lb	0.51	38.5 lb	0.57
Descent	10.3 lb	0.14	10.2 lb	0.15
Land	35.6 lb	0.49	33.4 lb	0.50
Total Weight	1179.2 lb	16.21	1339.6 lb	19.99
Total Weight with Safety Factor	1250.0 lb	17.18	1420.0 lb	21.18

3.6 Loiter & Range Performance

The several performance parameters can be optimized by flying in specific aerodynamic configurations based on the desired performance maximization. Fig 3.4 shows the plot of $\frac{C_L}{C_D}$, $\frac{C_L^{1/2}}{C_D}$, and $\frac{C_L^{3/2}}{C_D}$. Labeled are the maximum values of all of these values, which signify the configuration which yields the longest range for reciprocating aircraft and minimum gliding flight path angle, $\frac{C_L}{C_D}$, longest range for a jet aircraft, $\frac{C_L^{1/2}}{C_D}$, and highest endurance for a reciprocating engine aircraft as well as aircraft max rate of climb, $\frac{C_L^{3/2}}{C_D}$.

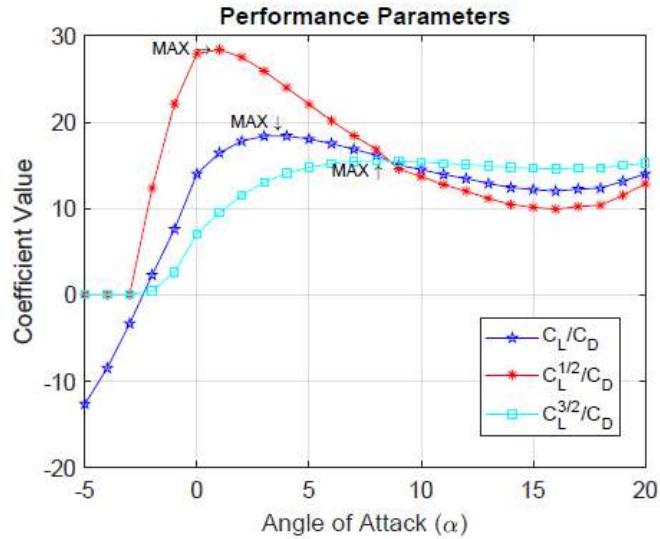


Figure 3.4: Performance parameters for both aircraft.

Using the fuel estimations for post-climb from the previous sections, in combination with TSFC engine data and prop derivative estimation methods found in Yechout [6], the maximum cruise range and loiter performance at cruise altitude for normal were calculated. The cruise range, loiter time, and lift over drag configuration are listed in Table 3.5 for the 6-seater and Table 3.6 for the 4-seater.

Table 3.5: Range and loiter performance for HT-LIT

Parameter	Value	Velocity	L/D
Max Range at Cruise Velocity	870 nmi	270 kt	15.2
Max Range	1045 nmi	175 kt	18.4
Max Loiter After Cruise	1.1 hr	151 kt	16.9
Max Loiter After Climb	9.0 hr	151 kt	16.9

Table 3.6: Range and loiter performance for HT-LITTLE

Parameter	Value	Velocity	L/D
Max Range at Cruise Velocity	1115 nmi	260 kt	14.4
Max Range	1335 nmi	169 kt	18.4
Max Loiter After Cruise	1.2 hr	145 kt	16.9
Max Loiter After Climb	10.1 hr	145 kt	16.9

Both aircraft configurations easily meet the requirements set within the RFP and well outperform the range requirements at optimal flight speeds and attitude, despite being weighed down by the maximum payload. The effects on range by substituting payload for additional fuel is shown by the payload diagrams in Fig. 3.5a and Fig. 3.5b. By following the method described in Roskam [7], a payload diagram for each aircraft was constructed, trading payload weight for fuel

until the volumetric limit was reached. A theoretical ferry mission with no payload is also shown as a best case cruise range.

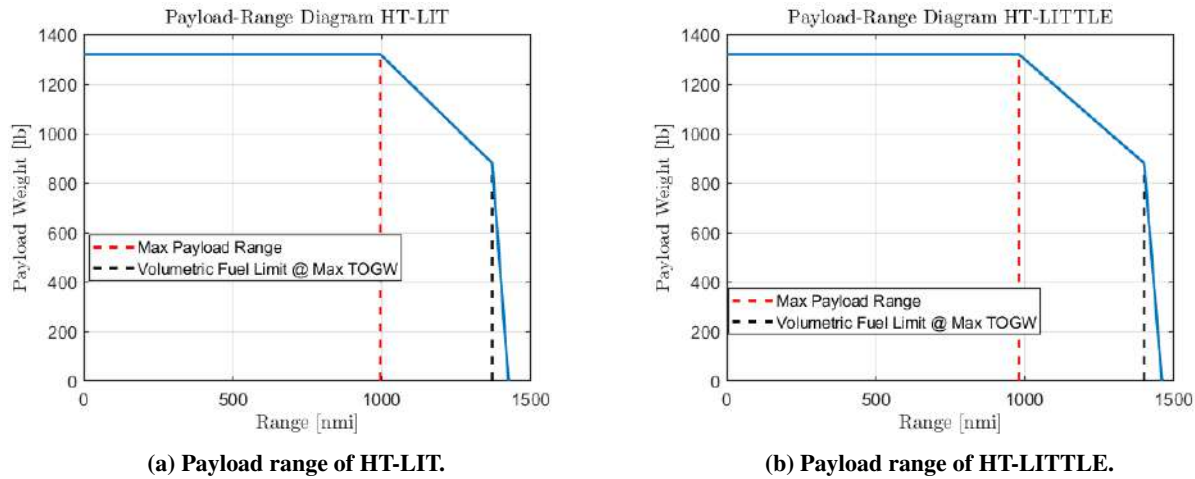


Figure 3.5: Payload range a) HT-LIT b) HT-LITTLE.

3.7 Emergency Divert

The emergency situation is considered when there is a single engine failure right after takeoff. Two cases need to be discussed under such circumstances. Either the aircraft will be powered by the electric propulsion system only, or both the electric propulsion system and the remaining operable turboprop. The Table 3.7 shows the emergency range performance of HT-LIT and HT-LITTLE with an 80 kWh battery pack.

Table 3.7: Divert capabilities at different altitudes

	Altitude 5,000 ft		Altitude 10,000 ft		Altitude 17,000 ft	
	HT-LIT	HT-LITTLE	HT-LIT	HT-LITTLE	HT-LIT	HT-LITTLE
Electric Motors Only	81.8 nmi	84.4 nmi	79.9 nmi	84.1 nmi	80.7 nmi	86.9 nmi
Electric Motors & 2nd ICE	173 nmi	178 nmi	171 nmi	180 nmi	177 nmi	189 nmi

It can be observed that there is little variance of the maximum range for the aircraft at different cruising altitudes. This is because even though the aircraft has a higher efficiency at high altitude, the increased battery consumption at climb will compensate the amount of power saved. Also, the HT-LITTLE can go a little further than the HT-LIT due to its better aerodynamic performance caused by its smaller size. Overall either of the two propulsion modes for both aircraft in the HT series can provide enough power for relocation and safe landing.

3.8 Trade Study: Cruise Velocity

After cruise altitude was determined, the next important decision was cruise velocity. By varying cruise velocity and evaluating constant speed max range for the HT-LIT aircraft variation, a plot of max range versus cruise range was generated. The turboprops selected for this family operate more efficiently for higher thrust outputs. The hard cutoff on c_{bhp} was set at 260 kts because that corresponds to approximately the thrust percentage at which the fuel efficiency decreases. The plot generated is shown in Fig. 3.6

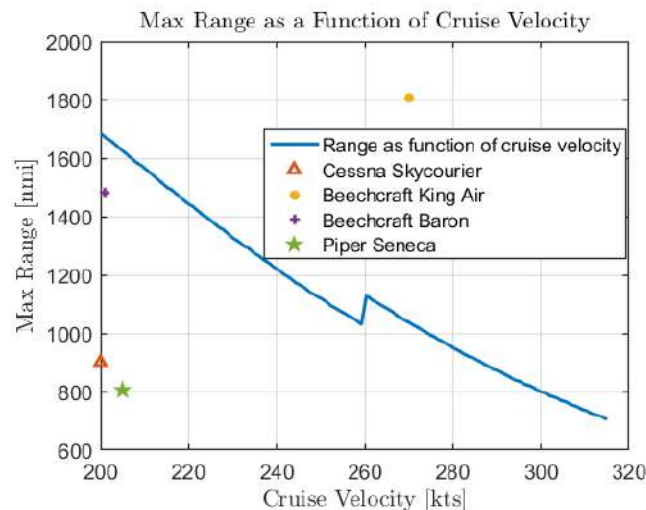


Figure 3.6: Effects of cruise speed on maximum cruise range.

As would be expected, a lower velocity yields better range when the fuel efficiency drops from running at a less efficient output. This would have led to a choice of a lower cruise velocity, but due to the unique difficulty of bringing a new and expensive aircraft to market, a typical aircraft was not an option if the HT-LIT and LITTLE were to be marketable. Co-plotted in the figure are ranges and cruise velocities of existing aircraft of several different types. This was used to attempt to establish a niche market in the velocity and range. Several cheaper aircraft, like the Piper Seneca and Beechcraft Baron, operate at lower velocities and often achieve higher ranges than that of the HT-LIT. There are also several regional planes, like the very popular King Air series of aircraft, which operate at velocities of 270 kts and up for significantly longer ranges than what is possible with the LIT and LITTLE. Armed with this information of the current market, the cruise velocity of the LIT was chosen to be 270 kts. This allows the HT family to stake land in a somewhat untapped market for fast, short trips while still maintaining some of the added efficiency of flying at the propulsion system's peak efficiency.

4 CONFIGURATION

The configuration section here is meant to detail the overall internal and external placement of major components and the iterations through the design process that have led to the designed aircraft. Additional information on the individual components of either aircraft may be explained in more detail in other sections of the report.

4.1 Design Morphology

When developing the aircraft family, a number of trade studies were performed to consider various components for these aircraft. These studies and the results obtained from them comprise the design morphology. A visual representation of some of the designs that were explored can be seen in Fig. 4.1

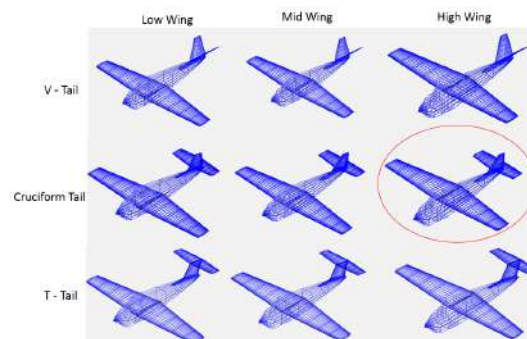


Figure 4.1: First stage of design iterations for wing and tail configuration.

Tail Configuration When designing the main points of external configuration (being the location of the main wing and the style of tail) major design decisions included tail design as well as wing location. For tail design, the main argument was whether to use a V-tail, cruciform tail, traditional tail, or T-tail. V-tail offered some advantages such as reduced drag and lower structural weight, which are in line with the efficiency ideals we set out to design around. On the other hand, the V-tail's design makes it more difficult to maintain control authority as neither of the control surfaces on the tail are orthogonal to the pilot's desired force vectors and the simultaneous pitch and yaw moment on the aircraft makes for a much more complicated flight control system. The conventional tail would be the most cost effective but less performance minded when one considers that both cruciform and T-tail deliver better control as the elevators lie outside of the wake generated by the main wing. Another major factor is weight with the V-tail and conventional tail being the lightest, followed by the cruciform tail with the T-tail at the end of the pack. When considering all of these factors it was determined that the cruciform tail configuration offered the perfect balance of weight, complexity and control authority for the HT-LIT and HT-LITTLE designs.

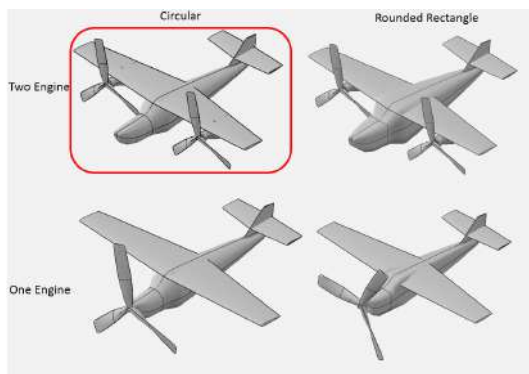
Wing Configuration Wing location was the next decision point of the aircraft which can also be seen in Fig. 4.1 displaying many aircraft concept models. Mid-wing was initially ruled out of contention due to the complicated integration

into the configuration of the aircraft as the wing box must pass through the fuselage. Although a mid-wing configuration offers less interference drag the added structural complexity renders it an inadequate design choice. A low-wing configuration would negate the structural complexity, and offers a location for retractable landing gear, though entering/exiting a low-wing aircraft proves more difficult and the limited downward visibility on approach can make landing more difficult. For these reasons the choice was made to pursue a high wing configuration. High-wings offer similar structural complexity compared to low-wing aircraft but have improved roll stability, are easier to enter and exit, and have an improved downward visibility. Seeing as how the design of the HT aircraft family is tailored towards luxury it was determined that the ease of entrance/exit would prove a vital advantage of the high-wing design.

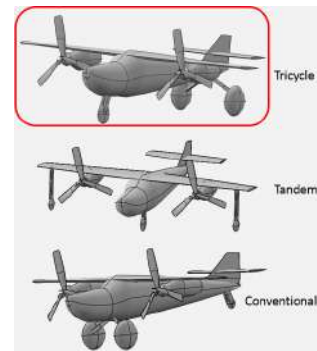
Fuselage Shape In the initial design of the aircraft a rounded rectangle was seen as the most desirable shape for the fuselage. The wide nature allowed for ample floor space and higher ceilings but made cabin pressurization (due to the added structural complexity) much more difficult. Going through multiple design iterations it was determined that the benefits seen from cabin pressurization (increased cruise altitude, increased cruise speed, increased passenger comfort, etc.) were too large to ignore and the decision was made to pressurize the cabin. In order to do this the cabin changed from a rounded rectangle shape into a circle to allow for a more even force distribution. The designs considered during this process can be seen in Fig. 4.2a.

Engine Selection/Location Due to the difficult stall speed requirement in an engine out scenario the decision was to equip the aircraft two Rolls Royce Allison Model 250 turboshaft engines which would easily provide the power needed to meet the one engine inoperative takeoff requirement. A piston-prop configuration was also considered for its benefit of low cost but it was determined that as the HT family was being marketed as a luxury aircraft and was going to be pressurized that the added power from a turboprop (let alone a twin-turboprop) configuration would see greater returns in profit. The designs considered during this process can be seen in Fig. 4.2a.

Landing Gear After looking at landing gear types such as tandem landing gear, tail wheel landing gear (also referred to as traditional landing gear), and tricycle landing gear (all of which are features in Fig. 4.2b) it was determined that the benefits of tricycle landing gear such as greater resistance to nosing over while braking, increased visibility from the flight deck, and prevention of ground-looping (which tends to be an issue of traditional landing gears) would prove most valuable. In addition, the benefit of landing gear configurations such as tandem landing gear would not provide significant advantage to our system as they excel in aircraft with flexible wings, which a general aviation aircraft of this size would not utilize. Though the initial thought was to pursue fixed landing gear for simplicity, the reduced drag along with cabin pressurization that coincide with retractable landing gear would allow the aircraft to operate at a higher speed and a higher altitude, making the aircraft family more appealing to the premium general aviation market.



(a) Second stage of design iterations - fuselage and engines.



(b) Third stage of design iterations - landing gear.

Figure 4.2: VSP models of multiple design iterations.

4.2 External Layout

4.2.1 General Sizing

The HT-LIT and the HT-LITTLE (the 6 and 4 seat variants respectively) share a nose and tail design with the main difference being the length of cabin. The cabin diameter is the same for each variant with a total diameter of 58 inches and a usable diameter (floor to ceiling) of 48 inches. The longer HT-LIT, the 6 seated aircraft, has a 120 inch (10 ft) cabin and a total length of 32 ft while the shorter HT-LITTLE, the 4 seated aircraft, has a 54 inch (4.5 ft) cabin resulting in a 26.5 ft long aircraft. These aircraft lengths result in very spacious and luxurious cabins for both the 4 and 6 seat variants.

The propulsion system for both aircraft consists of two turboprop engines and an electric motor powered by a 500 lb lithium ion battery. The takeoff weight of the HT-LIT is 7276 lbs while the smaller HT-LITTLE has a takeoff weight of 6547 lbs.

4.2.2 Engines

In the aircraft, mounted at 9 ft from the center of the fuselage on either end are two Rolls Royce Allison Model 250 turboprop engines each capable of delivering 420 shaft horsepower. Due to the nature of the electric motor being mounded directly above the M250, the nacelle is quite tall with a height of 40 inches and has a width of 20 inches. The lateral placement of the engine relative to the center of the fuselage was determined to ensure that the engines did not reside directly under the fuel tank for safety purposes. A more detailed dissection of the nacelle design can be found in Section 6.4

4.2.3 Landing Gear

The retractable tricycle landing gear was constructed in regard to nose gear loading and structural complexity. The front landing gear was placed approximately 5 ft aft of the nose of the aircraft while the rear landing gear was placed

approximately 13.14 ft in front of the tip of the tail - a configuration chosen to avoid forward over pitch, prevent tail strikes, and provide proper load paths throughout the aircraft structure. An animated gif of the landing gear motion can be found at <https://imgur.com/a/lrAYdRb>.

4.2.4 Wing & Empennage

Initial sizing wing loading directed the aircraft toward a main wing which has a surface area of 200 ft^2 and a small sweep of 4° . The design of the wing and airfoil (NACA 2415) is the same for both variants of the aircraft but its location changes. The HT-LITTLE has a leading edge 8.33 ft aft of the nose of the aircraft while the HT-LIT has its leading edge placed 13.83 ft aft of the datum (nose of the aircraft). Both wings span 40 ft and have root chords of 6.667 ft, tip chords of 3.333 ft, and a 4° sweep.

The cruciform horizontal tails also have a small sweep of 4° as well as a surface area of 54.2 ft^2 and a 15.79 ft span with its leading edge located 29.69 ft aft of the nose on the 6-seater and 24.65 ft aft of the datum on the 4-seater with the elevators sized to cover roughly 35% of the chord.

The vertical portion of the tail has a span of 5.5 ft, with an area of 58.72 ft^2 , of which 35% of the chord is the rudder. The root chord measures 5.8 ft and the tip chord measures 4.6 ft with a sweep of 32 degrees for the HT-LIT and HT-LITTLE respectively.

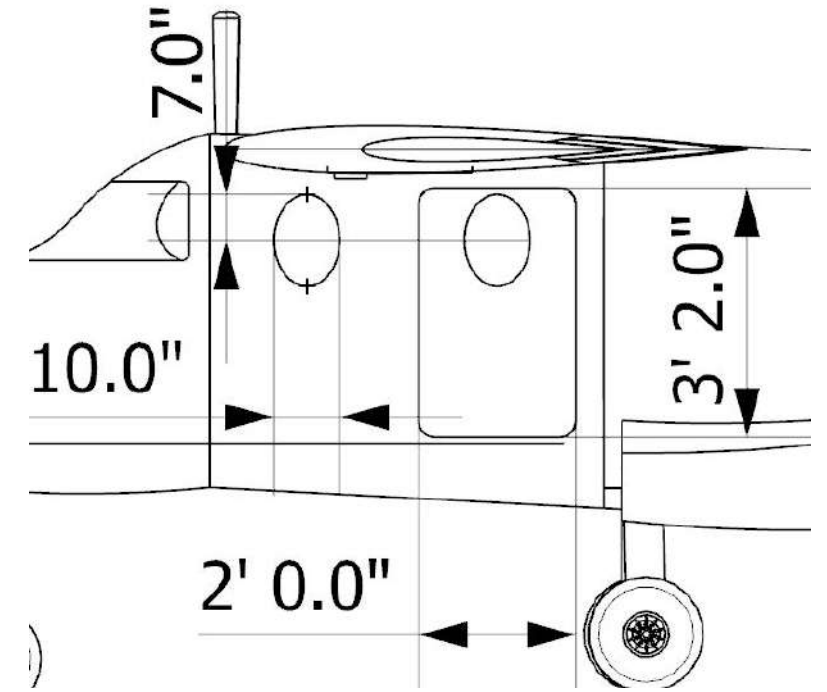
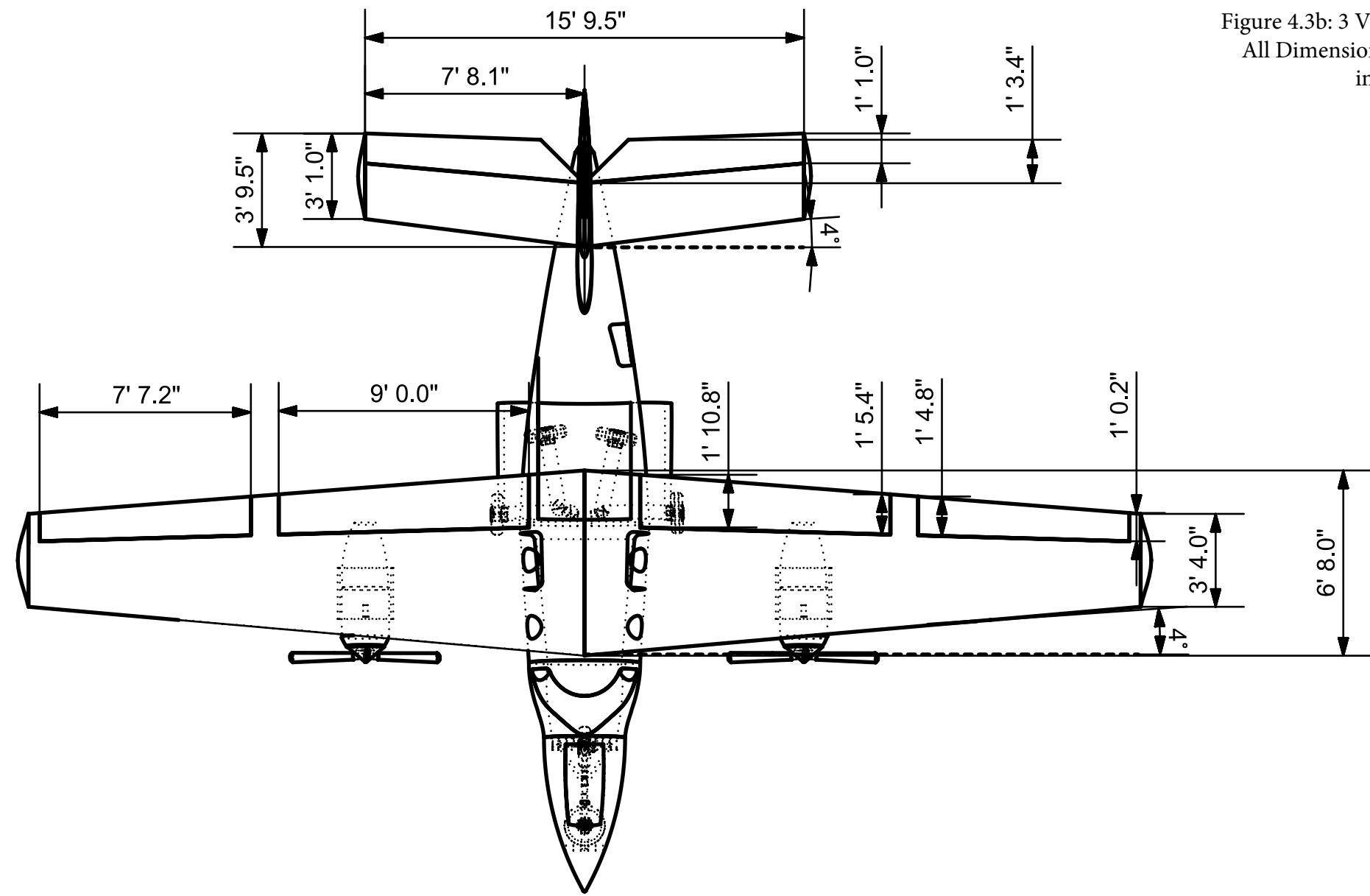
4.2.5 Windows

The number of windows varies widely between the two variants of aircraft in the HT family. Windows were placed in between the structural frames of the aircraft and were designed in elliptical shapes (each with a 7 inch major radius and a 5 inch minor radius) to minimize the stress concentration on the pressurized cabin. The HT-LIT, with a significantly larger cabin, has 5 windows on each side of the aircraft for a total of 10. The HT-LITTLE, being far smaller, has two windows on each side of the cabin for a total of 4 windows.

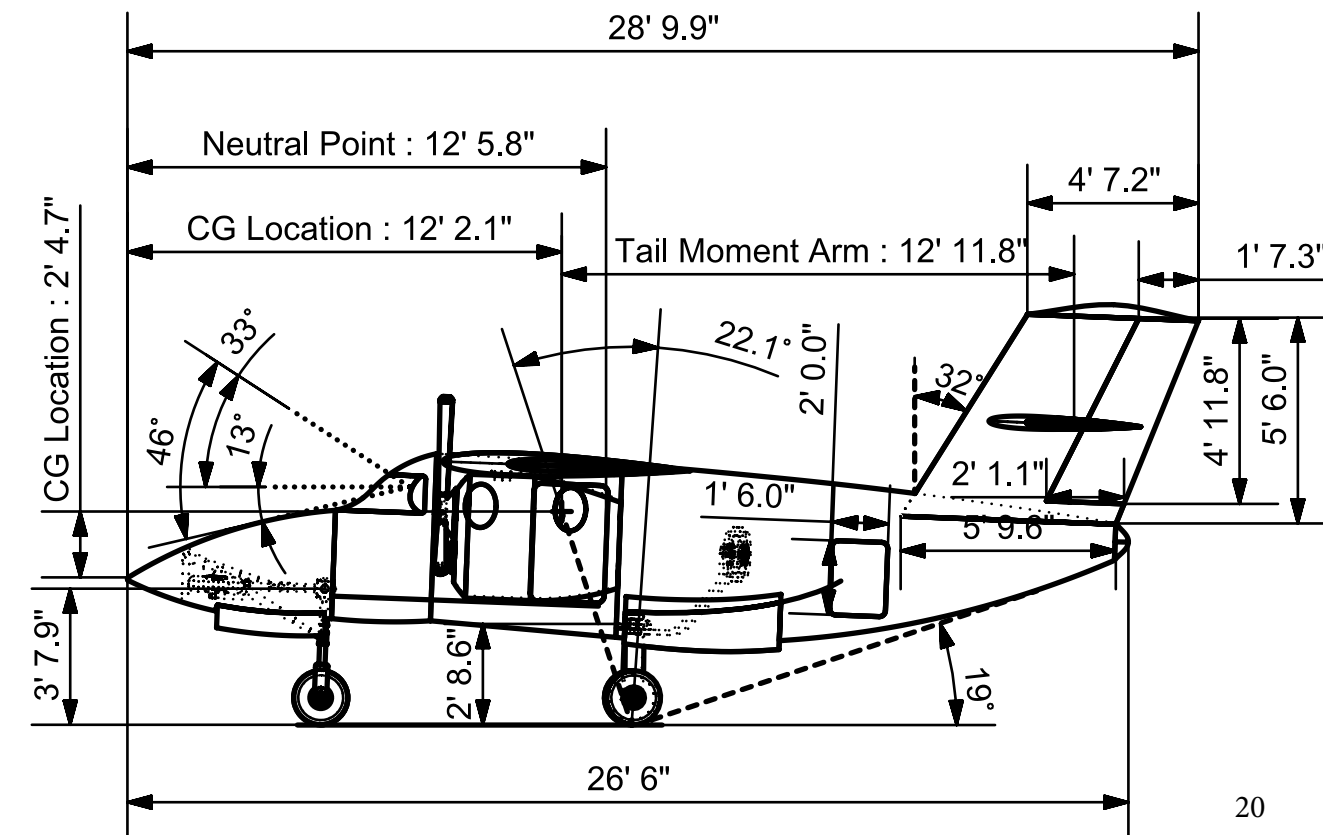
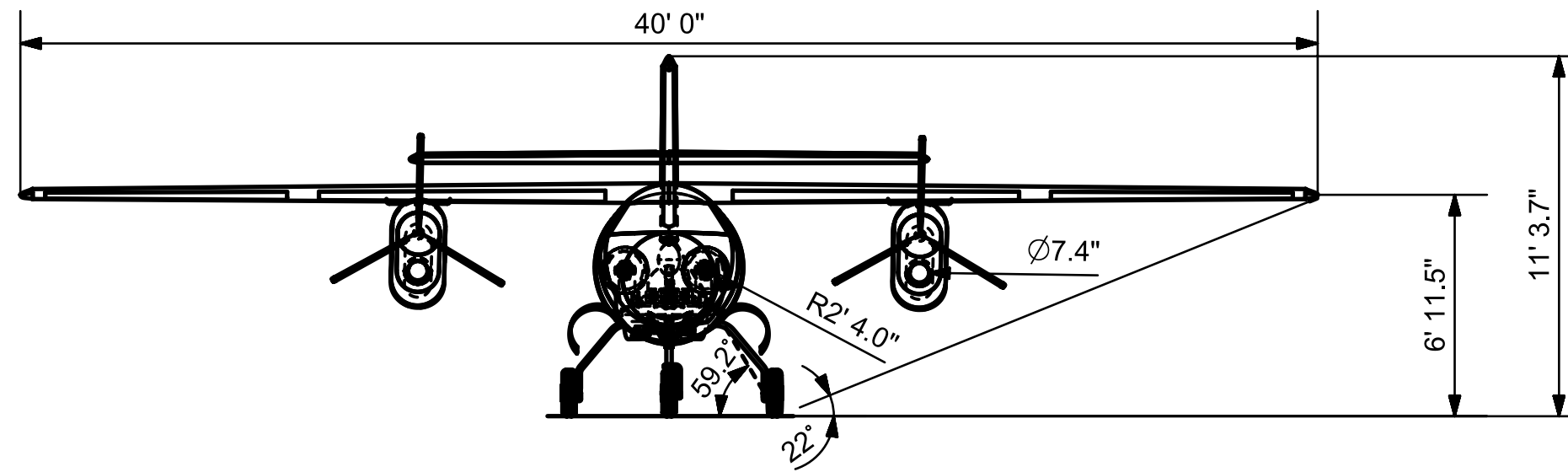
4.2.6 Doors

Each aircraft in the HT family is outfitted with two doors, each with the dimensions of 24 inches x 38 inches in order to lie between the frames of the aircraft and in between the structural longerons. The doors of the HT-LIT are located with the door beginning 8.25 ft aft of the datum while the doors of the HT-LITTLE begin 10.82 ft aft of the datum in order to ensure that both doors are clear of the propeller for passengers entering and exiting the aircraft.

Figure 4.3b: 3 View of HT-LITTLE
 All Dimensions are in feet and inches



Close up with nacelle removed



4.3 Internal Layout

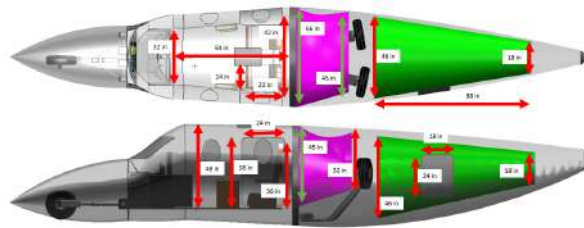


Figure 4.4: Interior layout of the HT-LITTLE.

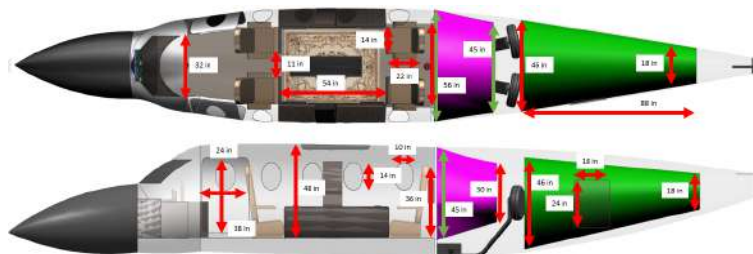


Figure 4.5: Interior layout of the HT-LIT.

The interiors of the HT-LIT and HT-LITTLE can be seen in Fig. 4.5 and 4.4. The HT-LIT is built to accommodate 5 passengers and a pilot while the HT-LITTLE is built to accommodate 3 passengers and a pilot. Both aircraft are outfitted with two doors and contain a large cargo area in the tail of the plane, which will be talked about more in Section 4.3.6.

4.3.1 Fuel Tanks

Fuel for the aircraft is stored in both wings with each wing containing an integral fuel tank which extends from the first wing rib to the fourth wing rib and then from the fifth wing rib to the second to last wing rib (located at the 98% point of the wing). Through analysis of the mission profile it was determined that the LIT requires 1250 lbs of fuel and the LITTLE requires 1300 lbs of fuel which can easily fit inside the large area of the main wing. Since the location of the wings differs between the two variants the fuel weight is evaluated as 11.81ft aft of the datum and 17.88 ft aft of the datum for the LITTLE and LIT respectively.

4.3.2 Avionics

The avionics system weight is between 85-95 lbs for both aircraft variants and was estimated using avionics packages present in existing similar aircraft available for sale. The avionics were placed at a distance 6.76 ft (LITTLE) and 7.12 ft (LIT) aft of the nose of the aircraft. An image of the avionics and cockpit view can be seen in Fig. 4.6. The avionics selection was made using information from existing aircraft and a more detailed walk through of the systems can be found in Section 10.5.



Figure 4.6: View from the cockpit of the aircraft.

4.3.3 Battery System

The battery system for the plane is a lithium-ion battery system that resides in the rear of the aircraft. This 7 ft³ battery along with its battery coolant and protection system are located behind the cabin and above the landing gear. The location of the battery and its necessary systems is approximately 15 ft aft of the datum for the LITTLE and 20 ft aft of the datum for the LIT - though the location is different for the two variants they both have the same total battery weight of 500 lbs or 725 lbs when adding in the cooling and protection systems.

4.3.4 Oxygen and Cabin Systems

The oxygen and cabin systems are located in the area behind the furthest aft row of seats above the main landing gear. With how the main landing gear operates there is a significant portion of the fuselage that remains out of the path of the retracting gear and out of the usable cabin space. This space can be represented from the pink mass just aft of the cabin seats in Fig. 4.4 and Fig. 4.5.

4.3.5 Seats

The aircraft contains 1 pilot seat, 1 copilot seat and either one or two rows of luxury seats in the cabin of the aircraft. The pilot and copilot seats are located 7.5 ft aft of the nose in both aircraft variants.

In the LITTLE variant the next row of seats is located 4.5 ft behind the pilots seats at 12.08 aft of the datum, spaced 5 inches apart from each other due to the lack of need for an aisle in the two seat variant.

In the LIT variant the two cabin rows are located 2.65 ft and 6.57 ft away from the pilot seats and about 10 inches away from each other. These seats have a cabin-inward facing orientation as that offers more ample leg room and provides a prime environment for socialization between passengers

The passengers seats themselves are meant to be incredibly luxurious. Made of fine leather with dimensions of

14 inches across, 22 inches deep and 36 inches tall. The seats and rest of the interior cabin can be viewed in more detail in Fig. 4.7.

4.3.6 Storage

Baggage for the passengers and pilot are to be located behind the landing gear in the tail of both the LIT and LITTLE aircraft. As shown in Fig. 4.4 and Fig. 4.5 the baggage area can be represented by the pink mass toward the rear of the plane. This area behind these seats provides a volumetric area 43 ft^3 in each variant, which surpasses the suggested 26 ft^3 by the RFI[3] for the 6 seat variant (and 16 ft^3 for the 4 seat variant). It is accessible from the outside of the aircraft from one cargo door located on the port side of the aircraft. Though the baggage storage is inaccessible from the cabin, the spacious cabin (which will be talked about more in the next section) allows the passengers on both the HT-LIT and HT-LITTLE to bring items with them into the cabin.

4.3.7 Consumer Appeal

Seeing as how the HT aircraft series is tailored to appeal to the wealthy and luxurious it only seemed right to include some luxury amenities in the HT-LIT, especially with such a large cabin to take advantage of it. For this reason, the HT-LIT comes with a mini bar located in between the ample leg room of the two rows of seating. As can be seen in Figs. 4.4 and 4.5 the aircraft have quite a bit of leg room with 54 inches of shared legroom on the LIT and 32 inches of individual legroom on the LITTLE. The luxurious nature of the aircraft is well represented in Fig. 4.7

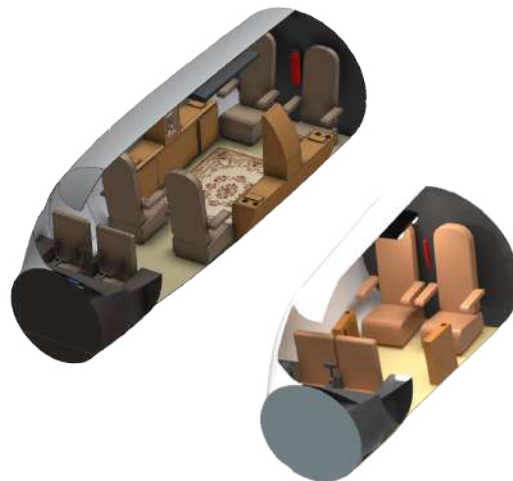
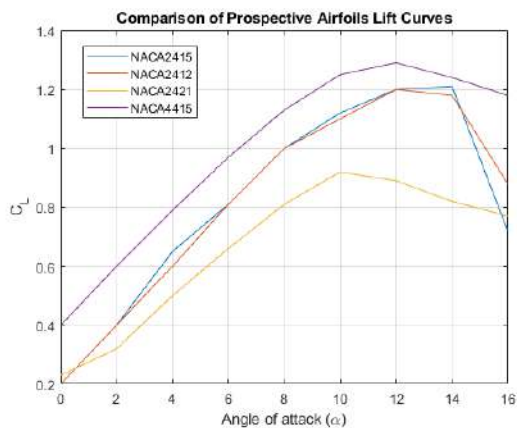


Figure 4.7: View of the cabin of the HT-LIT and HT-LITTLE.

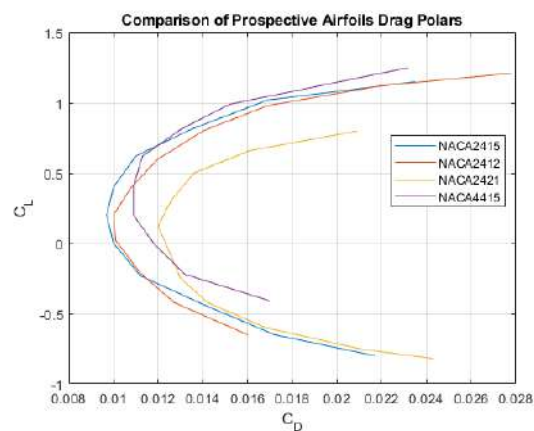
5 AERODYNAMICS

5.1 Airfoil Selection

The process of selecting an airfoil began with the creation of a list of airfoils that are used on general aviation aircraft similar in size to the concept aircraft. The list of airfoils was narrowed to the NACA 2412, NACA 2415, NACA 2421, and the NACA 4415. The data for drag polars, moments, and lift coefficient vs. angle of attack curves for each airfoil were accumulated from experimental data aggregated in Yechout [6]. They were then co-plotted to better compare the coefficient trends. The resulting comparisons are shown in Fig. 5.1a, Fig. 5.2 and Fig. 5.1b. These values were compiled from the highest Reynolds number available to try and match the flight subsonic 0.4 Mach, 9,000,000 Re flight regime. In this Regime compressibility does not need to be accounted for, but certain performance characteristics have noticeable deviation. The airfoil options were narrowed down based on lift, stall, moment and drag characteristics in the specified flight regime.



(a) The lift coefficient vs. angle of attack for each airfoil considered for main wing.



(b) Drag polars of airfoils considered for main wing.

Figure 5.1: Airfoil parameter comparisons.

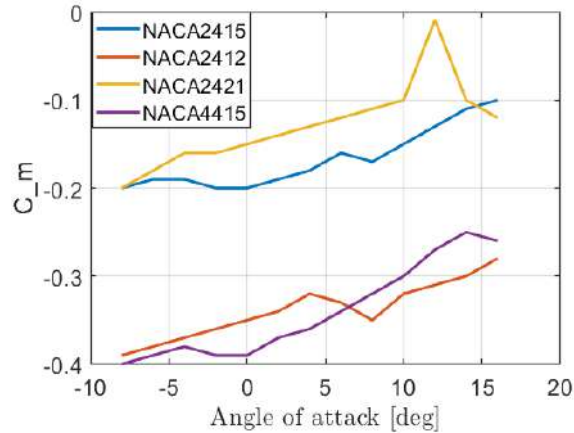


Figure 5.2: C_m curves of airfoils considered for main wing.

Looking at the lift curve slopes in Fig. 5.1a, all except for the NACA 2421 are rather comparable in slope. The NACA 2412 and NACA 2415 are extremely close but are beat out in $c_{L\alpha}$ by the NACA 4415; however, the NACA 4415 has a lower stall angle as compared to the NACA 2412 and 2415. Then evaluating the drag polar of each airfoil, the NACA 2421 once again was an outlier, posting impressively weak performance in comparison to the other airfoils. The NACA 4415 performed much worse in this analysis, with noticeably larger C_{Dmin} compared to both the NACA 2412 and 2415. The NACA 2415 reaches the lowest C_{Dmin} and also achieves this at a higher lift versus drag value than any of the other airfoils. The moment curves for the NACA 2412 and NACA 2415 are notably lower in magnitude than the other choices, which became preferable as the trim force in some configurations can be slightly decreased. The initial choice was the NACA 2412, but after increasing cruise velocity the NACA 2415 became preferable due to its comparably better stall angle and L/D values for higher Reynolds numbers. Upon evaluation, the NACA 2415 became the choice for the main wing airfoil due to its respectable lift curve slope, high stall angle, and prospective range efficiency, a matter which must be carefully accounted for due to the added weight of the hybrid electric propulsion system. The NACA 2415 airfoil is shown in Fig. 5.3. The airfoil and selection methodology and for the horizontal and vertical stabilizers can be found in section 7.1.2. The airfoil parameters of the NACA 2415 can be found in Table 5.1.

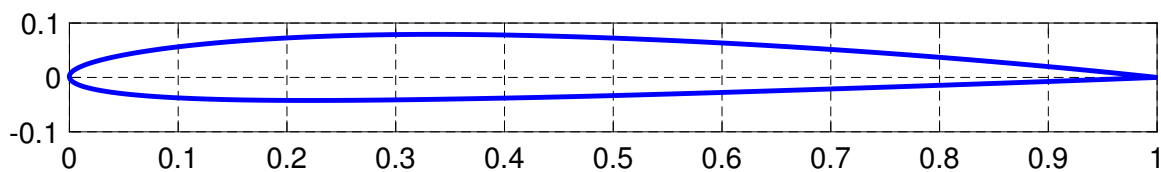


Figure 5.3: NACA 2415 airfoil used for the wing.

Table 5.1: NACA 2415 airfoil parameters

$\text{Max } C_l/C_d$	$\text{Max } C_l$	Stall Angle	C_m Cruise	t/c max
26.3	1.22	14°	-0.19	0.15

5.2 Wing Geometry

The sizing of the wing geometries for both the HT-LIT and HT-LITTLE began with an initial sizing analysis where the initial area of the wing was determined. The rest of the geometric parameters of the wing were determined using Roskam's method [7]. The taper ratio, sweep angle, aspect ratio, and dihedral angle were then determined by analyzing the effects of each parameter, outlined in detail in Roskam [7]. An incidence of zero degrees was chosen, because minimal angle of attack is necessary for cruise attitude and a zero incidence avoids stall in high angles landing approach. Taking the performance trends of each parameter into account, the wing geometry was determined to best accommodate the requirements set for each aircraft, including cruise velocity, takeoff performance, and desired efficiency. Upon further investigation, it became clear that with minimal adjustments to mission parameters of the HT-LITTLE the HT-LIT wing geometry could be used for both aircraft. This was determined to be advantageous from a manufacturing and price standpoint and provided very few detractive traits in performance. As a result, the wing geometries were merged to a single design. All of the geometric parameters of the wing are presented in Table 5.2. In addition, a diagram of the wings and control surfaces are presented in Fig. 4.3.

Table 5.2: Wing geometric parameters

Parameter	Symbol	Value
Planform Area	S	200 ft ²
Exposed Wetted Area	S_{wet}	387 ft ²
Leading Edge Sweep	Λ	4°
Span	b	40 ft
Aspect Ratio	AR	8
Root Chord	c_r	6.67 ft
Tip Chord	c_t	3.33 ft
Incidence	i	0°
Wing Loading (LIT)	$\frac{W}{S}$	36.38 lb/ft ²
Wing Loading (LITTLE)	$\frac{W}{S}$	33.5 lb/ft ²
Mean Aerodynamic Chord	MAC	5.18 ft
Dihedral Angle	Γ	2°
Twist Angle	ϵ_t	-2°

5.3 Flap Design

A high-lift device needs to be employed to satisfy many of the requirements, so a trade study was used to determine the best option for the aircraft's specifications. The leading candidates were the slotted flap, the plain flap, and the double slotted flap. A quality function deployment comparison again was employed to quickly evaluate the merit of each flap design, which is shown in Table 5.3.

Table 5.3: QFD of high-lift devices

	Importance	Plain Flap	Slotted Flap	Double-Slotted Flap
Simplicity	2	3	2	1
Lift increase	3	1	2	3
Weight	1	3	3	2
Maintenance	2	3	3	1
Total		18	19	14

The analysis was conducted by assigning point values, 3 for best fit and 1 for worst fit, along with a weighting system indicating the importance of each characteristic. The weighted sums were then used to determine the slotted flap was the best flap design for the HT-LIT and HT-LITTLE aircraft. The plain flap was a close competitor, but the importance of lift modification caused the slotted flap to pull ahead in total design value. Fig 5.4 shows the relative positions of the slotted flaps during takeoff and landing, with deflections listed in Table 5.4

Table 5.4: Flap dimensions and parameters

	HT-LIT	HT-LITTLE
Flap chord ratio	0.3	0.3
Flap deflection during takeoff	15°	12°
Flap deflection during landing	35°	35°
Flap span ratio	0.55	0.55
Max flap deflection	40°	40°
Longitudinal flap movement	1.3 %c	1.3 %c
Vertical flap movement	2.4 %c	2.4 %c

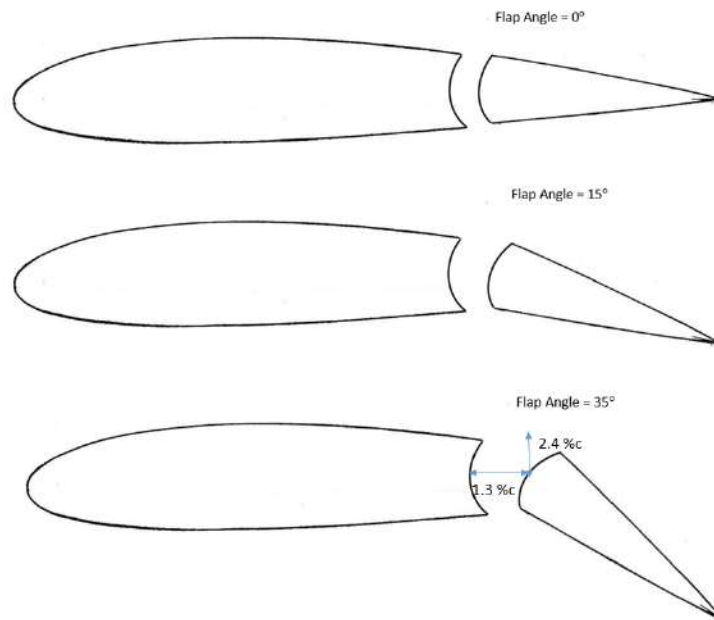
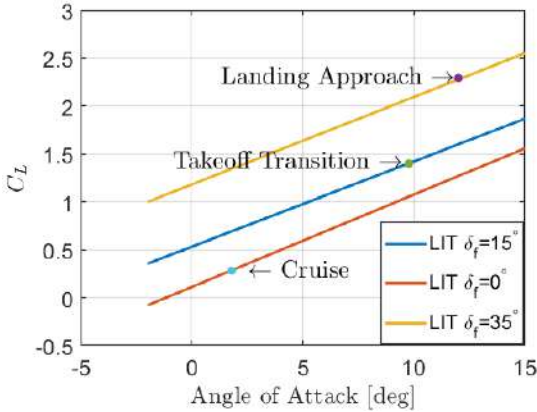


Figure 5.4: Flaps at take off and landing deflections.

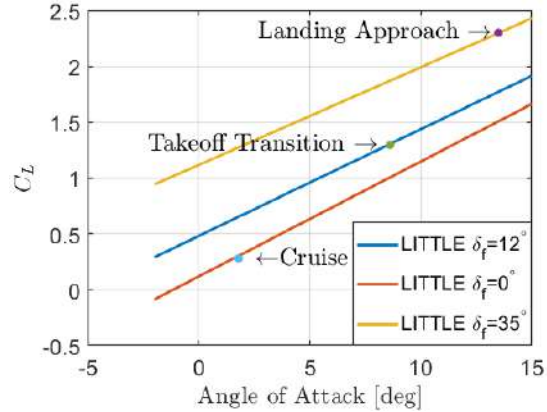
In its deflected position, the flap extends an additional 1.3 percent of local chord aft of the trailing edge and 2.4 percent down. This allows space for an air vane which reinvigorates the boundary layer on the flap, increasing its effectiveness. The decision on this geometry was made by analyzing optimized flap geometries for similar airfoils in McCormick [8]. The flaps are hinged on the adjacent rib at the inboard and outboard most ends of the flap, adding no additional disturbance to the slot airflow. Additional flap geometries were determined by utilizing historical data of flap geometries of similar aircraft, found in Sadraey [9]. In particular, the Jetstream 41 and Lockheed L-100 were used in determining the necessary flap dimensions for the desired aircraft design. The flap chord was held constant at 30% of the local wing chord and runs along the inboard 55% of the wing. The flaps run a slightly lower percentage of the span in order to allow a larger aileron section for lateral stability, as the higher cruise velocity necessitates greater attention to control authority and control surface sizing. The wing, flap, and aileron geometries are shown in Fig. 4.3 with relevant dimensions. Ailerons were sized using the method described in Sadraey [9] and sized to extend the later 40% of the wing at the same chord ratio. Relevant flap data are tabulated in Table 5.4.

5.4 Lift & Drag Models

The total lift coefficient values for both aircraft were found by modeling the all lifting surfaces in AVL, a 3-D panel method program, then running simulations for the various flight configurations and conditions of takeoff, cruise, and landing. Due to the linear nature of a panel method in approximating lift values, the stall conditions could not be accurately represented. As a result the lift-curves were cutoff at the airfoil stall angle shown in Fig. 5.1a. The resulting lift curves for the HT-LIT and HT-LITTLE are shown in Fig. 5.5a and Fig. 5.5b, respectively.



(a) Lift curve for mission segments of HT-LIT.

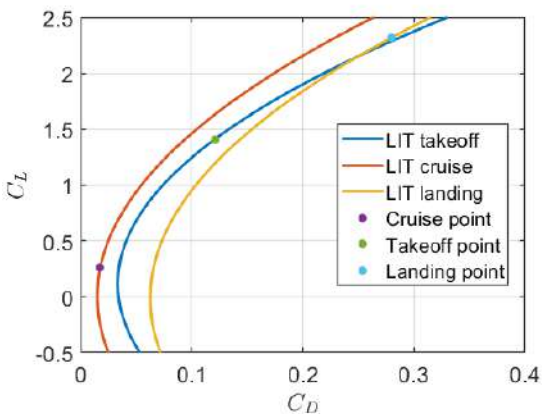


(b) Lift curve for mission segments of HT-LITTLE.

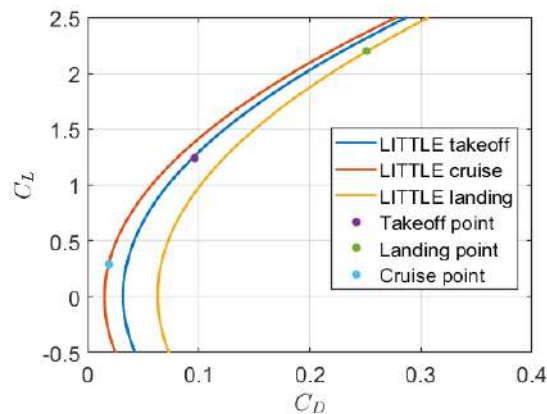
Figure 5.5: Lift curve for mission segments of both HT-LIT and HT-LITTLE.

The flap deflection angles during landing and takeoff were established by looking at historical data, found in Roskam [7], then optimized based on performance requirements. The HT-LIT flap deflection was determined to be 15° for takeoff and 35° during landing. The HT-LITTLE, due to its lighter airframe, has a takeoff flap deflection of 12° . The deflection during takeoff remains 35° in order to meet stricter landing requirements.

The parasite drag was calculated according to methods detailed in Roskam [7], using a combination of form factor analysis, drag approximations, and aircraft parameters. The parasite drag was then combined with the induced drag, calculated using AVL, for every angle of attack and flap deflection to complete the drag model. The resulting aircraft drag polar for the HT-LIT and HT-LITTLE is shown in Fig. 5.6a and Fig. 5.6b. The breakdown of drag, including trim and induced drag, is shown for each mission segment for both aircraft in Table 5.5.



(a) Drag polar of HT-LIT.



(b) Drag polar of HT-LITTLE.

Figure 5.6: Drag polar of a) HT-LIT and b) HT-LITTLE.

Table 5.5: Drag buildup of HT-LIT and HT-LITTLE

HT-LITTLE				HT-LIT			
Component	Cruise Parasite Drag Coefficient	Takeoff	Landing	Component	Cruise Parasite Drag Coefficient	Takeoff	Landing
Wings	0.0046	0.0051	0.0053	Wings	0.0046	0.0052	0.0053
Flaps	N/A	0.002	0.0082	Flaps	N/A	0.0022	0.0082
Cruciform Tail	0.0025	0.0026	0.0026	Cruciform Tail	0.0035	0.0036	0.0036
Nacelles and Pylons	0.0017	0.0017	0.0017	Nacelles and Pylons	0.0017	0.0017	0.0017
Fuselage	0.0047	0.005	0.0051	Fuselage	0.0052	0.0055	0.0056
Landing Gear	N/A	0.0122	0.0122	Landing Gear	N/A	0.0122	0.0122
Windshield	0.000747	0.000747	0.000747	Windshield	0.000747	0.000747	0.000747
Surface Roughness	0.000415	0.000415	0.000415	Surface Roughness	0.000415	0.000415	0.000415
Trim	0.0002	0.0039	0.0052	Trim	0.0001	0.0004	0.0014
Induced	0.0034	0.0674	0.2152	Induced	0.0023	0.0939	0.2459
Total	0.01871	0.096	0.2514	Total	0.01753	0.1207	0.2798

The angle of attack, C_L , and C_D values for each mission leg can be seen in Table 5.6.

Table 5.6: Aerodynamic Coefficients for various mission legs

Parameter	HT-LIT	HT-LITTLE
α Takeoff (transition)	10.5	8.2
α Cruise	1.6	1.5
α Landing (approach)	12.4	13.4
C_L Takeoff	1.4	1.31
C_L Cruise	0.2766	0.2748
C_L Landing	2.3	2.3
C_D Takeoff	0.1207	0.096
C_D Cruise	0.01753	0.01871
C_D Landing	0.2798	0.2514

6 PROPULSION

The design requirements listed in the RFI [3] necessitated the selection of engine, battery, and electric motor components that could be feasibly integrated to meet the performance requirements of the HT-LIT and HT-LITTLE aircraft. Due to the current nature of electric propulsion components, assumptions had to be made on the developmental trends of future technology. The performance specifications and costs of electric propulsion components such as the batteries and electric motors were determined from projections based on the current state of technology. The propulsion system was designed by choosing an existing internal combustion engine that best met the design goals of performance and reliability within the size and weight constraints and by choosing the electric components whose predicted perfor-

mance, size, weight, and efficiency were most promising based on current trends. An overview of the propulsion system components is shown in Table 6.1. An overview of the propulsion system integration into the aircraft is shown in Fig. 6.1 and the propulsion system layout within the nacelle is shown in Fig. 6.1

Table 6.1: Overview of main powerplant components

Powerplant Component	Number of Components	Make and Model
Engine	2	Rolls Royce M250-B17F Turboprop
Propeller	2	Hartzell HC-B3TF-7A T1017
Motor	2	Siemens 170kW EM
Batteries	1	Lithium Nickel Manganese Cobalt Oxide

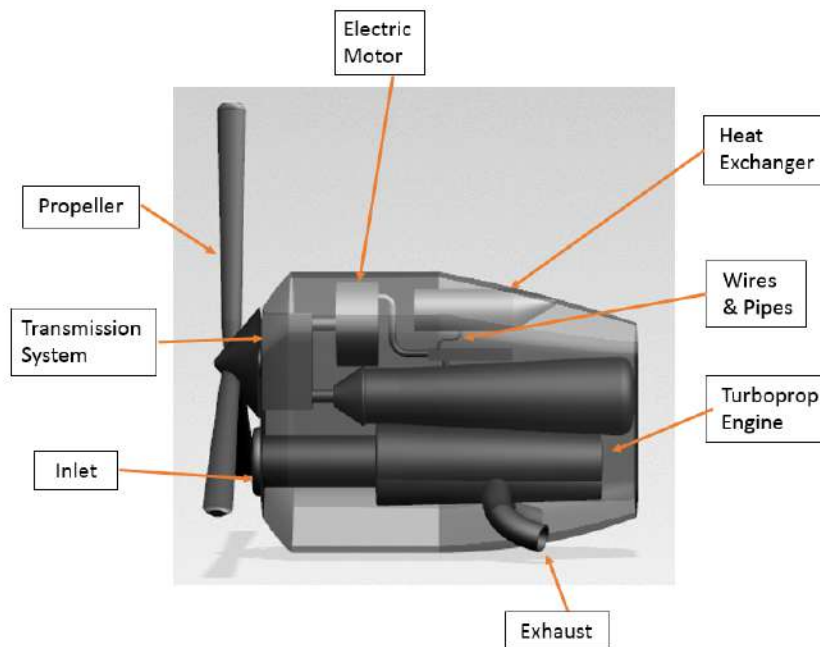


Figure 6.1: Nacelle layout diagram.

6.1 Engine Requirements

The primary design drivers behind the selection of the propulsion system were based on achieving desired performance, minimized weight, and high reliability. The design requirements for the aircraft necessitated the selection of a propulsion system that would provide a thrust to weight ratio capable of satisfying the performance requirements listed in the RFI, specifically the capability of the HT-LIT aircraft to maintain a target cruise velocity over 200 KTAS at an altitude of 20,000 ft. From the sizing analysis, the engine power required to satisfy the desired mission performance was found

to be roughly 400 hp at cruise conditions. Engine candidates needed to satisfy this power requirement at a minimum, and were then analyzed for optimal design decisions of displacement, weight, efficiency, and cost. The available thrust and power of the chosen propulsion system for the HT-LIT and HT-LITTLE aircraft were shown to meet the design mission requirements as shown in Table 6.2.

Table 6.2: Required vs. available thrust and power for cruise

Aircraft Variant	T_{req}	P_{req}	T_{avail} Cruise	P_{avail} Cruise	T_{avail} Takeoff	P_{avail} Takeoff
HT-LIT	449 lbf	371 SHP	748 lbf	620 SHP	2,395 lbf	706 SHP
HT-LITTLE	407 lbf	324 SHP	777 lbf	620 SHP	2,499 lbf	706 SHP

6.2 Engine Safety Considerations

A thorough examination of the performance in the case of single engine failure was explored on page 15 of the report in Section 4.7.

6.3 Engine Selection Process

6.3.1 Number of Engines

A twin-engine design was chosen as the basis of the propulsion system for the HT-LIT, which allowed for reduced complexity in structural design of the aircraft as well as a larger possible power output and TOGW.

6.3.2 Piston Engine vs. Turboprop Engine

The desired aircraft designs were a 6-seat and 4-seat, twin-engine general aviation aircraft. Almost all such aircraft utilize reciprocating engines or turboprop engines, due to the nature of the performance requirements and operating conditions of said aircraft. Turbojet, turboshaft, and turbofan engines were ruled out as candidates, because turbojets and turbofans provide much more than the required amount of thrust for the design specifications and add significant weight to the aircraft. Turboshaft engines generally provide more than the required amount of power, as well as being used in most cases for rotary aircraft applications, introducing added design complexity. A list of specifications of comparable turboprop and piston engines is shown in Table 6.3. The performance data for the engines was collected from Daly [10].

Table 6.3: Turboprop/piston engines weights & maximum power output

Engine Manufacturer	Model	Engine Type	Max Power	Dry Weight	P/W ratio
Continental	IO-550-N	Piston	310 hp	412 lb	$0.752 \frac{hp}{lb}$
Lycoming	IO-540-S	Piston	300 hp	441 lb	$0.680 \frac{hp}{lb}$
Lycoming	IO-720-A	Piston	400 hp	568 lb	$0.704 \frac{hp}{lb}$
Rolls Royce	M250-B17F	Turboprop	420 SHP	212 lb	$1.98 \frac{SHP}{lb}$
Pratt & Whitney	PT6A-110	Turboprop	475 SHP	334 lb	$1.42 \frac{SHP}{lb}$
Garrett (Honeywell)	TPE 331-43A	Turboprop	575 SHP	335 lb	$1.72 \frac{SHP}{lb}$

One of the primary design drivers behind engine selection was power output (ideally around 400 SHP). This narrowed down the possible engine candidates to three turboprop engines (the M25-0B17F, PT6A-110, and the TPE 331-43A) and one piston engine (the Lycoming IO-720-A). Another design driver behind the propulsion system and the HT-LIT and HT-LITTLE aircraft in general was the minimization of weight. Although the Lycoming reciprocating engine provided comparable power to the remaining turboprops, its dry weight was almost double the average weight of the turboprop candidates. Thus, the Lycoming IO-720-A was removed as a possible engine candidate and the remaining turboprop engines were further examined.

6.3.3 Candidate Engine Specifications

As seen in Table 6.4, all of the remaining turboprop engines provided more than the necessary maximum amount of power. Therefore the weight was taken to be the deciding factor. As all three candidates had similar specific fuel consumptions, the M250-B17F engine was chosen because its dry weight was significantly lower than the other two engines.

Table 6.4: Candidate turboprop engine specifications

Engine Manufacturer	Model	Max Power	Dry Weight	Displacement	SFC_{max}
Rolls Royce	M250-B17F	420 SHP	212 lb	11.42 ft^3	$0.673 \frac{lb}{hr \cdot shp}$
Pratt & Whitney	PT6A-110	475 SHP	334 lb	10.17 ft^3	$0.657 \frac{lb}{hr \cdot shp}$
Garrett (Honeywell)	TPE 331-43A	575 SHP	335 lb	16.59 ft^3	$0.660 \frac{lb}{hr \cdot shp}$

6.3.4 Rolls Royce M250-B17-F Turboprop Performance

Table 6.5: Rolls Royce M250-B17F performance and specifications [2]

Takeoff Power	Cruise Power	Takeoff SFC	Cruise SFC	Compressor Pressure Ratio
420 SHP	370 SHP	$0.673 \frac{lb}{hr} \frac{1}{shp}$	$0.656 \frac{lb}{hr} \frac{1}{shp}$	7.9

The values for available power output were calculated first by determining the thrust generated by the propeller and jet of the turboprop. The available power was determined by multiplying the sum of the thrust from the turboprop by the cruise speed of the aircraft. These values were plotted against altitude in Figure 6.2.

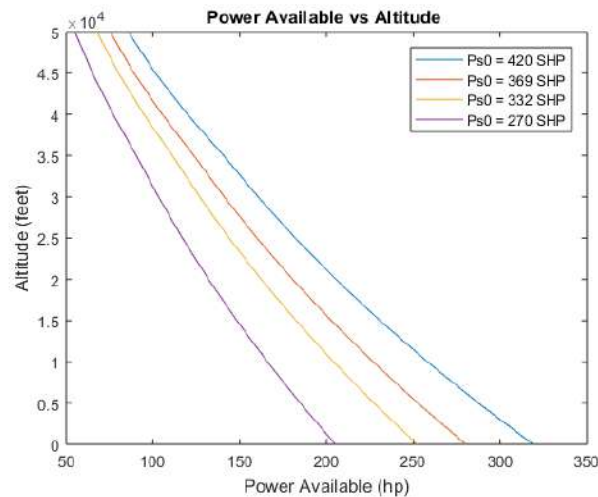


Figure 6.2: Available power output as a function of altitude.

6.3.5 Propeller Selection

After the M250-B17-F engine was selected a corresponding propeller system was chosen that was specifically produced to be compatible with the aforementioned engine. Produced by Hartzell Propellers, the Hartzell HC-B3TF-7A T10173 model consists of a 3-aluminum-blade, constant-speed propeller with full-feathering and anti-icing systems [11]. The propeller specifications are shown in Table 6.6. The thrust produced by the powerplant was seen to satisfy the cruise and takeoff thrust requirements.

Table 6.6: Propeller system specifications

Propeller Parameter	Values at Cruise Conditions
Number of Blades	3
Blade Length	41.75 in
Frontal Propeller Area	5475.9 in^2
Tip Velocity	739.605 $\frac{ft}{s}$
Mass Flow	21.96 $\frac{lb}{s}$
Thrust Produced	1,198 lbf (takeoff) - 356 lbf (cruise)

6.4 Inlet & Nacelle Design

The nacelle design of the HT series was based heavily on the design of existing aircraft that are using the same turboprop engine. However, due to the addition of the electric motor the height of the nacelle was made to be larger than that of comparable aircraft. This was due to the design choice that the electric motor be placed directly above the turboprop engine. The dimensions of the nacelle design were that of an ellipse cross section with a 40 in semi-major axis and 20 in semi-minor axis at the largest cross section. The total length of the nacelle was 60 in . Moreover, the air inlet design for the turboprop engine had an area of 0.302 ft^2 due to the intake air flow rate requirement (1.733 kg/s) and was placed directly below the propeller. The inlet pressure recovery of such design is about 0.72, which still allows the turboprop engines to provide enough power mentioned in Table 6.2. The exhaust for the ICE locates at the bottom of the nacelle with an area of 0.246 ft^2 . A view of the nacelle and inlet is presented in Fig. 6.3.

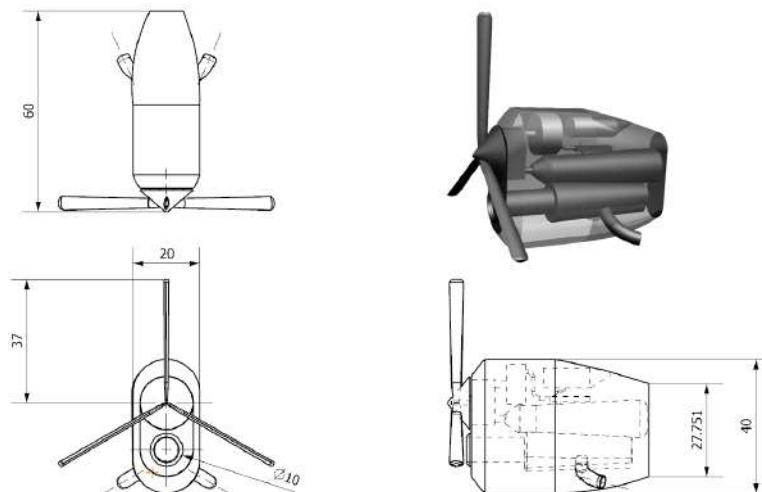


Figure 6.3: Views of the nacelle and inlet design.

6.5 Propulsion Architecture Selection

It was very important to determine which type of hybrid electric propulsion architecture would be the best choice for the HT series. Related requirements that needed to be satisfied included the emergency divert range with only electric power. The cost and feasibility of the design were crucial as well. There are currently three major hybrid electric propulsion architectures that have been either already implemented to actual aircraft or considered for testing in the near future. By discussing the advantages and disadvantages of these three architectures showing in Table 6.7, Table 6.8, and Table 6.9, a best option can be chosen for the HT series.

Table 6.7: Summary table for series HEP

Series Hybrid Electric Propulsion System
Advantage
<ul style="list-style-type: none"> • Lowest power management complexity due to the least number of potential power paths [12]. • Compatible with distributed propulsion concepts in which uses multiple small electric motors [12].
Disadvantage
<ul style="list-style-type: none"> • Limited thrust it can provide due to the technology limit of the electric motor. • Greater mass it has due to the multiple electric motors/generators required.
Conclusion
Not realistic to meet the desired cruise speed for both the six-seat model and the four-seat model by using such propulsion system in the next two decades [3] even with the decrease of motors weight and increase in their performance capabilities.

Table 6.8: Summary table for parallel HEP

Parallel Hybrid Electric Propulsion System
Advantage
<ul style="list-style-type: none"> • Extra safety redundancy since the electric motor and internal combustion engine are almost independent from each other [13]. • Lower mass compares to other architectures because it requires only one electric motor.
Disadvantage
<ul style="list-style-type: none"> • Power management complexity significantly increased due to the requirement of transmission system to connect two propulsion systems. • Larger size for the entire architecture and requires a larger nacelle than usual.
Conclusion
Capable of providing enough thrust to satisfy the mission requirements but need to consider the system complexity and size for such architecture [14].

Table 6.9: Summary table for series-parallel HEP

Series-Parallel Hybrid Electric Propulsion System
Advantage
<ul style="list-style-type: none"> • Mature technology in the usage of automobiles. • Strong power output and providing safety redundancy.
Disadvantage
<ul style="list-style-type: none"> • System complexity made maintenance hard to implement. • Too heavy for weight sensitive vehicles, especially for aircraft.
Conclusion
Even though this type of propulsion system can provide enough power to meet the requirements, the weight and system complexity made such architecture not the best choice for the design [15].

In conclusion, the most ideal choice for HEP system architecture showing in Fig. 6.4 was determined to be the parallel hybrid electric propulsion system. The key contributing factors to this decision were the moderate system complexity, relatively light system weight, and desirable thrust output.

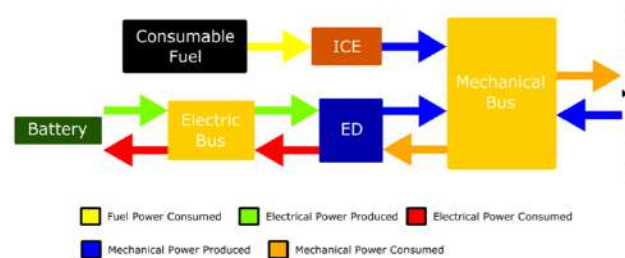


Figure 6.4: Parallel HEP system layout.

6.6 Batteries Selection Trade Study

When choosing the ideal battery for the HT-LIT aircraft it was necessary to consider and weigh performance factors such as specific energy, cost, life span, and safety for each battery candidate. From the macro perspective, the lithium-ion battery appeared to be the best choice under current technology, because it has already been widely used in many areas and has shown a large potential for improvements in the immediate and near future. However there are many different types of lithium-ion batteries, each having different advantages and disadvantages. Therefore, a trade study was required to compare different types of lithium-ion battery candidates.

Table 6.10 shows the features of the most common lithium-ion batteries. Ideal candidates had a high specific energy, corresponding to the ability to store a greater amount of energy within a lower weight battery. Ideal candidates also had a large cycle life, reducing the cost of maintenance. Thermal runaway was another important factor, since it

directly related to the safety consideration. Higher thermal runaway temperatures corresponded to a safer battery. The manufacturing costs were important to consider, as battery cost contributed to the total cost of the HT-LIT aircraft.

Table 6.10: Comparison of different lithium ion batteries

	Specific Energy	Cycle Life	Thermal Runaway	Cost
Lithium Cobalt Oxide ($LiCoO_2$)	150–200 Wh/kg	500–1000	150°C (302°F)	3
Lithium Manganese Oxide ($LiMn_2O_4$)	100–150 Wh/kg	300–700	250°C (482°F)	3
Lithium Nickel Manganese Cobalt Oxide ($LiNiMnCoO_2$)	150–220 Wh/kg	1000–2000	210°C (410°F)	3
Lithium Iron Phosphate ($LiFePO_4$)	90–120 Wh/kg	1000–2000	270°C (518°F)	3
Lithium Nickel Cobalt Aluminum Oxide ($LiNiCoAlO_2$)	200-260 Wh/kg	500- 800	150°C (302°F)	2
Lithium Titanate ($Li_4Ti_5O_{12}$)	50–80 Wh/kg	3000–7000	210°C (410°F)	1

Combining these points of concern, the resulting trade study was summarized quantitatively as follows:

Table 6.11: Parameter priority table for battery trade study

Feature	Weight (From Level 1 to 4)
Specific energy	4
Cycle life	3
Thermal runaway	1
Cost	2

Table 6.12: Ranking table for battery trade study

	Specific Energy	Cycle Life	Thermal Runaway	Cost
Lithium Cobalt Oxide ($LiCoO_2$)	4	3	2	4
Lithium Manganese Oxide ($LiMn_2O_4$)	3	1	5	4
Lithium Nickel Manganese Cobalt Oxide ($LiNiMnCoO_2$)	5	5	4	4
Lithium Iron Phosphate ($LiFePO_4$)	2	5	6	4
Lithium Nickel Cobalt Aluminum Oxide ($LiNiCoAlO_2$)	6	2	2	5
Lithium Titanate ($Li_4Ti_5O_{12}$)	1	6	4	6

Table 6.13: Final score of battery trade study

Type of Battery	Score
Lithium Cobalt Oxide ($LiCoO_2$)	35
Lithium Manganese Oxide ($LiMn_2O_4$)	28
Lithium Nickel Manganese Cobalt Oxide ($LiNiMnCoO_2$)	47
Lithium Iron Phosphate ($LiFePO_4$)	37
Lithium Nickel Cobalt Aluminum Oxide ($LiNiCoAlO_2$)	42
Lithium Titanate ($Li_4Ti_5O_{12}$)	38

Table 6.11, Table 6.12, and Table 6.13 above present the quantitative evaluation of the trade study. The parameter priority table shows the importance ranking of each parameter. In this case the specific energy was the most important parameter, followed by cycle life, cost, and thermal runaway. The ranking table presents the score received for each of the parameters for different types of battery. From these two tables, the final scoring table was determined. Based on the quantitative analysis of the different types of lithium-ion batteries, the Lithium Nickel Manganese Cobalt Oxide ($LiNiMnCoO_2$) received the highest score with 47 points. Therefore, the decision to use this type of battery for the design was justified in maximizing specific energy, life cycle, and thermal runaway, as well as minimizing the production cost. The current state Lithium Nickel Manganese Cobalt Oxide battery technology was shown to possess a specific energy of 150–220 Wh/kg. The trend of technology development suggested that by the year 2030 such type of battery would be capable of possessing a specific energy of 350 Wh/kg. With this value of specific energy, an 85-kWh battery pack was found to weigh 535.41 lb and a 100-kWh battery was found to weigh 629.89 lb. The aforementioned energy storage values for batteries have been observed as the most common values used in current electric automobiles, which were used as references for the HT-LIT aircraft design. An air cooling system will be used in order to bring down the temperature of the battery pack when it is operating.

6.7 Electric Motor Selection

A major factor for electric motor selection was its power output. In order to satisfy the requirements for the case of an emergency divert to landing on the support of the electric propulsion system alone, the power output of the electric motor needed to be able to decrease the aircraft's sinking rate to increase the aircraft's gliding range. A reasonable power output of the electric motor was found to be about 25% of the power output of the turboprop engine. For the design of the HT-LIT, the turboprop engine was selected to be the Rolls Royce M250-B17F which possessed a maximum power output of 420 SHP at takeoff. This indicated that the electric motor needed to have about 80 kW of available power output. The final selection for the electric motor was the Siemens 170 kW electric motor with a continuous power output of 170 kW and 95% efficiency at 6,250 rpm. The weight of this electric motor was 53.8 lb and its dimensions were 5.91 *in* length and 12.2 *in* diameter. Fig. 6.5 represents the electric motor.



Figure 6.5: Siemens 170 kW electric motor.

For the HT series, the electric motor is designed to engage during takeoff and cruising in order to minimize the takeoff runway length and to reduce fuel consumption or to increase cruise range. This means the electric motor will provide maximum power output during takeoff and partially engage during cruise. The battery will not be recharged during flight and the charging process only occurs on the ground. A thorough discussion of the system operation over mission profile is in the Mission Profile section under Concept of Operations in page 4.

Moreover, customers will have two options for the size of battery pack – either 80 kWh or 100 kWh. The performance on range of two different combinations is shown in Table 6.14.

Table 6.14: Performance of the electric propulsion section

Model	HT-LIT		HT-LITTLE	
Battery Size (kWh)	80	100	80	100
Maximum Percentage Contribution of Thrust in Cruise (%)	6	8	5	7
Maximum Fuel Saving Compare to Only Using ICE (lb)	42.6	68.2	49.4	69.1
Maximum Range Increase Compare to Only Using ICE (nmi)	42.4	67.8	52.9	74.1

6.8 Fuel System

The fuel tanks will be distributed inside the wing in between the ribs and spars. For HT-LIT to operate a regular cruise mission it will need a fuel weight of 1250 lb, and for HT-LITTLE a fuel weight of 1420 lb is required to meet the mission requirements. This means the fuel tanks need to have a total volume of 183 US gallons (24.5 ft^3) for HT-LIT and 208 US gallons (27.8 ft^3) for HT-LITTLE. There will be four fuel tanks in total, two on each wing; one will be located inside the wing section that is in between the nacelle and the fuselage and the other will be located inside the wing section that is in between the nacelle wingtip. The outboard fuel tank will supply fuel to the engine first due to roll stability concerns and the inboard fuel tank will be used after the outward fuel tank is drained. Fig. 6.6 shows the schematic of the fuel system.

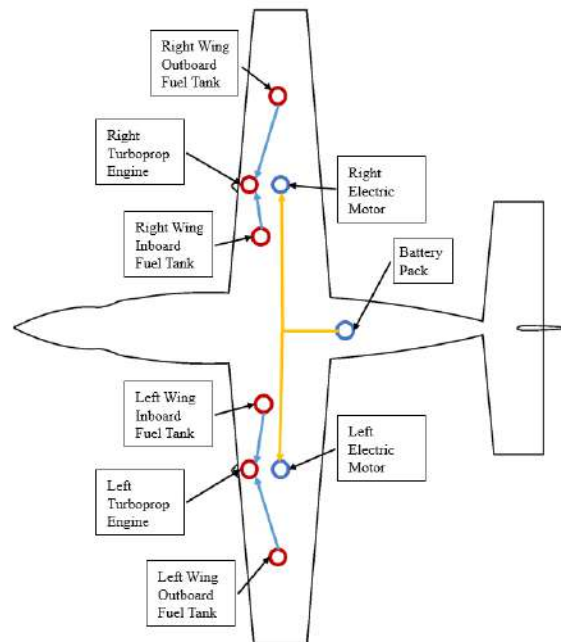


Figure 6.6: Fuel system schematic diagram.

7 STABILITY & CONTROL

7.1 Empennage

In initial designs, the HT-LIT and HT-LITTLE were to have separate empennages to ensure stability with the changing moment arm of a shortened fuselage. Upon, further investigation and careful placement of systems within available fuselage space it was determined the empennage could remain common between the two aircraft without compromising stability of either, thus reducing complexity and massively increasing manufacturing efficiencies for the family aircraft design.

7.1.1 Tail Configuration

A cruciform tail, shown in Fig. 7.1, was selected for the aircraft. This configuration was selected because of several reasons. The taller stabilizer position helps to keep it free of washout from the main wing during higher angle of attack maneuvers which could lead to deep stall in extreme cases. This also allows the tail to experience "fresher" free stream air, less inhibited by down wash from the main wing and able to provide greater control authority for its area, introducing the opportunity to comparably reduce area. It is relatively low complexity while maintaining a moderate weight and having a plethora of aircraft to draw from in aiding in the design process. Although a conventional tail configuration is very appealing, the lower efficiency due to increased interaction with the main wing circulation detracted from it enough to warrant a slightly heavier, more complex cruciform design.

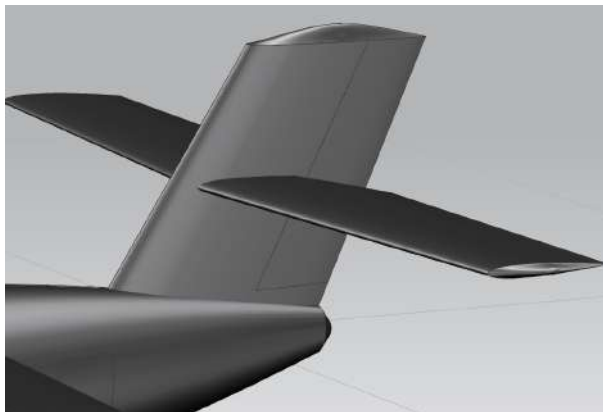


Figure 7.1: Overview of the tail configuration.

7.1.2 Airfoil

The airfoil selection process for the tail started with exploring airfoils that are commonly used for the tails of general aviation aircraft. The NACA 0009 airfoil was selected for the horizontal stabilizer because it was in the middle of the range of symmetric airfoils typically used for horizontal stabilizers. The NACA 0009 airfoil was also selected for the

vertical stabilizer because it was on the thicker end of the range of typical airfoils for vertical stabilizers, making it ideal for enclosing the structure required for a cruciform tail. A NACA 0009 airfoil contour is shown in Fig. 7.2.

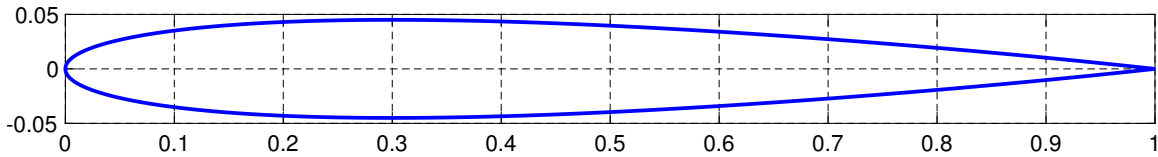
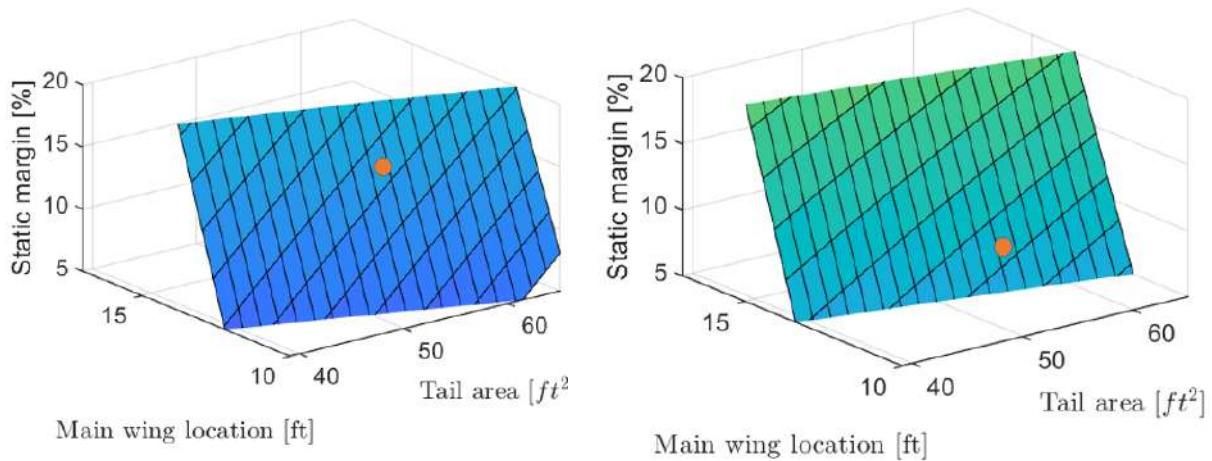


Figure 7.2: NACA 0009 airfoil used for the horizontal and vertical stabilizers.

7.1.3 Sizing

The horizontal and vertical stabilizers were sized using the method outlined in Sadraey [9]. Parameters for the horizontal stabilizer that were not numerically determined using Sadraey’s approach were selected based on typical values for comparable aircraft, such as the Jetstream 31, Cessna T303, and the Swearingen Merlin, also detailed in Sadraey. The parameters that were estimated include sweep angle, dihedral angle, aspect ratio, and taper ratio.

Center of gravity and neutral point are the main drivers in the calculation of static margin. Through manipulation of the aerodynamic center, or neutral point, nearly any CG configuration could be made stable. By varying horizontal tail area and wing position, the main drivers in determining neutral point, a set of combinations which yield adequate static margin can be found. Varying both tail area and wing location simultaneously and calculating static margin for every set, Fig. 7.3a and Fig. 7.3b were created, showing possible stable configurations for every wing position and tail area.



(a) Static margin over a range of tail areas and wing locations HT-LIT.

(b) Static margin over a range of tail areas and wing locations HT-LITTLE.

Figure 7.3: Stability envelopes of HT-LIT and HT-LITTLE.

The design points indicated in Fig. 7.3a and Fig. 7.3b represent a wing position and tail area for both aircraft, which yields a static margin of 13.49% and 10.1% for the LIT and LITTLE, respectively. This is well within the stable

boundaries, indicating there may be more flexibility if changes arise. The geometric parameters of the horizontal stabilizer are presented in Table 7.1.

Table 7.1: Horizontal stabilizer geometric parameters

Parameter	Symbol	Value
Planform Area	S_h	54.2 ft ²
Exposed Wetted Area	S_{wet_h}	104 ft ²
Leading Edge Sweep	Λ_h	4°
Span	b_h	15.8 ft
Actual Semi Span	s_h	7.9 ft
Root Chord	c_{r_h}	3.8 ft
Tip Chord	c_{t_h}	3.04 ft
Incidence	i_h	0°
Mean Aerodynamic Chord	MAC_h	3.43 ft
Volume Coefficient	\bar{V}_{HT}	0.0872 (LIT) 0.085 (LITTLE)
Dihedral Angle	Γ_h	1°
Aspect Ratio	AR	4.6
Taper Ratio	λ	0.8
Moment Arm	l_v	13.29 ft (LIT) 12.98 ft (LITTLE)

An incidence angle of 0 degrees was chosen as it allowed the aircraft to trim at a reasonable low elevator deflection for cruise and retained as much control authority as possible in the high deflection mission segments, specifically landing. A normal rudder that spans most of the vertical stabilizer was considered, but required the horizontal stabilizer to be notched to allow clearance for the rudder to deflect. Additionally, a double rudder system with one rudder above the horizontal stabilizer and another below the horizontal stabilizer was also considered. The double rudder system negated the need to make 45° notches in the horizontal stabilizer; however, the double rudder system was heavy and added unnecessary complexity to the tail structure. As a result, a tail configuration with a normal rudder and a notched horizontal stabilizer was chosen. The notched portions are visible in the engineering drawing of the horizontal stabilizer presented in Fig. 4.3.

Like the sizing of horizontal stabilizer, the volume coefficient, aspect ratio, and taper ratio of the vertical stabilizer were calculated and estimated based on information presented in Sadraey [9], but then were optimized through use of a trade study on the vertical tail's surface area. By varying surface area for a given aspect ratio and taper ratio, the stability derivative $C_{n,\beta}$ was calculated. A lower boundary was established using the minimum tail area to be able to counteract engine out asymmetrical thrust at takeoff and landing for the four seat variant due to its higher required yaw moment for trimming. An upper bound was established through comparison to heritage aircraft and by evaluation of tail aesthetics as a whole on the plane. A design point was established from these bounds and carried through in determining the remainder of the geometries. A representative plot is shown in Fig. 7.4 with the chosen design point. All of the geometric parameters

of the vertical stabilizer are presented in the Table 7.2. An engineering drawing of the vertical stabilizer is also presented in Fig. 4.3.

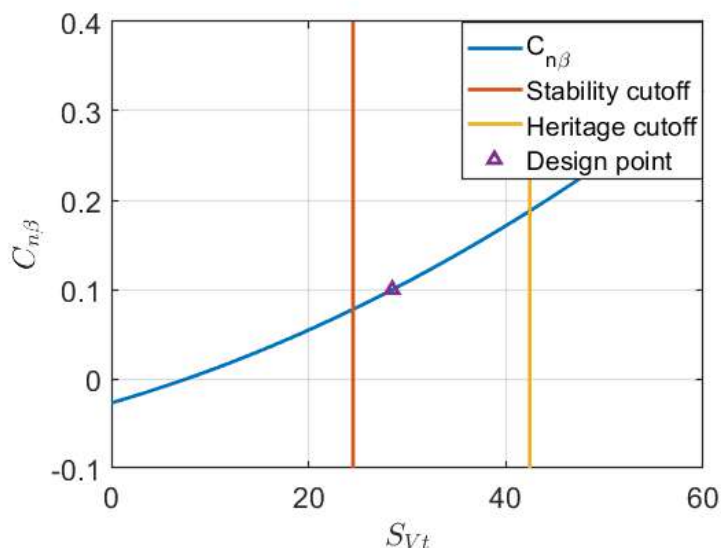


Figure 7.4: Trade study of vertical tail size.

Table 7.2: Vertical stabilizer geometric parameters

Parameter	Symbol	Value
Planform Area	S_v	28.6 ft ²
Exposed Wetted Area	S_{wet}	59 ft ²
Leading Edge Sweep	Λ_v	32°
Span	b_v	5.5 ft
Root Chord	c_{r_v}	5.8 ft
Tip Chord	c_{t_v}	4.6 ft
Incidence	i_v	0°
Mean Aerodynamic Chord	MAC_v	5.22 ft
Volume Coefficient	\bar{V}_{VT}	0.046 (LIT) 0.045 (LITTLE)
Dihedral Angle	Γ_v	0°
Aspect Ratio	AR	4.6
Taper Ratio	λ	0.8
Moment Arm	l_v	12.79 ft (LIT) 12.48 ft (LITTLE)

7.2 Control Surface Sizing

The control surfaces were sized using the method outlined by Sadraey [9]. Specifically, the geometric parameters were determined based on the method presented then modified to meet control authority and stability requirements for lateral and directional stability found in AVL. The deflection ranges of the control surfaces and general geometries are

presented in Table 7.3. In addition, diagrams of the aileron, elevator, and rudder are once again presented in Fig. 4.3. Details on flap and aileron design can be found in section 6.3. Relative locations of the tails can be found in section 4.2.4.

Table 7.3: Deflection ranges of the control surfaces

Control Surface	Deflection Range	Chord Ratio	Span Ratio	Tip Chord (ft)	Root Chord (ft)	Length (ft)
Aileron	$-20^\circ - 30^\circ$	0.3	0.4	1.1	1.4	7.6
Elevator	$-30^\circ - 30^\circ$	0.35	0.97	1.1	1.3	7.6
Rudder	$-30^\circ - 30^\circ$	0.35	0.9	1.6	2.1	5

7.3 Stability Derivatives

Using the finalized geometries of the wing and empennage and flight parameters of varying mission segments the various stability derivatives, which were used in stability analysis, were calculated by simulation in AVL. The resulting stability derivatives are shown in Table 7.4 and Table 7.5. They were used for all stability analysis.

Table 7.4: Stability derivatives

Generation	Mission Segment	$C_{l,\beta}$	$C_{n,\beta}$	$C_{L,a}$	$C_{m,a}$	$C_{m,\delta,e}$
LIT	Takeoff	-0.1362	0.0936	5.15	-1.367	-0.03439
	Cruise	-0.0635	0.0878	5.87	-0.86	-0.03736
	Landing	-0.1913	0.106	4.62	-1.193	-0.0312
LITTLE	Takeoff	-0.1372	0.09161	5.82	0.093468	-0.0353
	Cruise	-0.078	0.0842	5.844	0.1829	-0.035606
	Landing	-0.1861	0.1118	4.573	-1.599	-0.0339

Table 7.5: Stability derivatives (continued)

Generation	Mission Segment	ϵ_a	$C_{l,r}$	$C_{n,r}$	$C_{l,\delta,r}$	$C_{n,\delta,r}$
LIT	Takeoff	0.2	0.2819	-0.0891	-0.000267	0.001195
	Cruise	0.2	0.04513	-0.07961	-0.000326	0.001334
	Landing	0.2	0.4073	-0.1043	-0.000335	0.001157
LITTLE	Takeoff	0.2	0.0956	-0.0769	-0.000416	0.001329
	Cruise	0.2	0.0478	-0.0747	-0.000401	0.00129
	Landing	0.2	0.422	-0.1127	-0.000249	0.00177

7.4 Trim Configurations

Using the stability derivatives and known angle of attack values for every mission leg of both aircraft shown in Table 5.6, the trim configuration of the elevator was found using an interpolation of data collected from AVL. The specific deflections for each plane and mission leg are shown with an indicative trim line. The elevator deflections for each mission segment are shown in Table 7.5a and Table 7.5b for the HT-LIT and HT-LITTLE, respectively.

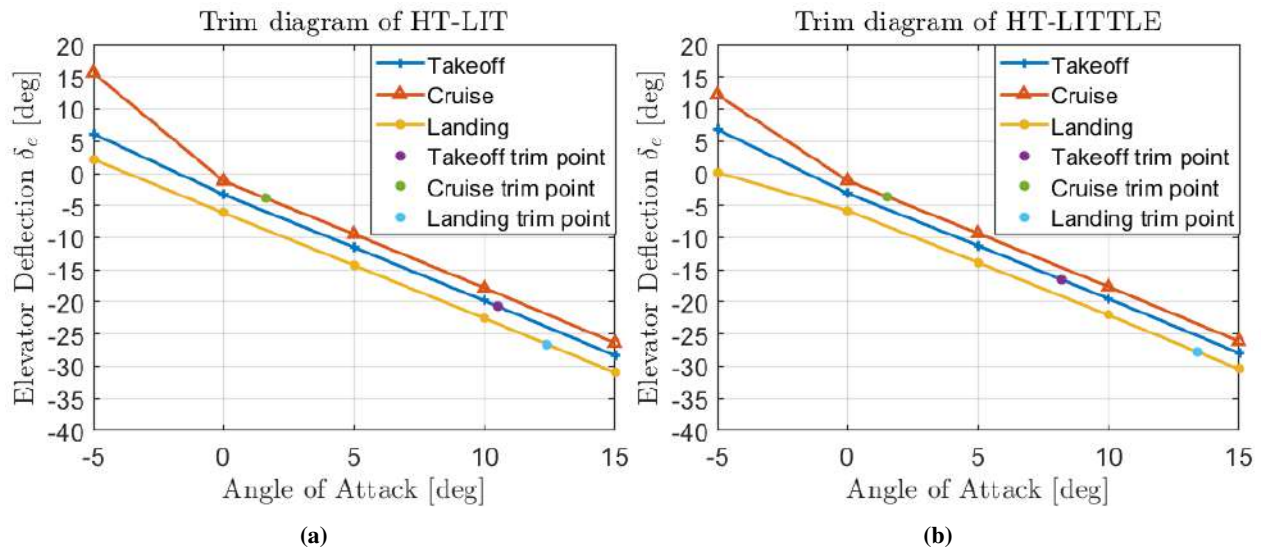


Figure 7.5: Trim diagrams of HT-LIT and HT-LITTLE.

The elevator deflection angles are tabulated for each section of their respective aircraft in Table 7.6. Corresponding angles of attack can be found in Table 5.6.

Table 7.6: Tabulated trim deflections

Generation	Mission Segment	C_L	δ_f [deg]	δ_e [deg]
LIT	Takeoff	1.4	15	-20.6
	Cruise	0.2766	0	-3.8
	Landing	2.3	35	-26.6
LITTLE	Takeoff	1.31	12	-16.6
	Cruise	0.2748	0	-3.7
	Landing	2.3	35	-27.8

7.5 Longitudinal Stability

The longitudinal static stability of the concept aircraft was evaluated using the method outlined in Yechout [6]. All stability derivatives were calculated in AVL except ϵ_α which had to be estimated based on empiric historical data found in Raymer [4]. The resulting stability derivatives are presented in Table 7.7.

These values held true for both aircraft because of the identical tail moment arm and wing geometries. With all stability derivatives found using the calculated neutral point and center of gravity, the static margin range for both aircraft were determined for best case and worst case stability weight balances. The HT-LIT ranged from 10.21-19.12% in its most extreme cases, C.G. of 16.7 ft and 17.3 ft, with a TOGW static margin 13.49%. The HT-LITTLE ranged from 8.39-10.9% under the same extremes, C.G. of 12.12 ft and 12.26 ft, with a TOGW static margin of 10.11%. The neutral

Table 7.7: Longitudinal static stability parameters

Parameter	Value
$C_{L,\alpha}$	0.083717
$C_{M,\alpha}$	-0.01875
τ_e	0.4%
C_{M,δ_e}	-0.0181
C_{M,i_e}	-0.0453
ϵ_α	0.2
i_{wing}	0°
i_{tail}	0°

Table 7.8: Requirements for various levels of dynamic longitudinal stability [1]

Phugoid Mode		
Level 1	$\zeta > 0.04$	
Level 2	$\zeta > 0$	
Level 3	$T_2 > 55$ s	
Short-Period Mode		
Level	ζ_{sp} min	ζ_{sp} max
1	0.35	1.3
2	0.25	2
3	0.15	-

points of the HT-LIT and HT-LITTLE are 18.53 ft and 12.48 ft aft of the nose, respectively. These values were found using the methods described in Yechout [6] and subsequently confirmed by the estimations from AVL.

The dynamic longitudinal stability was evaluated per the Cooper-Harper scale. The goal of an aircraft is to achieve Level 1 flying qualities, which are defined as "excellent" and "highly desirable" by the Cooper-Harper scale. The level below Level 1 is Level 2, at which a pilot will be able to fly the aircraft well, but with a noticeable increase in pilot workload or a notable decrease in mission effectiveness. The final safe level an aircraft can get is Level 3, at which point the pilot is doing excessive amount of work to keep the aircraft flying. The flight qualities which defines each of these three levels are shown in Table 7.8. The value of $\omega_{n,sp}$ is also important and can be related to ζ_{sp} per Fig. 7.6.

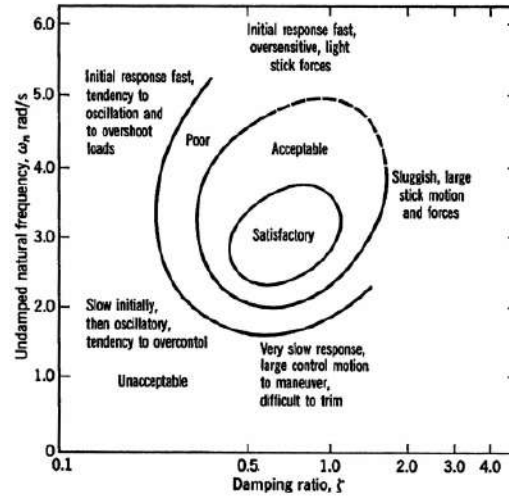


Figure 7.6: Desirable flying qualities for dynamic longitudinal stability [1].

The natural dynamic longitudinal stability of the HT-LIT and HT-LITTLE aircraft was evaluated per the approach outlined in Nelson's *Flight Stability and Automatic Control* [1]. To determine the natural frequencies and damping coefficients for the short-period and phugoid modes, it is necessary to define a state-space system that describes the dynamics of the aircraft. A and B matrices were determined as follows:

$$\dot{x} = Ax + B\eta$$

$$\begin{bmatrix} \dot{u} \\ \dot{w} \\ \dot{q} \\ \dot{\theta} \end{bmatrix} = \begin{bmatrix} X_u & X_w & 0 & -g \\ Z_u & Z_w & u_0 & 0 \\ M_u + M_{\dot{w}}Z_u & M_w + M_{\dot{w}}Z_w & M_q + M_{\dot{w}}u_0 & 0 \\ 0 & 0 & 1 & 0 \end{bmatrix} \begin{bmatrix} u \\ w \\ q \\ \theta \end{bmatrix} + \begin{bmatrix} X_{\delta_e} \\ Z_{\delta_e} \\ M_{\delta} + M_{\dot{w}}Z_{\delta} \\ 0 \end{bmatrix} \begin{bmatrix} \delta_e \end{bmatrix}$$

Plugging in the stability coefficients from AVL for cruise, these A and B matrices become:

$$A_{HT-LIT,long} = \begin{bmatrix} -0.0017 & 0.0034 & -0.0109 & -32.18 \\ -0.0126 & -0.3250 & 453.7 & 0 \\ 0 & -0.0039 & -0.2006 & 0 \\ 0 & 0 & 1 & 0 \end{bmatrix} \quad B_{HT-LIT,long} = \begin{bmatrix} -0.0012 \\ -0.3584 \\ -0.0764 \\ 0 \end{bmatrix}$$

$$A_{HT-LITTLE, long} = \begin{bmatrix} -0.0018 & 0.0039 & -0.131 & -32.18 \\ -0.0145 & -0.3460 & 437.0 & 0 \\ 0 & 0.0008 & -0.1819 & 0 \\ 0 & 0 & 1 & 0 \end{bmatrix} \quad B_{HT-LITTLE, long} = \begin{bmatrix} -0.0020 \\ -0.3664 \\ -0.0672 \\ 0 \end{bmatrix}$$

The natural flying qualities of the HT-LIT and HT-LITTLE are shown in Table 7.9. For the HT-LIT, neither the short-period of phugoid Level 1 requirements are met. The eigenvalues for the HT-LITTLE are not listed because one of the four has a positive real part, signifying system instability. Therefore, a stability augmentation system must be implemented for both the dynamic longitudinal stability of the HT-LIT and HT-LITTLE aircraft.

Table 7.9: Natural flying qualities of HT-LIT and HT-LITTLE aircraft

	λ_{sp}	λ_{phug}	ζ_{sp}	$\omega_{n,sp}$	ζ_{phug}	ω_{phug}
HT-LIT	-0.2629 ± 1.3285	-0.0007 ± 0.0294	0.194	1.35	0.0248	0.0294
HT-LITTLE	-	-	1	0.861	0.0570	0.0359

A simple feedback system was set up using MATLAB and Simulink to adjust the flying qualities of the HT-LIT and HT-LITTLE aircraft; the Simulink model can be seen in Figure 7.7. Gains were only implemented for w and q since all other entries in the B-matrix were zero or near-zero. Using MATLAB's linear-quadratic regulator functionality to optimally tune gains per the Ricatti equation, gains were found to maximize aircraft controllability and pilot comfort. The chosen gains are shown in Table 7.10, along with the adapted flying qualities of each aircraft. The short period flying qualities are also plotted on the short-period flying qualities graph, originally introduced by Fig. 7.6, in Fig. 7.8.

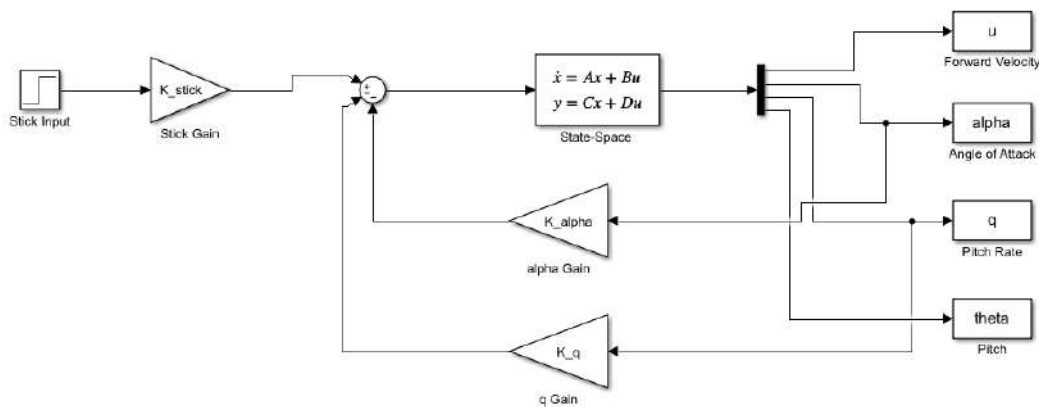


Figure 7.7: Simulink block diagram of longitudinal controller.

Table 7.10: Final gains for longitudinal control design

	K_w	K_θ	ζ_{sp}	$\omega_{n,sp}$	ζ_{phug}	ω_{phug}
HT-LIT	0.0510	-41.4	1	3.36	0.699	0.0013
HT-LITTLE	-0.0159	-42.6	1	3.00	0.0801	0.0103

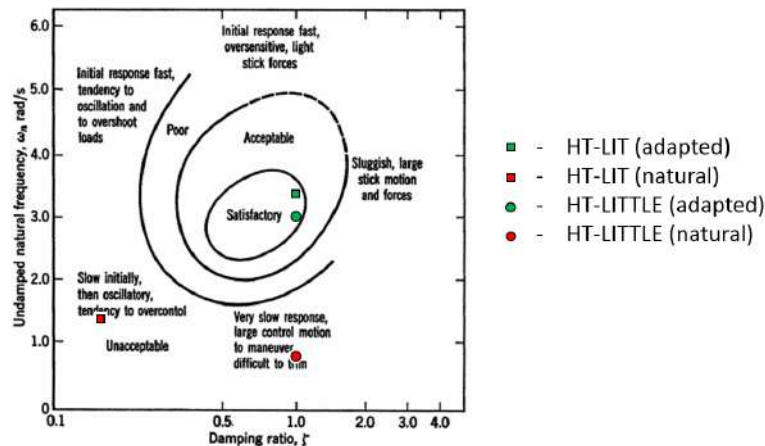


Figure 7.8: HT-LIT and HT-LITTLE short-period flying qualities shown before and after feedback control.

After the longitudinal control system is implemented, both aircraft satisfy the Level 1 flying criteria for short-period and phugoid modes.

7.6 Lateral Stability

The static lateral stability was evaluated for both aircraft by finding the sign of the roll moment coefficient with respect to yaw angle, $C_{l,\beta}$. A negative value for this stability derivative is indicative of a static laterally stable aircraft. The stability derivatives were found using AVL and tabulated in Table 7.4. All of the derivatives are negative, indicating that both aircraft have static lateral stability in all mission segments.

The dynamic lateral stability of the HT-LIT and HT-LITTLE aircraft was evaluated on the basis of the ability of both aircraft to meet Cooper-Harper Level 1 handling quality rating. A detailed analysis of the dynamic lateral stability follows, the results of which determined that the design and implementation of a state-feedback controller based SAS allowed the HT-LIT and HT-LITTLE aircraft to meet the Cooper-Harper Level 1 requirements.

For the evaluation of the aircraft handling qualities, A and B matrices representing the state-space system of dynamic lateral equations of motion were determined and subjected to eigenvalue analysis to evaluate natural frequency, damping ratio, time to half amplitude, and time constants for the dutch roll mode, roll mode, and spiral mode. The state space system of the lateral dynamic equations of motion was represented by the following equations, where the state vector x contained the variables y-velocity, yaw rate, bank angle, and roll rate respectively and the control vector η contained the aileron and rudder deflections as inputs.

$$\dot{x} = Ax + B\eta$$

$$\begin{bmatrix} \dot{v} \\ \dot{p} \\ \dot{\phi} \\ \dot{r} \end{bmatrix} = \begin{bmatrix} Y_v & Y_p & g_0 \cos \theta_0 & Y_r - u_0 \\ L_v & L_p & 0 & L_r \\ 0 & 1 & 0 & 0 \\ N_v & N_p & 0 & N_r \end{bmatrix} \begin{bmatrix} v \\ p \\ \phi \\ r \end{bmatrix} + \begin{bmatrix} Y_{\delta_r} & 0 \\ L_{\delta_r} & \delta_a \\ 0 & 0 \\ N_{\delta_r} & \delta_a \end{bmatrix} \begin{bmatrix} \delta_r \\ \delta_a \end{bmatrix}$$

The A and B matrices were evaluated using stability derivatives obtained with AVL analysis in conjunction with aircraft geometric and performance parameters. The evaluated A and B matrices for the HT-LIT and HT-LITTLE aircraft are shown below.

$$A_{HT-LIT,lat} = \begin{bmatrix} -0.0752 & -0.410 & 32.18 & -455 \\ -0.0113 & -1.90 & 0 & 0.160 \\ 0 & 1 & 0 & 0 \\ 0.00043 & -0.00065 & 0 & -0.0078 \end{bmatrix} \quad B_{HT-LIT,lat} = \begin{bmatrix} -0.420 & 0 \\ -0.0263 & 0.450 \\ 0 & 0 \\ 0.00298 & 0.000314 \end{bmatrix}$$

$$A_{HT-LITTLE,lat} = \begin{bmatrix} -0.0752 & -0.469 & 32.2 & -455 \\ -0.0123 & -1.91 & 0 & 0.169 \\ 0 & 1 & 0 & 0 \\ 0.00041 & -0.00048 & 0 & -0.0073 \end{bmatrix} \quad B_{HT-LITTLE,lat} = \begin{bmatrix} -0.420 & 0 \\ -0.0324 & 0.449 \\ 0 & 0 \\ 0.00288 & 0.000361 \end{bmatrix}$$

Using MATLAB, eigenvalue analysis produced eigenvalues shown in Table 7.11. The eigenvalues generated for the dutch roll mode, using superficial examination alone, were seen to be inadequate as they featured positive values for the real portion of the eigenvalues.

Table 7.11: Eigenvalues for Dutch roll, roll, and spiral roll modes

Lateral Mode	HT-LIT eigenvalues	HT-LITTLE eigenvalues
Dutch Roll	$0.0057 \pm 0.6084i$	$0.0097 \pm 0.6147i$
Roll	-1.99	-2.009
Spiral	-0.0008	-0.0008

In order to improve the dynamic lateral stability of the HT-LIT and HT-LITTLE aircraft, an optimal controller was developed to be used as a stability augmentation system. Using the **lqr** MATLAB function to solve the algebraic Riccati equation, an optimal gain matrix K was found and implemented into the linear control law $\eta = -Kx$. This

control law was used to find the modified state matrix $A_m = A - BK$. Eigenvalue analysis of the modified A matrices was used to find the modal eigenvalues as shown in Table 7.12.

Table 7.12: Lateral mode eigenvalues for state-feedback control

Lateral Mode	HT-LIT eigenvalues	HT-LITTLE eigenvalues
Dutch Roll	$-1.31 \pm 1.917i$	$-1.30 \pm 1.911i$
Roll	-2.748	-2.754
Spiral	-0.0428	-0.0417

The modal eigenvalues were then used to determine the natural frequencies, damping ratios, time to half amplitude, and time constants of each mode and compared to the level 1 handling quality requirements. The results are shown in Table 17.3 and Table 17.4 and indicate that the HT-LIT and HT-LITTLE aircraft meet the dynamic lateral motion level 1 handling requirements with the introduction of the state-feedback controller. The Simulink model of the controller is shown in Fig. 17.1.

Table 7.13: HT-LIT lateral mode performance vs. requirements

Lateral Mode	Performance	Level 1 Requirement
Roll	$\tau_{roll} = 0.364$	$\tau_{roll} < 1$
Spiral	$t_{\frac{1}{2}} = 16.2$ s	$t_{\frac{1}{2}} > 12$ s
Dutch Roll	$\omega_n = 2.319$	$\omega_n > 1$
	$\zeta = 0.563$	$\zeta > 0.19$
	$\zeta\omega_n = 1.305$	$\zeta\omega_n > 0.35$

Table 7.14: HT-LITTLE lateral mode performance vs. requirements

Lateral Mode	Performance	Level 1 Requirement
Roll	$\tau_{roll} = 0.363$	$\tau_{roll} < 1$
Spiral	$t_{\frac{1}{2}} = 16.6$ s	$t_{\frac{1}{2}} > 12$ s
Dutch Roll	$\omega_n = 2.312$	$\omega_n > 1$
	$\zeta = 0.563$	$\zeta > 0.19$
	$\zeta\omega_n = 1.30$	$\zeta\omega_n > 0.35$

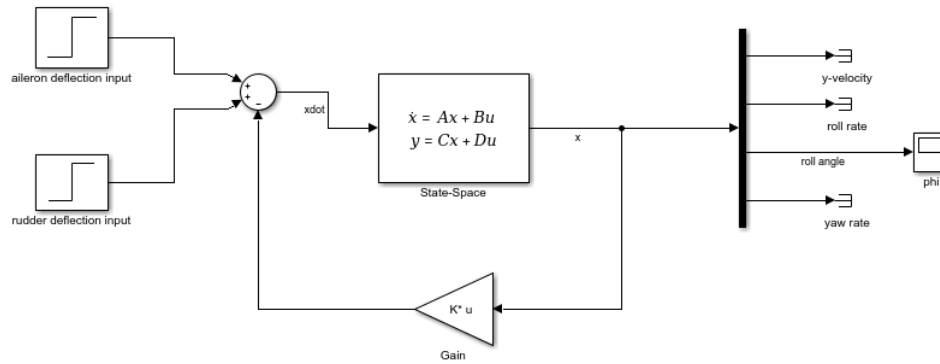


Figure 7.9: Simulink block diagram of lateral/directional controller.

7.7 Directional Stability

The static directional stability was evaluated for both aircraft by finding the sign of the yaw moment coefficient with respect to yaw angle, $C_{n,\beta}$. A positive value for this stability derivative is indicative of a static directionally stable aircraft. The stability derivatives were found using AVL and tabulated in Table 7.15. All of the derivatives are positive, indicating that both aircraft have static directional stability in all mission segments.

Table 7.15: Directional static stability derivatives

Generation	Mission Segment	$C_{n,\beta}$
LIT	Takeoff	0.0936
	Cruise	0.0878
	Landing	0.106
LITTLE	Takeoff	0.09161
	Cruise	0.0842
	Landing	0.1118

Additionally, an engine out asymmetric thrust scenario was evaluated for both aircraft at takeoff and landing. The necessary rudder deflections to negate the asymmetric thrust yaw moment in listed in Table 7.16.

Table 7.16: Engine-out rudder deflection

Generation	Mission Segment	δ_r
LIT	Takeoff	24°
	Landing	25°
LITTLE	Takeoff	25°
	Landing	27°

With the capabilities of our rudder, the asymmetric thrust moment can be counteracted in all cases, but control authority is limited so any maneuvers must take the limitation into account.

8 STRUCTURES & LOADS



Figure 8.1: Structural layout of HT-LIT aircraft.

8.1 Materials Selection

The aircraft market over the past 30 years has been dominated by sheet metal aluminum aircraft. Aluminum is a very light metal, and yet it can maintain very high loads in compression and tension for its density. Aluminum also has been developed into many different alloys; common aluminum alloys are infused with zinc, copper, and magnesium. These alloys can have properties which are significantly better than pure aluminum, proving aluminum to be a very versatile metal.

The approach that was taken to these aircraft, however, was to almost exclusively use composite materials. Carbon fiber/epoxy matrix composites have had a huge spike in popularity over the past ten years. The Boeing 787 was a pioneer in the field of composites, and its make of over 50% composite materials showed people that composites could be used for many more aerospace applications than previously thought. Carbon fiber/epoxy matrix composites, as opposed to other composite types, have become popular because of their well-documented test history in aviation from the drone to the commercial scale and their exceptionally low density and relatively high tensile strength.

Carbon fiber composites are made up of strands of carbon fiber embedded in a matrix of epoxy resin. In aerospace

uses, composites with continuous strands are favored for their superior load-carrying capability in predetermined directions. When making a layer of composites, many fibers are oriented unidirectionally and put into one layer of epoxy, forming a component called a laminate. Laminates are layered, each having its own unique fiber direction, to make sandwiched composites. The sequence in which the composites are stacked is generally called a lay-up, and one or more lay-ups will form a sandwich. Composites are so low in density yet high in tensile strength because they optimize their material allocation for a given loading scenario. As an example, if a material will be only loaded axially, a unidirectional carbon fiber composite will serve much better than an isotropic sheet of aluminum.

The fuselages of these aircraft are inspired by the fuselage of the Boeing 787 in a few ways. One huge benefit of composites is that, depending on the fiber orientation of the skins, the skin can hold very large loads, much larger than conventional aluminum skins. There is also the potential for large portions of a carbon fiber fuselage skin to be made as a single piece, as opposed to sheet metal aircraft which are made of countless skin panels, all bound together with thousands of rivets. The frames and stringers in the fuselages of these aircraft are also made of carbon fiber composites. Once a skin is chosen to be carbon fiber, it is unwise to choose stringers or frames which are made of a metal such as aluminum because of the thermal expansion of the metal. When an aircraft flies at altitude, it is much colder than the ground temperature, and aluminum contracts in cold temperatures. Continuous use of an aircraft with a composite skin and aluminum frames would result in early-onset fatigue. Additionally, unidirectional composites are perfect for use in stringers due to their penchant for loading in their fiber direction, which can be oriented along the stringer.

Nearly all the lifting surfaces and skeletal structures of those surfaces are made up of carbon fiber composite laminates or carbon fiber composite sandwiches. This is inspired by the work done by other modern aircraft companies. Diamond Aircraft recently came out with the DA-62, an aircraft with a completely composite structure, excluding the landing gear. It is in the general aviation market, and it is only slightly smaller than our aircraft. The Boeing 777X will be out soon, and the wings of the 777X are almost completely composite, only excluding the wing ribs which are metal to aid with lightning strikes. While it is not officially in service yet, the 777X has been proven to work and be flyable on a world scale. The 777X is an extreme case of wing loading, and with a much smaller aircraft like the DA-62, both the skins and internal structures of all lifting surfaces can likely be made using composites. Even if this is not true in 2017 for an aircraft like the HT-LIT or the HT-LITTLE, these aircraft are set to enter service in 2030. There are copious amounts of research being done by both aerospace companies and research institutes on the improvement of composite materials, and by 2030, it should be expected that an all-composite wing and empennage structure can be made usable for a general aviation aircraft of this size, use, and scale of production.

To better highlight the strengths of composite materials in structural applications, densities and Young's Moduli for multiple composite materials and one metal are laid out in Table 8.1. All composite material properties were obtained from the Department of Defense Materials Handbook [16]. Celion 12k/E7K8 unidirectional tape is used in the skins of the fuselage of both HT-series aircraft. On the other hand, Celion 12k/938 unidirectional tape is used in the wing skins

Table 8.1: Properties of various composite materials compared with aluminum 6061-T6

	ρ [$\frac{g}{cm^3}$]	E_1 [Msi]	E_2 (if applicable) [Msi]
Celion 12k/E7K8	1.59	20	1.28
T-300 3k/934	1.55	9.1	9
Celion 12k/938	1.54	19.7	1.35
Aluminum 6061-T6	2.7	10	-

for the HT-series aircraft due to its thinner lamina. T-300 3k/934 plain-weave fabric is used in the spars and other main structural members of the HT-series lifting surfaces and fuselages. The plain weave fabric offers a quasi-isotropic set of properties while also offering the low density of a carbon-fiber composite. Finally, aluminum 6061-T6 is one of the most prevalent aluminum alloys in the general aviation market for general structural applications.

While aluminum 6061-T6 does have isotropic properties, which have been proven to work well for modern aircraft, the fact that unidirectional composites can exhibit Young's moduli of twice that of aluminum 6061-T6 and yet can be only a fraction of the weight is very hard to beat. Still, composites have other drawbacks like a notably bad fracture toughness. For this reason, the HT-series aircraft were designed with a small exception to their "all-composite" lifting surfaces. The leading edge of each lifting surface is lined with a metallic material. In this case, Aluminum 2024-T3 was chosen for its strong tensile strength and its relatively low cost, in comparison to nickel or titanium. This is to make sure that the integrity of the wing remains if a bird strike or other unexpected collision event occurs. The nose of the fuselage is also made of Aluminum 2024-T3 for the same reason as mentioned above.

The landing gear of the aircraft is made up of 300M alloy steel. This material was chosen for its great fatigue strength, durability, and impact strength. The main landing gear of each of these aircraft is not damped using oleos or other damping mechanisms, so the material that the landing gear is made of will need to solely be capable of withstanding extreme bottoming loads upwards of 10,000 pounds. The primary alternative option for this was to make the landing gear out of titanium, but this was not feasible because of titanium's exceptionally high cost. The main drawback to using 300M alloy steel is its tendency to place high amounts of stress on the steel structure when landing on soft runways. This drawback, however, is far outweighed by the positive characteristics of the alloy and the low cost. While the HT-LIT and HT-LITTLE are capable of soft runway landings, it is predicted that the average HT-LIT/HT-LITTLE customer will not often be landing on runways like these due to the aircraft's luxury appeal and superior range capabilities.

A huge drawback to using composite materials in a general aviation setting is the cost. While comparisons were drawn earlier to large-scale Boeing jets, Boeing aircraft are built on a completely different scale than a standard general aviation aircraft. Costs will be much higher for the manufacturer due to lower amounts of aircraft being manufactured over the life of the program, and this will result in much higher sales prices. Yet, this upcoming trade study outlines how, despite having a high price tag, composite general aviation aircraft can save a customer money in the long run.

8.1.1 Trade Study: Fuel Cost Savings of Composite Materials

The choice of using composite structural materials in the design of the HT-LIT and HT-LITTLE aircraft correlated to a 20% increase in the estimated manufacturing and materials costs. To justify the use of composite manufacturing materials, a trade study was completed to explore the effect of the reduced weight of composites on the fuel cost savings over the life cycle of the aircraft. The empty weight of HT-LIT was determined for use of aluminum manufacturing materials for comparison. The empty weight when using aluminum was found to be 682.6 pounds heavier than that of the composite aircraft. A performance analysis was carried out to find that, given the heavier empty weight, the cruise speed of the HT-LIT would have to be reduced to 264 knots (as opposed to 270 knots using composites) to maintain design specifications such as range and fuel capacity. Due to the constant fuel consumption rates of the turboprop engines at cruise, the increase in cruise endurance at the lower speed was found to determine the increase in fuel consumption when using aluminum materials. The values of cruise endurance and fuel consumption during cruise for each material are shown in Table 8.2.

Table 8.2: Cruise performance for composite vs aluminum manufacturing materials

	Composite Aircraft	Aluminum Aircraft
Empty Weight	4706 lb	5210 lb
Cruise Speed	270 kts	264 kts
Cruise Endurance	2.78 hr	2.84 hr
Fuel Consumed	672 lb	688 lb
Fuel Cost	\$517	\$529

The composite aircraft consumed 16 pounds less fuel than the aluminum aircraft, correlating to \$11.75 saving in fuel cost per design mission cruise segment. The cruise fuel savings were divided by the cruise endurance to find the fuel cost savings per flight hour of the composite aircraft of \$4.23 per hour. This value was then multiplied by a range of yearly flight hours to reflect the annual savings in fuel cost of \$2,117, \$4,233, and \$8,467 for 500, 1000, and 2000 flight hours per year respectively. The manufacturing and materials costs for aluminum versus composites were calculated and tabulated to examine the significance of the fuel cost savings found for composites. This was done for a maximum production quantity of 600 aircraft over 5 years. As shown in Table 8.3, the manufacturing and materials cost increase per aircraft when using composites is only roughly \$32,000 at maximum production rate. For an owner of the HT-LIT with an average yearly flight hour rate of 1000 FH/yr, the fuel cost savings of the composite materials would overcome the increased cost due to manufacturing and materials in only 7.5 years.

Table 8.3: Manufacturing cost differences for aluminum vs composite materials (in millions of dollars)

	Composite Aircraft	Aluminum Aircraft
Manufacturing and Materials Cost of Program	264	244
Manufacturing and Materials Cost per Aircraft	0.439	0.407

8.2 Internal Structural Element Layout

This section elaborates on the internal component layout of the major aircraft structural elements for the HT family of aircraft. Each part is designed to distribute loads efficiently over the body of the aircraft and to ensure structural stability throughout the operation of the aircraft. The HT-LIT structure is specifically examined in the figures for the following section; this is because the structures of the two aircraft are identical except for the center fuselage and nose landing gear areas. All rib, longeron, and frame spacings were determined using Roskam [17].

8.2.1 Wing Structure

The wing structure consists of a series of wing ribs connected by two main spars. Primary wing ribs have inter-rib spacings of anywhere from 19 inches to 27 inches. The front and rear spars are located at 25% and 65% of the wing chord, respectively. The rear spar is placed at 65% of the chord to give proper clearance for the flap and aileron (both 30% of the chord). The front spar is located at 25% of the chord to provide a minimal lever arm for lift forces, all of which act at approximately 25% of the wing chord. The internal wing structure can be seen in Fig. 8.2.

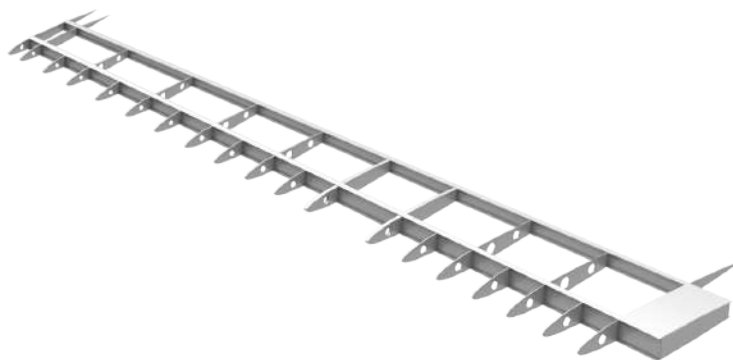


Figure 8.2: Internal structure of right HT-LIT aircraft wing.

The areas enclosed within the two spars from the most inboard rib to the fourth most inboard rib and from the fifth rib to the outermost rib are integral fuel tanks. The ribs passing through this area contain cutouts, making it possible

for fuel to freely flow between them. For this reason, the ribs in this section each have an extra nose rib in between them; the presence of fuel and fuel holes in this section weakens the structure of that area, so the nose ribs are there to help support the aerodynamic drag loads and transfer lifting loads throughout the skin in that area. Any bolts or other external parts that are in the fuel area of the wings are coated with a strong sealant to prevent corrosion. All nose ribs have small holes in them to help cut down on structural weight. The standard rib thickness through the wings is 0.25 inches. This holds for all the wing ribs excluding two of them which lie at eight and ten feet from the wing root. Each of these ribs is 0.2 inches thick and attach to the nacelle attachment plate, which spans the two feet in between the two ribs. These ribs will be supporting the weight of the powerplant, so they must be significantly thicker than the surrounding ribs to account for the extra loading. Both the front and rear wing spars are the height of the airfoil of the wing at the given point along the length of the wing. They are made up of 0.5-inch-thick webs with 3-inch spar caps, each of which is 0.2 inches thick. The general I-beam shape of each of these spars is to best counteract bending lift loads while simultaneously being weight efficient.

The aileron is attached to the rear spar at the ends of two of the wing ribs spanning that area. Where the sixth and ninth full wing ribs end, a pivot point is built in, upon which the aileron rotates. The flap has a similar configuration. The flap is rotated at two points, as it is connected at two pivot points. These two points are located at the ends of the second and fifth wing ribs. Both the flaps and the ailerons have rib structures that mimic the structure of the wing ribs. This is so that each connection point attaches to an attachment point which extends from a rib on the control surface, ensuring optimal structural stability and clear load paths. Between the ribs of the surfaces, a composite honeycomb structure is built in to increase the overall rigidity of the structure. All control surfaces are powered by the aircraft hydraulic system.

The inboard ends of each wing meet in the center of the aircraft over the fuselage in a wingbox structure. The wingbox is the intersection between the wing ribs, the wing spars, and the fuselage supporting structure. This area is the main load transfer area from the wing to the fuselage of the aircraft. It is an integral structural component of the HT-LIT and HT-LITTLE aircraft.

To verify the elastic properties and strength of the HT-LIT/HT-LITTLE wing design, a finite element model was created using NX NASTRAN. The internal structure of the model can be seen in Fig. 8.3. The internal structure was modeled using the elastic properties of T-300 3k/934 plain weave fabric, and the skin of the wing was modeled using a [0/90/45/-45]S laminate made of Celion 12k/938 unidirectional tape plies, each of thickness 0.006 inches. All skins and ribs were modeled with a 0.5-inch element CQUAD4 mesh, and all spars and spar caps were modeled with a 0.1-inch element CQUAD4 mesh. The FEM model begins at the first rib outward of the wingbox, and the model is simulated as being fixed along that rib due to the high stiffness of the wingbox area. Therefore, the simulated wing has a span of 18.75 feet instead of the full 20 feet. The analysis was performed at the maximum loading condition of the HT-LIT aircraft (cruise with 50 fps gusts), resulting in a load factor of 3.8. The aircraft was assumed to be fully loaded as a worst-case scenario. This maximum loading condition is illustrated by each aircraft's V-n diagram later in this section.

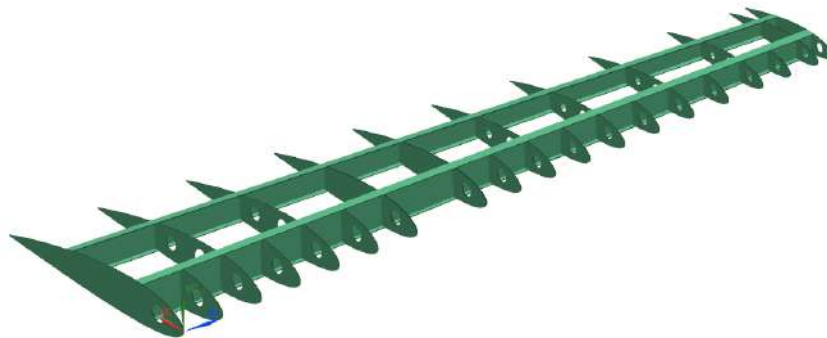


Figure 8.3: Internal structure of HT-LIT/HT-LITTLE wing FEM model.

The spanwise lift distribution of the wing for the loading conditions was calculated using AVL. The Trefftz plots showing these distributions for both the HT-LIT and HT-LITTLE aircraft are shown in Fig. 8.4. The lift distribution for the HT-LIT aircraft was used in this simulation. This distribution was normalized by the taper of the wing and propagated chordwise along the wing according to NACA2415 airfoil C_p data calculated using XFOIL. The pressure distribution due to lift along the skin of the FEM model is shown in Fig. 8.5.

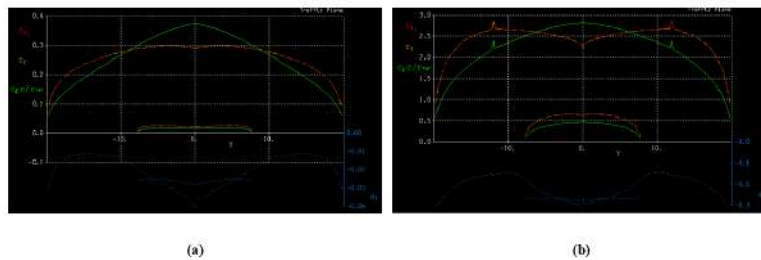


Figure 8.4: Trefftz plot for a) HT-LIT and b) HT-LITTLE at cruise.

Lift Pressure
Pressure - Elemental, Scalar
Min : -1.562, Max : 2.129, Units = lbf/in²(psi)

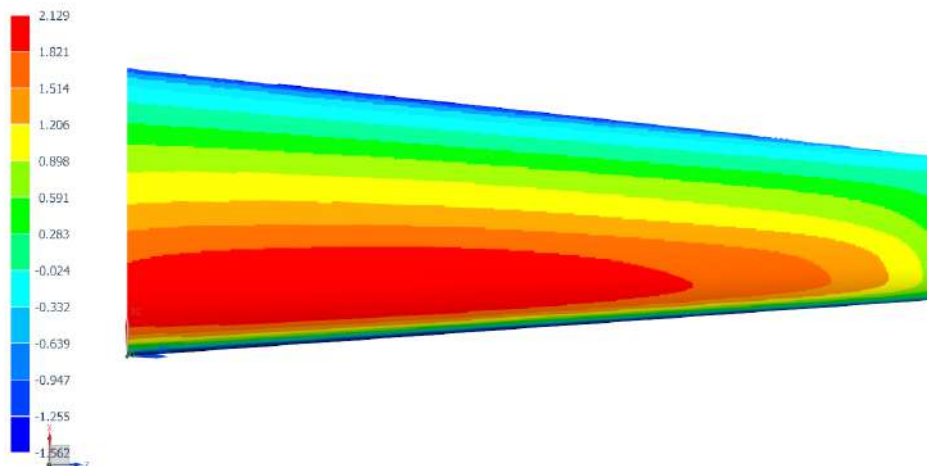


Figure 8.5: Lift pressure distribution along HT-LIT/HT-LITTLE wing FEM model.

Additional forces were added to the FEM simulation to simulate the pressure of the fuel inside the integral wing tanks. This pressure assumed that the wing tanks were full. A gravity load was added to the structure of the wing as well. Additionally, four point loads were added to the engine attachment ribs to simulate the powerplant weight. The displacement results of the FEM simulation are shown in Fig. 8.6. All deflections are amplified by a factor of 1.5 for better visibility.

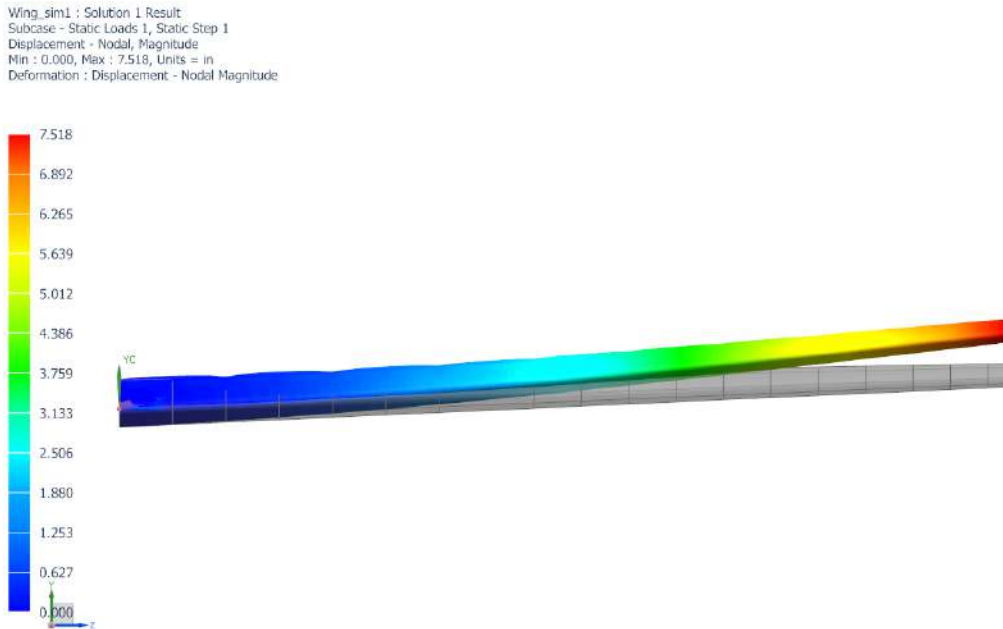


Figure 8.6: Deflection along HT-LIT/HT-LITTLE wing FEM model.

A lower-order approach was also utilized to ensure accuracy of the results of the finite-element simulation. This lower-order method is a modified version of the approach outlined in Nicolai's *Fundamentals of Aircraft and Airship Design* [18]. The primary difference between this approach and the one outlined in Nicolai is that the lift on each panel was found by integrating the known AVL data from Fig. 8.4 in MATLAB as opposed to using the assumption of an elliptic/trapezoidal lift distribution along the wing. The results of the Nicolai approach are shown in Fig. 8.7. The moment of inertia at each cross-section along the wing was found NX. Using this approach, a maximum deflection of 7.2 inches was calculated. This value is within 5% of the FEM maximum deflection shown in Fig. 8.6. This approach also validated the spar cap sizing of 3 inches in width for this wing model. Because of this, the spar cap was not changed from this initial estimated width value.

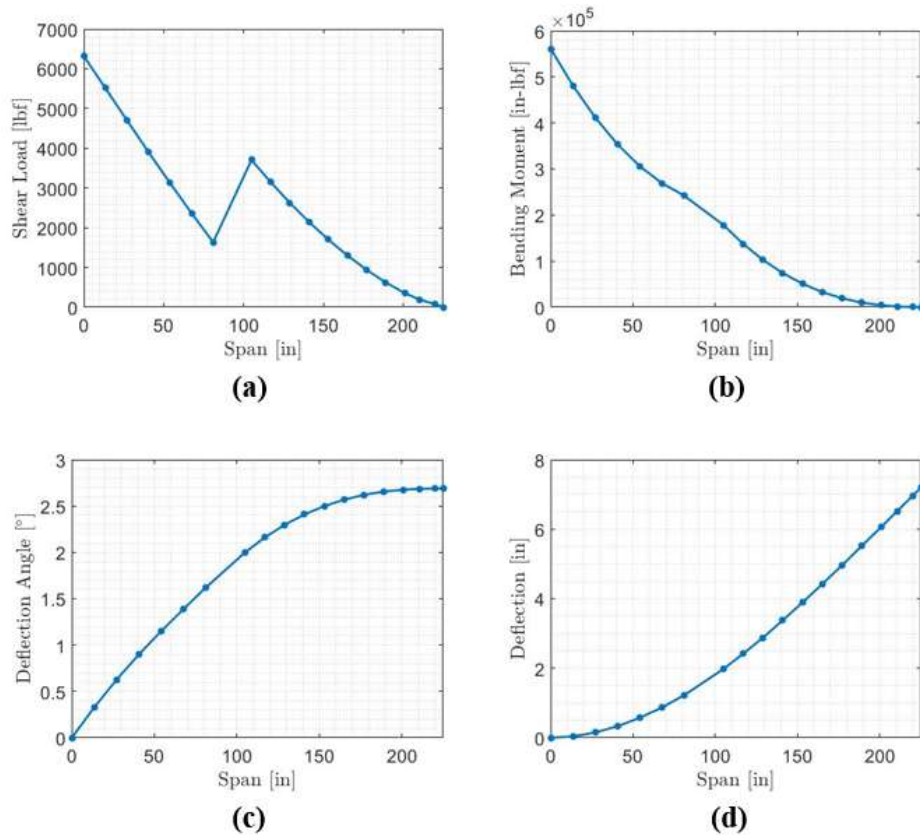


Figure 8.7: Lower-order method results for a) shear load, b) bending moment, c) deflection angle, and d) deflection along wing.

8.2.2 Fuselage Structure

The fuselage of this aircraft has a semi-monocoque structure. The skin of the fuselage is supported by seven longerons, a keel beam, frames, and bulkheads, all of which are designed to carry major structural loads. Both the farthest forward and farthest back cross-sectional supports are bulkheads. These are situated in their respective places to support the longerons and the loads that they carry. By being situated on each end, longeron loads will always be supported by both bulkheads, with the exception of the longeron passing through the door which will be supported by a bulkhead on one end and a frame or partial bulkhead on the other. The exact locations of the bulkheads are 15, 68, 220, and 378 inches aft of the nose. All frames in the fuselage are located roughly 2-3 feet apart.

On either end of the pressure vessel is a pressure bulkhead - the second and third bulkheads in the fuselage. In many passenger aircraft, the pressure bulkheads are bowed out into hemispheric shapes to better deal with the pressure loading. However, the pressure difference that the walls of the cabin are experiencing at 17,000 feet do not compare to those felt at 40,000 feet, and hence it is reasonable to assume that with a properly thickened and reinforced bulkhead at each side of the pressure vessel, the bulkheads do not need to bulge out. Each of these bulkheads in the HT-LIT and HT-LITTLE aircraft are 0.8 inch thick and composite stiffeners are applied across the stiffener on the aft pressure bulkhead to

increase stiffness.

The seven longerons that run along the length of the aircraft are the primary stiffening members in the fuselage, excluding the keel beam. These longerons are located at 45° increments around of the circumference of the fuselage, anchored about the keel beam which fills in the eighth spot in the circle and runs along the bottom of the plane. These longerons are all made up of unidirectional composite layups so that they can best resist longitudinal loading and stiffen the fuselage. Each longeron is designed similar to a standard composite hat stringer, as seen in the design of the 787 aircraft. The void encapsulated by the HT-LIT/HT-LITTLE longerons is reinforced with a composite filler material. The shape of the longeron increases its moment of inertia and, therefore, stiffness in comparison to a longeron with its only flange attached to the fuselage. These types of structural members are currently used by companies like Boeing and Airbus in their large-scale composite aircraft, so the method has been proven to be valid. Each of these has a thickness throughout of 0.1 inches.

At the top of the fuselage, the wingbox resides between the wings. As mentioned before, this is the main load transfer mechanism between the wings and the fuselage of the aircraft. The wingbox is integrated into the bulkhead and partial bulkhead to which the wings attach. All partial bulkheads, as well as all spars, have a general rotated I-beam shape to them with a height of 1.5 inches, a web thickness of 0.2 inches, a spar cap width of 1 inch, and a spar cap thickness of 0.1 inches.

The keel beam spans from the nose landing gear attachment point, which is just forward of the forward pressure bulkhead, to the last frame directly forward of the rear bulkhead. This keel beam is one foot wide and much thicker than the surrounding longerons, each of which is only 0.05 inches thick as opposed to the 0.5-inch thickness of the keel beam. The keel beam must start only at the nose landing gear because the path of the nose landing gear goes directly through the line of the keel beam. The aft landing gear does not clear the vertical flanges of the keel beam, but it clears the horizontal section, so the keel beam can extend almost all the way to the rear bulkhead. A simple cutout is made at the location the landing gear needs to pass through each flange of the keel beam, and the thickness of the composite structure is increased in this area to help account for the loss in bending thickness.

Aft of the door, there is a partial bulkhead at the front of the wingbox and a full pressure bulkhead at the aft of the wingbox. Each of these structures is aligned with one of the two wing spars. Around this area, Fig. 8.8a also highlights multiple holes in the fuselage structure for windows and doors. These holes are structurally significant, but each is surrounded by structure which attaches to the skin of the aircraft and keeps the fuselage structurally sound.

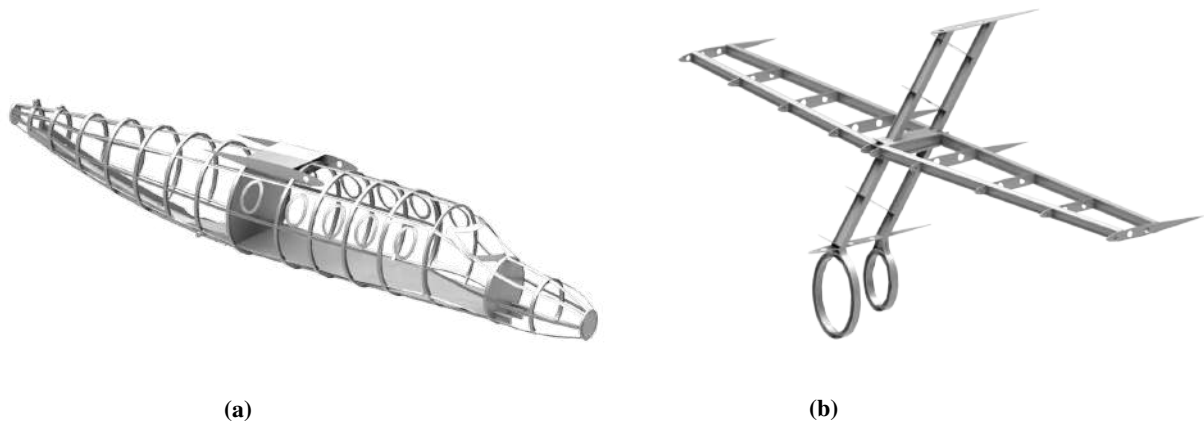


Figure 8.8: Diagrams of internal structural layouts of a) fuselage and b) empennage.

At the aft end of the fuselage, the two spars of the vertical stabilizer attach to two frames in the rear fuselage, as can be seen in Fig. 8.8a. This integration will be discussed in the next subsection.

All windows and doors, excluding the landing gear doors, have surrounding structure to ensure functionality under cabin pressure loads. Landing gear doors are all open to the atmosphere, so reinforced door structure is not necessary. Each landing gear door attaches to a series of hinges. The hinges will start at one end of the door on a complete frame, and they will extend until the next complete frame. In between, the frames are cut out in the door areas so that the landing gear members can pass through. This loss in strength is not ideal, but it is inevitable in the case of retractable landing gear.

The fuselage is the only major structural section which is different between the HT-LIT and HT-LITTLE aircraft. The HT-LITTLE is 5.5 feet shorter than the HT-LIT aircraft, and a few frames had to be removed to make it that length. By removing the two frames directly forward of the partial bulkhead at the front of the wingbox, the cabin is shortened by approximately 5.5 feet, and the HT-LITTLE aircraft fuselage is formed.

8.2.3 Empennage Structure

The empennage consists of both the horizontal and vertical stabilizer assemblies, joined to create a cruciform tail. The vertical stabilizer attaches directly to the fuselage at two attachment frames into which the vertical stabilizer spars are seamlessly integrated. This integration allows for smooth load transfer between the tail structures and the fuselage members. The vertical and horizontal stabilizers have six and ten ribs, respectively. Spacings between the vertical stabilizer ribs generally are about 13 inches, and spacings between the horizontal stabilizer ribs generally are about 25 inches. The ribs in the vertical stabilizer structure are slanted to be perpendicular to the spars and the leading edge of the fin, allowing them to best absorb oncoming loads while also remaining flush to the leading edge skins. Towards the aft of the vertical stabilizer, the rudder is attached at four points, all of which extend from terminated ribs. This configuration is like how the control surfaces were attached on the wings of the aircraft. Each point of attachment is outfitted with an actuator used to move the rudder. The rudder itself has ribs that stem from the connection points, just as the earlier control

surfaces did. The rudder is also made using a composite honeycomb structure to help strengthen the internal structure of the control surface.

The front spar of the vertical stabilizer is located at approximately 15% of the chord, and the rear spar is located at approximately 55% of the chord. The rear spar is so far forward due to the sheer size of the rudder. The rear spar must be located far enough in front of the rudder's leading edge to allow for the installation of hinges on which the rudder will be pivoted using the aircraft's hydraulics. The front spar of the vertical stabilizer is farther forward than the front spar of the wing to help compensate of the abnormally far forward rear spar. The farther apart the two spars are, the more strength the entire surface has in crosswinds.

The horizontal tail joins together with the vertical tail at a sort of wingbox in the middle of the vertical tail structure. The tail wingbox is made up of the two spars of the horizontal stabilizer along with auxiliary composite support structure, closing off the area as a structural box.

The front spar of the horizontal stabilizer is located at approximately 18% of the chord, and the rear spar is located at approximately 55% of the chord. The methodology for the spar placement was very similar to that used in the vertical stabilizer spar placement, although the front spar was placed a bit farther back to be closer to the center of the empennage spar location envelope of 15% - 25% recommended by Roskam [17].

The elevators of the horizontal stabilizer are attached at two spots, utilizing the exact methodology used to attach the other control surfaces. The elevator is made up of ribs along with a composite honeycomb which is identical to the honeycomb used in the other control surfaces.

Holes were made in the ribs throughout the empennage for weight savings in non-structurally integral parts of each body. These hole locations, as well as the rest of the empennage structure, can be seen in Fig. 8.12b. The thicknesses of the spars and ribs are the same as the thicknesses seen in the main wing structure.

8.3 Landing Gear

The sizing of the landing gear is dependent on the loads which it experiences. The nose and main landing gear for both the HT-LIT and HT-LITTLE aircraft were placed in strategic locations to optimize the load paths through the aircraft. The main landing gear was attached to the keel beam aft of the rear pressure bulkhead and the nose gear was placed forward of the front pressure bulkhead and avionics. These placements both maximize cabin space in the aircraft and direct the load paths through the keel beam, a primary structural component of the aircraft.

For the HT-LIT, the nose and aft landing gear contact the ground 5.0 and 18.2 feet aft of the nose, respectively. For the HT-LITTLE, the nose and aft landing gear contact the ground 5.0 and 13.6 feet aft of the nose, respectively. For a landing gear placement to be valid, the nose landing gear must take between 5% and 20% of the aircraft weight in ground roll. This ensures that the plane is not too front-weighted to lift the nose at takeoff while also ensuring that the nose wheel can get proper traction in ground roll for steering purposes. For the HT-LIT aircraft, the nose gear will see load

percentages ranging from 6.05% to 9.96% of the aircraft ground load. The nose gear of the HT-LITTLE will see load percentages ranging from 16.27% to 17.83% of the ground load. Both ranges are entirely within the range of 5% to 20% of aircraft ground load, so this placement was deemed valid.

For each aircraft's tire sizing, the takeoff and landing conditions were each analyzed for both a ferry mission and a standard fully-loaded configuration. Per Raymer, a gear load factor of 3.0 was put on the landing gear weights to account of the load transfer between the gear and the airframe when the landing gear is deflected. Raymer also says to apply a factor of 1.25 to all weights to account for future growth; this was done for all loads on both aircraft [4]. After determining all loads that go through the aircraft landing gear configurations at takeoff and landing for both mission setups (ferry and fully-loaded), the maximum loads were identified, and the Goodyear tire catalog was referenced [19]. Tires were chosen that were as small as possible while being able to take the dynamic, bottoming, and static loads of each aircraft and preferably having tire pressures at or below 45 psi to allow for wet grass landings on soft soil. For the HT-LIT aircraft, a Flight Custom III 606C66-8 tire was chosen for the nose landing gear and two Flight Custom III 850C86-2 tires were chosen for the main landing gear. The Flight Custom III 606C86-3 wheel was chosen for the HT-LITTLE nose landing gear, and the HT-LITTLE main landing gear has two Flight Custom III 850C86-2 tires, just like the HT-LIT. Specifications for each of these tires can be found in Table 8.4.

Table 8.4: Tire Specifications for HT-LIT and HT-LITTLE aircraft

	Size	Outside Diameter [in]	Rated Inflation [psi]	Rated Load [lbs]
606C66-8	6.00-6	17.5	42	1,750
850C86-2	8.50-10	25.65	55	4,400
606C86-3	6.00-6	17.5	55	2,350

In order for our aircraft to land on wet grass and soft soil, the tire pressures should be at most 45 psi. While two of the three tires in the above table do not operate at 45 psi naturally, they can be underinflated to 45 psi if the user wants to land on such runway conditions. According to the Goodyear Aircraft Tire Care & Maintenance Manual, tires operating in underinflation will experience earlier failure on taxi and takeoff [20]. While it is not recommended to land and take off on these types of runways, it is a possibility at the discretion of the aircraft owner. Since the aircraft are designed to land on wet grass and soft soil, they are also capable of landing on surfaces like dirt, dry grass, metal mat, gravel, asphalt, and concrete. All of these surfaces are less harmful to the tires and landing gear than wet grass and soft soil, but landing on a standard aircraft runway is still preferable to any other surface. It is recommended that, unless intentionally landing on these surfaces, the tires rated for 55 psi are kept at their rated pressure to minimize chance of premature failure.

The purpose of the landing gear is to absorb the loads encountered upon landing and to safely transition the aircraft from a flying state to a ground state without damaging the airframe. Fig. 8.9 shows the solution that was devised for the nose landing gear. Note that the landing gear sections of the HT-LIT and HT-LITTLE aircraft are virtually identical

since the two planes have identical nose and rear sections. The only notable difference between the two is the tire types for the nose landing gear, and each of the selected tires has the same outer diameter so no structure will change.

The nose gear is rotated forward by 7° and attached to a rotating rod mechanism which passes through the sides of both the keel beam and a U-shaped composite brace which is attached to the bulkhead aft of the nose landing gear. This setup allows for an 83° retraction sweep up to a stowed position. The rotating rod also has two side struts designed to take any off-axis loads encountered on landing. These struts end at a cuff which is fastened loosely around the main rod of the nose landing gear such that the gear can move freely through the cuff. The forward-facing side of the cuff is attached to a telescoping rod which also attaches to the forward end bulkhead of the aircraft. This telescoping rod has a built-in locking mechanism which secures the rod in the down position until the landing gear is signaled to retract. While in the locked position, the telescoping rod takes all drag and dynamic loads on landing which run along the axis of the fuselage. When the nose gear retracts, the nose wheel rotates 90° about a pivot at the bottom of the main rod, about which it is constrained for landing, for space-effective storage. All landing gear retraction is powered using the aircraft's hydraulic systems. The nose landing gear has an oleo system installed for shock absorption. The oleo length for both the HT-LIT and HT-LITTLE is approximately 16.5 inches, and they each have a maximum stroke on landing of 6.6 inches. All oleo sizing was done per Raymer [4]. The diameter of the HT-LIT is approximately 2 inches, while the diameter of the HT-LITTLE oleo is approximately 2.5 inches. This is because the HT-LITTLE, while a smaller aircraft, experiences larger bottoming loads than the HT-LIT aircraft due to its center of gravity placement.

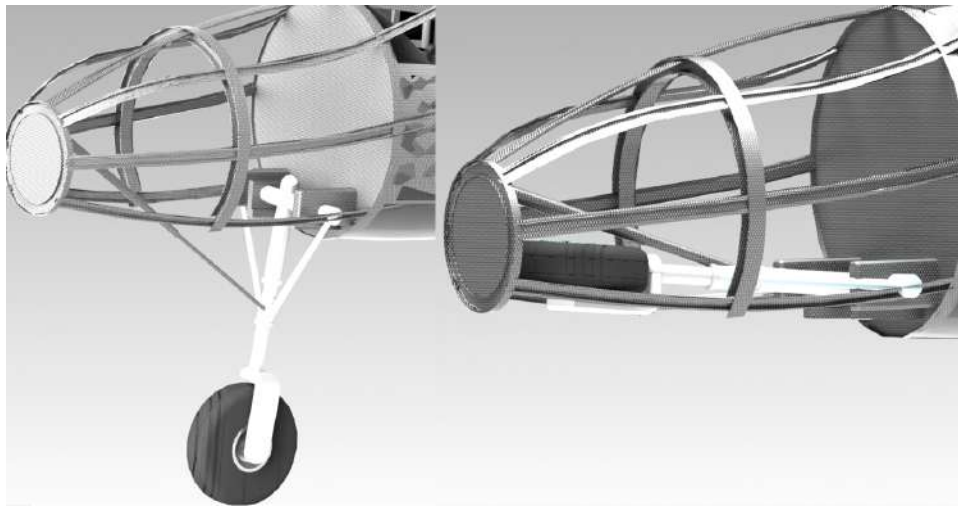


Figure 8.9: Nose landing gear retraction system design.

The main landing gear of the aircraft is shown in Fig. 8.10. The system consists of two curved steel beams, each joining a wheel of the main gear to a rotating steel constraint in the center of the keel beam. When the landing gear is in the down position, the steel constraint effectively joins the two main landing gear sections and allows it to bend as one large beam-like member. During retraction, the constraint rotates 45° , and the landing gear is free to rotate about its pivot. The main landing gear rotates a full 180° , swinging through the open landing gear doors under the fuselage and

into the aft fuselage for storage. When in the storage position, two steel pegs extend from the keel beam under the landing gear and constrain the landing gear to its retracted position. The movement of these pegs is linked to the rotating steel constraint such that when the constraint rotates, the pegs will extend or contract, depending on the direction of constraint rotation. This design is similar to the design of the Cessna Skymaster landing gear, so it is a proven system of constraint and retraction. The entire retraction process is, once again, powered by the hydraulic system of the aircraft.

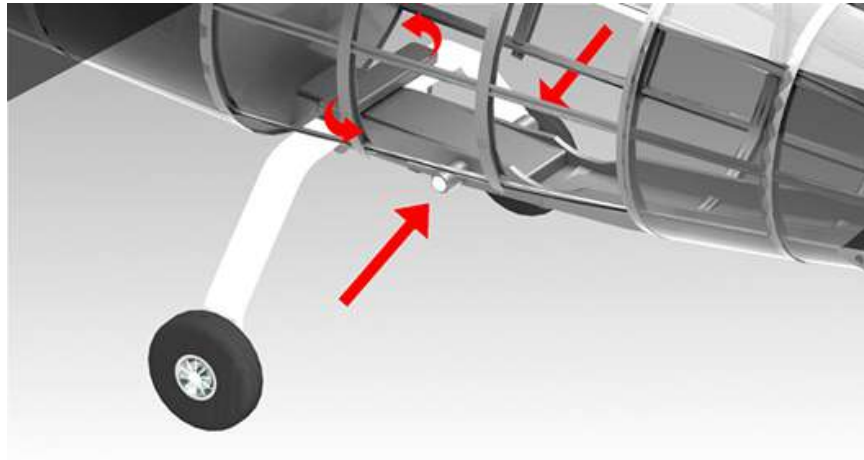


Figure 8.10: Main landing gear retraction system constraint design.

Fig. 8.11 is an illustration of the angles between the relevant tip-over lines and the C.G. of the HT-LIT aircraft with decompressed nose gear. The decompressed nose gear shifts the C.G. up and aft, shrinking the longitudinal tip-over angle and enlarging the lateral angle pictured in part (a) of Fig. 8.11, hence decreasing the lateral tip-over angle. In this scenario, the wing strike angle is 21.965° , which is much smaller than the 30.5° until tip-over in this scenario. The tail strike angle here is 19° , 6.2° less than the longitudinal tip-over angle in this scenario. Therefore, the case of decompressed landing gear for the HT-LIT aircraft meets all lateral and longitudinal tip-over requirements. As mentioned earlier, the decompression of the nose gear only worsens all of the tip-over angles, so if the HT-LIT satisfies these requirements here, it will satisfy them for compressed nose gear as well.

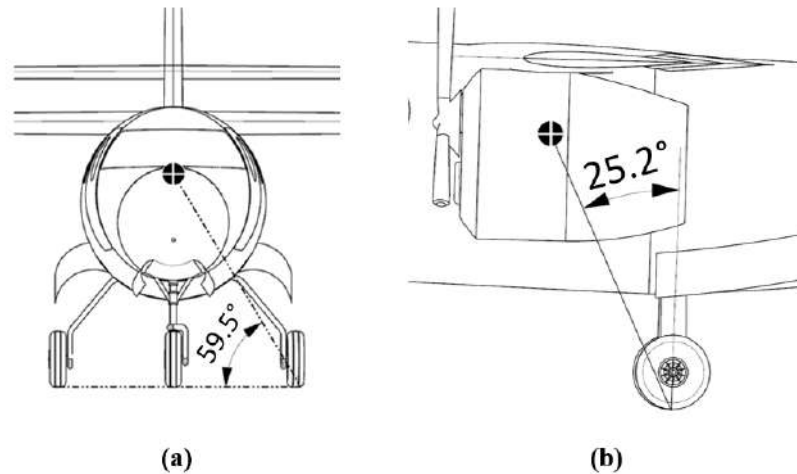


Figure 8.11: Lateral and Longitudinal tip-over relevant dimensions for the HT-LIT aircraft with decompressed nose gear.

The HT-LITTLE aircraft has a higher C.G. by 0.1 feet, and its x-placement of the C.G. is similar to the HT-LIT, relative to the aircraft size. Due to the slightly higher C.G., the decompressed landing gear lowers the lateral tip-over angle by another 0.2° , but it is not nearly enough to allow for lateral tip-over, seeing as the wing strike angle is 22.1° for the HT-LITTLE. Since the rear of the HT-LITTLE is nearly identical to the aft section of the HT-LIT, the tail strike angle is identical to the HT-LIT. However, the longitudinal tip-over angle, while smaller than the HT-LIT's, is still 22.1° . Since this number is larger than the tail strike angle, the requirements are met for the HT-LITTLE in a decompressed state and, consequently, for the compressed state as well.

8.4 Aircraft Loads

This section evaluates the primary loads that the HT-LIT and HT-LITTLE will experience in all parts of their mission profiles. Since the load paths of the two aircraft are identical, this section will refer to both aircraft in a singular sense.

8.4.1 Ground Loads

The aircraft will be in ground roll at both the start and end of its missions. At each of these points in the mission, the amount of load going through the aircraft will be determined by the current aircraft weight. The force of gravity acting on the aircraft is counteracted by the ground on which the aircraft is rolling, pushing upward on the landing gear. The weight forces of the aircraft act on all structural members, but in the end, all of the forces will move into the fuselage of the aircraft. From there, the loads are transferred through the skins, longerons and stringers, the frames, and the bulkheads into the keel beam the constraint joining the main landing gear, and the main and nose landing gear of the aircraft.

In addition, if the engines are on and the aircraft are in ground roll, the engines are producing thrust forces which act at the powerplant attachment ribs on each wing. These loads will quickly be transferred to the spar of each wing and brought towards the wingbox, at which point they are transferred to the full and partial bulkheads encompassing the wingbox and are spread via the lengthwise fuselage structural members and the skin along the length of the aircraft. Since the forces are along the axis of the fuselage, the forces then travel through both the telescoping rod of the nose landing gear and the constraint of the main landing gear.

8.4.2 Landing Loads

When an aircraft lands, there is additional loading on the landing gear. Aerodynamic forces created by crosswinds will often induce loads which are off-axis, pushing the aircraft from side to side. The landing gear will also take high frictional loads the first few seconds after landing while the wheels of the aircraft have not achieved the angular velocity needed to maintain a steady roll. These static frictional loads will push the landing gear aft along the length of the fuselage. All these loads will need to be taken by struts attached to the nose gear structure and nose landing gear bulkhead and by a beam joining the two sides of the main landing gear. All of these loads are created by the inertia of the aircraft and the stopping force that the landing gear is applying, so all loads will travel through the main members of the fuselage and end up in the landing gear. Landing is a sudden transition to ground roll and in ground roll, all loads go towards the members touching the ground.

8.4.3 Flight Loads

The primary loading during flight will be an upward lifting force at the quarter chord point along the length of the wing. Assuming the front wing spar does not lie along the quarter chord of the wing, both the front and rear spar will experience upward bending and torsion due to the off-axis nature of the loading. The front spar is much closer to the quarter chord point than the rear spar, so its loading will be close to pure bending. The great majority of the forces applied on the rear spar will be torsional. These bending and torsional loads will be transferred down the spars to the torque box, which is located between the wings at the top of the fuselage. The skin and ribs along the wing stiffen the wing in torsion, so they will take a portion of the torsional force. The wingbox transfers the loads to both the stringers running through the wingbox and the bulkheads on the wingbox's outer edges.

The entire forward-facing profile of the aircraft also experiences a drag force acting along the lengthwise axis. These forces are initially taken by the skins and then are transferred to the frames in the fuselage and the ribs in the lifting surfaces. Drag force acting on the engines is transferred straight from the nacelles to the attachment points along the wing ribs, and the drag forces on the landing gear are transferred to the landing gear bulkheads, just as the frictional forces on landing are. These loads are then carried along the aforementioned load paths for the wings and fuselage. An aircraft in flight may also experience crosswinds. These forces will be picked up by the skins of the aircraft just as the streamwise

drag forces are. The crosswind forces on the nacelles will be transferred to the attachment points, once again, and the cross wind forces on the landing gear will be transferred to the fuselage just as the sideways forces are during landing.

Finally, the engines are producing a thrust force much more powerful than the thrust force seen in ground roll. Yet, the load path is still the same as the load path experienced in ground roll. All forces will travel into the wingbox and into the partial bulkheads, which eventually distribute the loads across the aircraft fuselage.

8.4.4 V-n Diagram

A V-n diagram is a visual representation of the loading that the aircraft can withstand as a function of flight speed. The V-n diagrams for the HT-LIT and HT-LITTLE aircraft can be seen in Fig. 8.12a and 8.12, respectively. Aircraft performance equations from Roskam were used to make this diagram [21].

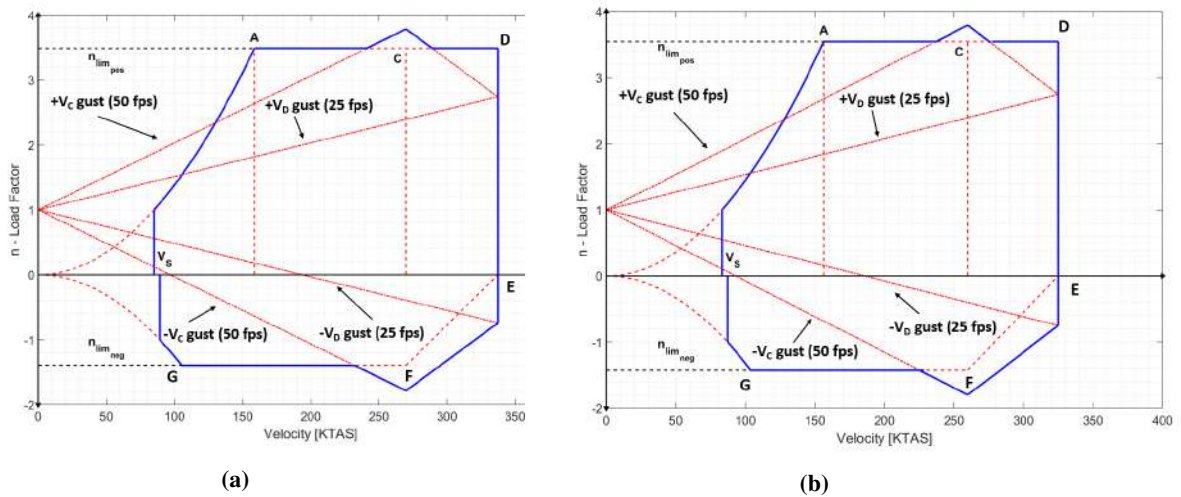


Figure 8.12: Diagrams of internal structural layouts of a) fuselage and b) empennage.

The four dotted red lines spanning the width of the graph are gust lines. It is standard for all FAR 23 aircraft to consider 25 fps and 50 fps gust winds in their V-n diagrams. The design loads at a given speed are dictated by the furthest positive and negative lines. Often, the gust lines will define the loads at higher speeds, as they clearly do for the HT-LIT and HT-LITTLE aircraft on the bottom half of each V-n diagram and for a section of the top half. The positive load limits of the HT-LIT and HT-LITTLE aircraft, $n_{lim_{pos}}$, were found to be 3.49 and 3.56, respectively. The negative load limits of the HT-LIT and HT-LITTLE aircraft, $n_{lim_{neg}}$, were found to be -1.40 and -1.42, respectively.

8.5 Pressurization

Both the HT-LIT and HT-LITTLE aircraft are pressurized aircraft due to their high operating altitude, cruise speeds, and target market. Pressurized aircraft constantly feel radial loads acting outward from the pressure vessel of the aircraft. The pressure vessel must be designed to withstand these pressure loads. Composite fuselage structures are

particularly good at taking radial loading when designed correctly.

The cabins of the HT-LIT and HT-LITTLE aircraft will each be pressurized to 0.96 atm, or the standard air pressure at 1,000 feet above sea level - this will allow for superior passenger comfort. When cruising at 17,000 feet, the surrounding air pressure is approximately 0.52 atm, creating a pressure difference of 0.44 atm. This pressure will act omnidirectionally on the cabin structure. The pressure bulkheads on each side of the cabin have been designed to take high pressure loads. These bulkheads are very thick - approximately an inch - to not only hold the pressure loads, but also to minimize surface deflection, maximizing room aft of the rear pressure bulkhead for aircraft systems and maximizing room forward of the forward pressure bulkhead for the lose landing gear retraction system. The aircraft both have a cylindrical main cabin section to minimize stress concentration points and to best distribute pressure loading.

For the main skin, a lay-up must be defined to extract material properties for a large body. The three main types of loading that the fuselage will be seeing during flight will be pressurization, longitudinal, and shearing. These can each be counteracted by plies of composites laid around the circumference of a cross section, along the length of the fuselage, and at a $-45^{\circ}/45^{\circ}$ orientation along the length of the fuselage, respectively. The chosen ply orientation for the HT-LIT and HT-LITTLE aircraft is $0^{\circ}/90^{\circ}/+45^{\circ}/-45^{\circ}/-45^{\circ}/+45^{\circ}/90^{\circ}/0^{\circ}$. This particular lay-up is known for its quasi-isotropic behavior and is able to resist each of the three aforementioned loads that will be seen by the aircraft.

The main skin thickness was determined by performing a composite hoop stress analysis. Based on estimated tensile properties of the fuselage composite laminate, a thickness of 0.088 inches was chosen for all fuselage skins. This thickness will provide the aircraft skin with a safety factor of greater than 3, ensuring passenger safety in unexpected loading cases. This skin thickness warrants one lay-up of eight plies in the orientation mentioned before, each with a thickness of 0.011 inches.

8.6 Fuselage Manufacturing & Weight Commonality

The HT-LIT and HT-LITTLE fuselages are produced in three main sections: forward, center, and aft. The forward fuselage runs from the nose tip to the frame behind the cockpit area, and the center fuselage runs from the last forward frame to the rear pressure bulkhead of each aircraft. The forward and aft sections of the HT-LIT and HT-LITTLE fuselages are identical for ease of manufacturing. Assuming that each fuselage section is made on a different assembly line with different forming jigs, this means that the fuselage similarity between the two models eliminates one third of the six lines that could have been used to produce these two aircraft. The sections are joined together utilizing aluminum rivets for ease of use, history of composite material integration, and lack of cost.

The center fuselage is the only primary structural component other than the nose landing gear which changes from HT-LIT to HT-LITTLE. Since the two aircraft have the same powerplant, their overall weight similarity is quite high. The ratio of HT-LITTLE to HT-LIT Structural & Powerplant weight is 2353 pounds to 2493 pounds, or 94.4% weight commonality. This meets the RFP's requirement of a weight commonality for structures and powerplant of 75%

or greater.

All main sections of the aircraft are co-bonded and co-cured. This ensures maximal section strength and entangled properties for a tunable and predictable behavior. It also creates a reduction in necessary fasteners for production, reducing cost and chance of error on the line during the production cycle.

9 WEIGHTS & BALANCE

9.1 Major Component Weights & Locations

The calculation of the component weights was done in a variety of ways to account for specific components added to the aircraft. Aircraft structural weights (excluding landing gear) were determined by adapting the methods found in Roskam [21] for structures weight estimation for carbon fiber composite materials. This was done by multiplying the weights by a density multiplier of $\frac{2}{3}$ to scale them down from a standard metal aircraft. For the engines, propellers, and electric motors, reference materials were available and the exact weights could be determined. The weight of the battery was determined as discussed in Section 6. The Battery cooling systems and battery protection were determined based on historical data and the volume of the battery. All other weights were determined using Roskam Class II weight estimation methods [21].

The summation of all of the weights & balances work for the HT-LIT and HT-LITTLE aircraft can be found in Tables 9.1 and 9.2. All locations are determined with respect to the nose of the aircraft. Visualizations of the major weight component layouts of the HT-LIT and HT-LITTLE aircraft can be seen in Figures 9.1 and 9.2, respectively. Most every item in Tables 9.1 and 9.2 that has a Y arm of zero feet is made up of two components which are symmetric about the fuselage. While the Y arm is zero for the pair of each of these objects, the individual Y arms come into play when moments of inertia are calculated for the aircraft. Moments of inertia were found by breaking each part down into simplified constituent shapes and utilizing parallel axis theorem to make their moments of inertia about the aircraft center of gravity.

Table 9.1: Weights and balance table for the HT-LIT

	Weight [lb]	X arm [ft]	Y arm [ft]	Z arm [ft]	M_x [ft-lb]	M_y [ft-lb]	M_z [ft-lb]	I_x [sl-ft ²]	I_y [sl-ft ²]	I_z [sl-ft ²]
Fuselage	500	18.2	0.0	1.6	9,114	0	2,311	483	1,592	4,365
Nose LG	127	4.7	0.0	-1.0	595	0	256	284	53	219
Main LG	276	18.9	0.0	-1.0	5,214	0	542	479	89	366
Wing	447	16.7	0.0	3.6	7,459	0	2,940	252	2,966	3,481
Powerplant	954	15.1	0.0	2.1	14,418	0	4,895	232	2,262	2,611
V. Stab	93	32.0	0.0	5.6	2,967	0	801	2,480	1,427	761
H. Stab	97	31.8	0.0	5.6	3,070	0	828	845	1,502	2,405
Fuel Sys.	148	15.6	0.3	3.5	2,307	44	522	13	7	9
Controls	507	14.1	0.1	2.9	2,089	15	1,481	138	7	125
Pneumatics/Hydraulics	79	15.3	0.1	2.1	2,269	15	167	7	1	6
Avionics	92	7.1	0.0	1.6	1,054	0	150	293	2	275
Interior	370	16.0	0.0	0.8	2,373	0	285	40	27	11
Op. Items	10	8.9	-1.0	1.1	1,314	-148	11	22	1	20
Aux. Items	66	9.1	0.8	0.2	1,347	118	15	141	10	125
Paint	15	16.4	0.0	1.6	2,434	0	23	31	0	27
Battery	500	20.8	0.0	3.1	3,072	0	1,556	279	29	254
Battery Cooling	75	20.9	0.0	2.5	3,096	0	191	39	1	38
Battery Protection	150	20.3	0.0	2.5	3,001	0	377	57	1	54
Cabin Systems	177	19.6	-0.1	3.1	2,902	-15	550	47	4	41
Oxygen Systems	25	19.9	0.0	2.2	2,945	0	53	7	0	7
Fuel	1,250	17.9	0.0	3.5	22,354	0	8,115	100	4,268	4,747
Passengers/Pilot	1,140	13.0	0.0	1.7	14,817	0	5,344	687	169	714
Baggage	180	28.1	0.0	2.0	5,064	0	906	782	11	740
Total	7,276	16.9	0.0	2.3	122,206	128	38,957	7,738	14,429	21,402

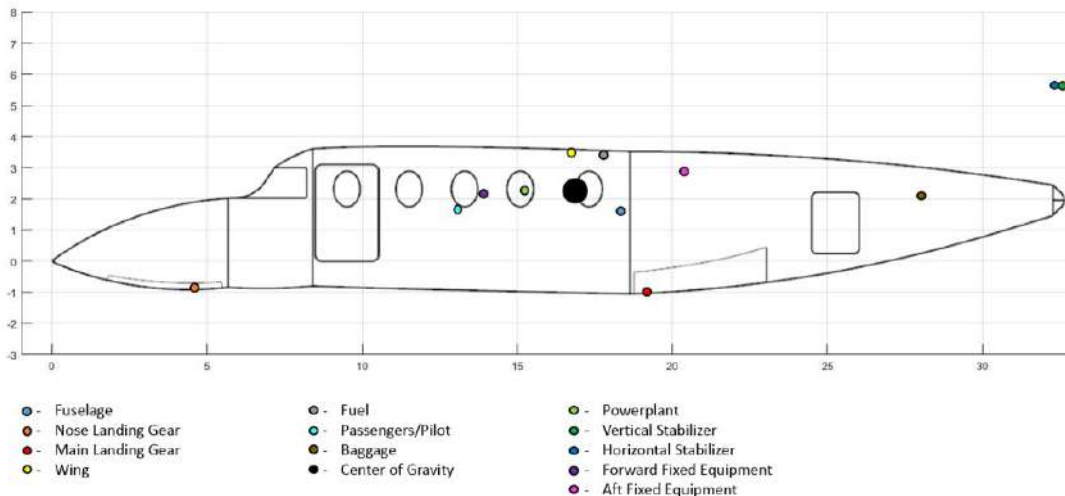


Figure 9.1: Component weight layout for HT-LIT aircraft.

Table 9.2: Weights and balance table for the HT-LITTLE

	Weight [lb]	X arm [ft]	Y arm [ft]	Z arm [ft]	M_x [ft-lb]	M_y [ft-lb]	M_z [ft-lb]	I_x [sl-ft ²]	I_y [sl-ft ²]	I_z [sl-ft ²]
Fuselage	429	14.1	0.0	1.6	6,062	0	1,526	511	1,332	4,273
Nose LG	113	4.7	0.0	-1.0	532	0	119	255	50	196
Main LG	247	14.1	0.0	-1.0	3,468	0	246	426	83	326
Wing	425	11.1	0.0	3.4	4,725	0	2,288	257	3,018	3,499
Powerplant	954	9.7	0.0	2.0	9,212	0	3,839	342	2,310	2,717
V. Stab	91	26.5	0.0	5.6	2,407	0	687	2,373	1,454	684
H. Stab	95	26.3	0.0	5.6	2,485	0	718	758	1,530	2,327
Fuel Sys.	152	9.7	0.3	5.4	1,483	46	824	56	6	49
Controls	467	8.9	0.1	5.2	4,158	47	2,428	183	11	165
Pneumatics/Hydraulics	70	9.4	0.1	4.7	655	7	325	41	0	39
Avionics	87	6.6	0.0	3.4	570	0	292	111	3	103
Interior	286	11.6	0.0	3.5	3,312	0	1,007	35	8	27
Op. Items	10	8.4	-1.0	3.0	84	-10	30	29	1	28
Aux. Items	58	8.5	0.8	2.5	494	47	145	55	7	47
Paint	15	14.0	0.0	3.6	210	0	54	27	0	25
Battery	500	15.4	0.0	4.8	7,696	0	2,403	239	24	225
Battery Cooling	75	15.2	0.0	4.5	1,140	0	339	50	0	48
Battery Protection	150	15.6	0.0	4.5	2,342	0	668	89	1	85
Cabin Systems	126	14.6	-0.1	4.9	1,839	-13	614	54	1	51
Oxygen Systems	19	14.6	0.0	4.1	271	0	75	29	0	27
Fuel	1,300	11.8	0.0	3.5	15,355	0	7,130	61	4,522	4,909
Passengers/Pilot	760	10.5	0.0	1.6	7,957	0	2,731	154	120	185
Baggage	120	22.4	0.0	1.5	2,693	0	423	440	10	417
Total	6,548	12.2	0.0	2.4	79,493	123	28,913	6,576	14,490	20,451

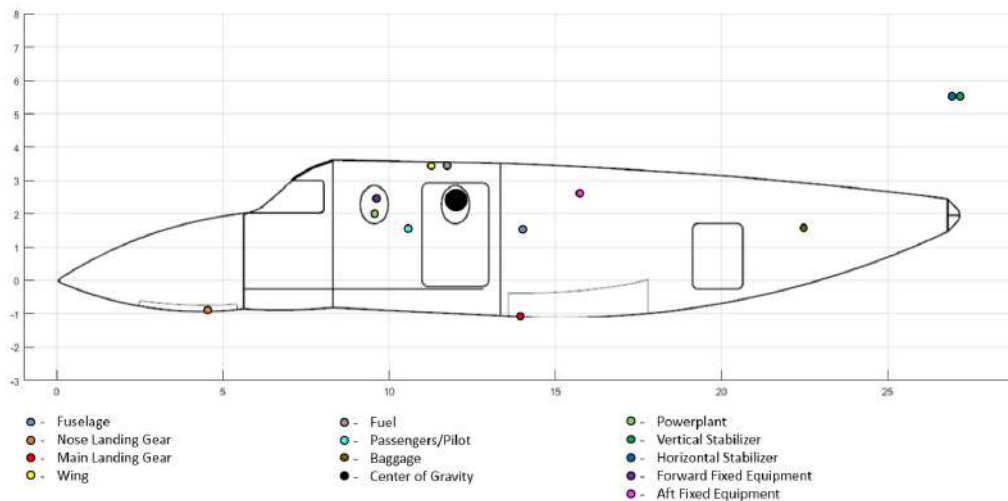
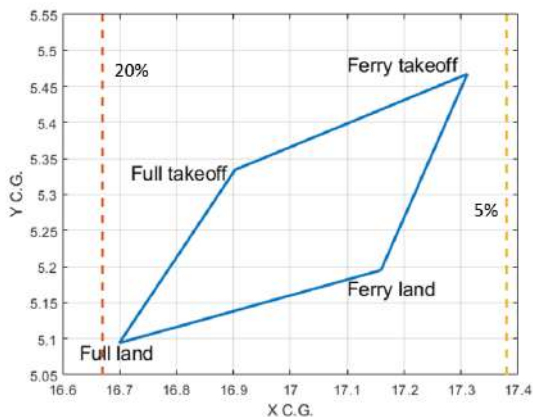


Figure 9.2: Component weight layout for HT-LITTLE aircraft.

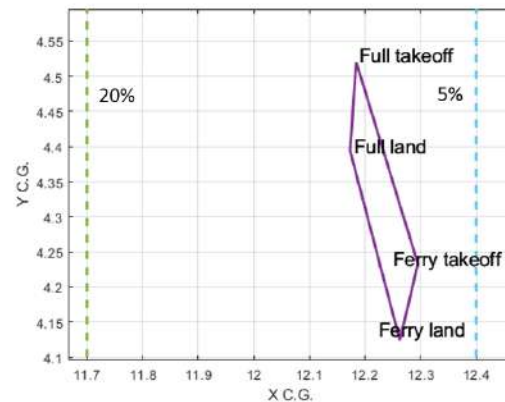
9.2 Center of Gravity Envelope

Throughout the course of the mission, the aircraft center of gravity (CG) changes. As fuel burns, the total center of gravity moves away from the center of gravity of the fuel. As discussed in Section 8.3, the CG envelope is much larger than the actual amount of CG migration for each aircraft under a standard mission. Both of these aircraft will see extreme loading conditions based on the type of mission they are flying. The furthest forward CG that the HT-LIT will encounter will be on a full standard mission during landing, where is it landing with 43 remaining pounds of fuel per performance specs. Upon landing, the aircraft will weigh 6069 pounds and have a CG of 16.71 feet from the nose. The furthest back CG that the HT-LIT will likely experience will be a CG of 17.18 feet behind the nose while weighing 6146 pounds. This will be during a ferry mission takeoff, in which the aircraft is full of fuel and there is no payload. The HT-LITTLE will experience its extreme loads during the same two cases: During the standard landing, the CG along the x-axis will be 12.25 feet aft of the nose. At this time, the aircraft will weigh 5291 pounds. During a ferry takeoff, the CG of the aircraft will be 12.13 feet aft of the nose with a weight of 5857 pounds.

The full CG envelopes for the HT-LIT and HT-LITTLE aircraft can be seen in Fig. 9.3a and 9.3b.



(a) CG envelope for the HT-LIT aircraft.



(b) CG envelope for the HT-LITTLE aircraft.

Figure 9.3: CG envelopes for HT-LIT and HT-LITTLE aircraft.

10 AUXILIARY AIRCRAFT SYSTEMS

10.1 Engine Controls

The engine control system of both the HT-LIT and HT-LITTLE aircraft consists of a FADEC (Full Authority Digital Engine Control) system attached to each turboprop engine. The FADEC system consists of two channels that control and monitor the engines given information from the aircraft air data system. Each FADEC channel is supplied with electrical power from a permanent magnet alternator on each engine driven off the accessory gearbox, giving the engine control system independence of the aircraft electrical system in case of a failure of aircraft electrical power [22].

A diagram of the engine control system within the aircraft is shown in Figure 10.1a.

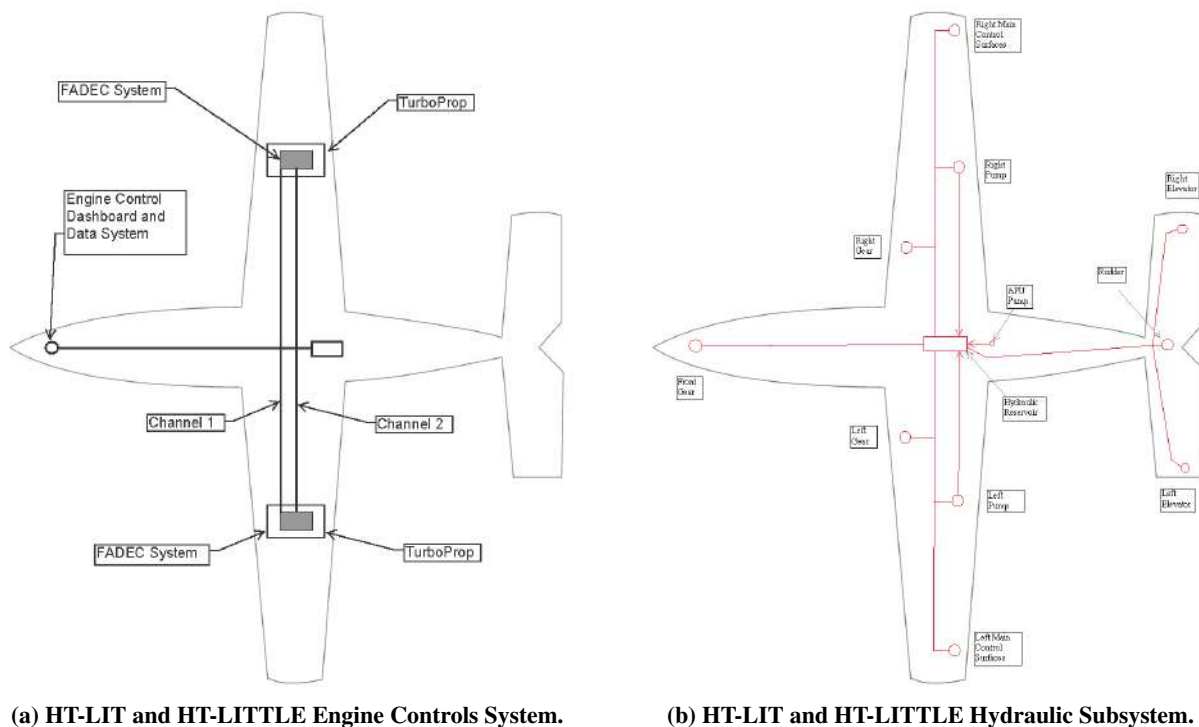


Figure 10.1: Diagrams of the engine control systems and hydraulic systems.

10.2 Hydraulics System and Flight Controls

The hydraulic subsystem for HT-LIT and HT-LITTLE controls the aircraft by applying pressure to the gears, control surfaces, elevators, and pumps. Both Aircraft are consisted of control surfaces (controlled by actuators), pumps that are connected to the engine, and gears. There is also a forward gear to control the landing gear. In the rear, there are the elevators and the rudder is connected directly to the reservoir. One main reservoir and an APU pump are located in the center of the aircraft, which are responsible for the control of the entire aircraft. An overview of the electric system is represented in Figure 10.1.

10.3 Electric and Emergency System

The electric subsystem for HT-LIT and HT-LITTLE has generators, control unit, cables, and breakers set up around the aircraft. The generators are installed in the two engines of the aircraft. One control system is placed in the front of the plane to give the pilot power to the required flight electronics. Both aircraft designs share the subsystem. An overview of the electric system is presented in Fig. 10.2b. The emergency subsystem for HT-LIT and HT-LITTLE have smoke detector and a fire extinguisher on each aircraft. Two smoke detector are installed in both aircrafts, one between the cabin and pilot, and one in the baggage space. The fire extinguisher is located in the cabin. An overview of the emergency

system is presented in Fig. 10.2b.

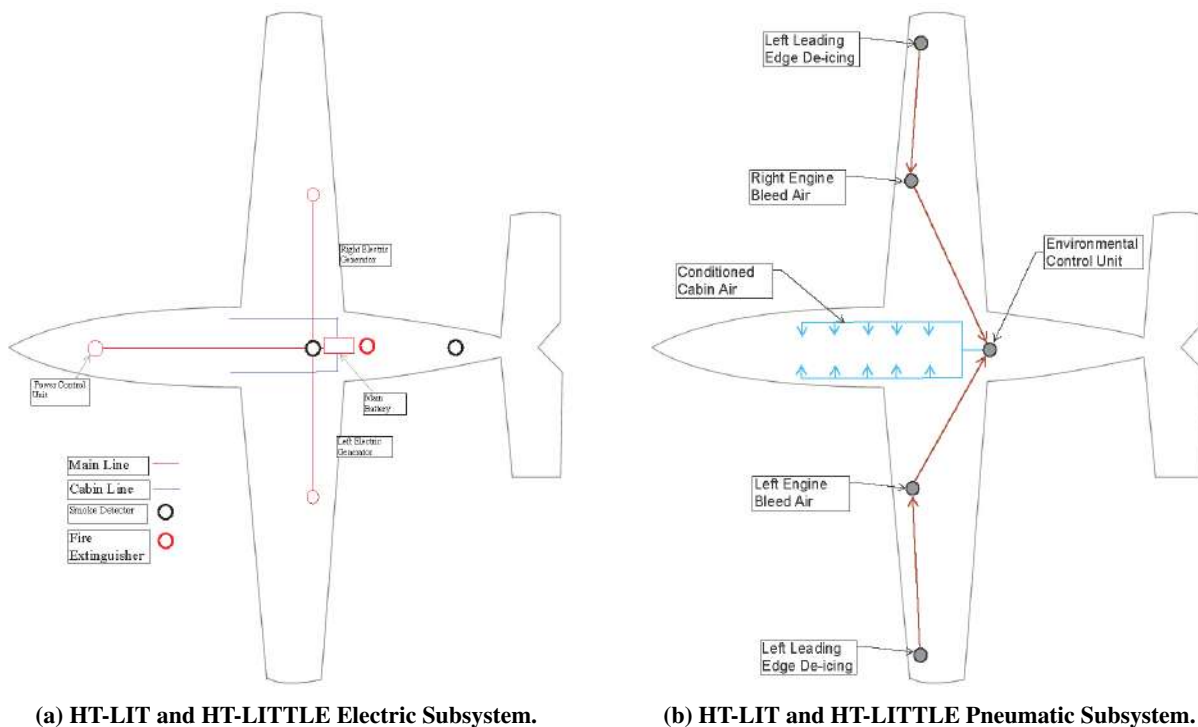


Figure 10.2: Diagrams of the electrical and pneumatic systems.

10.4 Pneumatic System and Environmental Control System

Common to both HT-LIT and HT-LITTLE, the pneumatic system primarily functions to pressurize the cabin as well as to provide conditioned air in order to offer a comfortable cabin environment to the passenger. Supplemental Oxygen is located in the back of the aircraft. Moreover, the hot bleed air is also supplied to the wing leading edge for deicing and ice protection. Fig. 10.2 shows an overview of the pneumatic system for both HT-LIT and HT-LITTLE.

10.5 Avionics

To maintain compliance with FAA, the aircraft were equipped with modern communication equipment and navigation. The aircraft was fitted with standard ADS-B for secure communication and navigations in the 21st century airspace. The pilot has access to the tool through the multi-functional flight deck display, providing necessary information such as navigation, surveillance, weather, and local traffic to navigate safely under several conditions. The plane is also quipped with an autopilot system for semi-autonomous flight, as mentioned in the RFI [3]. Selection started by looking at other comparable aircraft designs. The selection also depended on the available information and pricing of current systems. In the end, Garmin products were selected for the avionic systems, as these provide the aircraft with the best and up-to-date avionic system in the market.

The Garmin G500 flight deck contains all of the operations required for the pilot to control the aircraft and it is also certified and designed for FAR part 23 Class 1/Class 2 aircraft, fulfilling the requirement specified. The Garmin G500 carries all of the required navigation and communication systems and is fully integrated into the flight deck display. It also can integrate an operational autopilot to the aircraft, allowing for semi-autonomous flight. Other important components can be integrated into the Garmin G500 very easily, important components such as those listed in Table 10.1.

Table 10.1: Avionics components of HT-LIT aircraft

Avionics Components	Model
Surveillance	Garmin GTX 330
Navigation/Communication	Garmin GTN 750
Audio Panel	Garmin GMA 340
Flight Deck Display	Garmin G500
Autopilot	GARMIN G600
Weather	GDL 69 SXM
Active Traffic System	GTS 800 TAS

11 COST ANALYSIS

11.1 Initial Cost Estimate & Breakdown

The method used to estimate the RDT&E costs for the aircraft was the DAPCA IV cost model featured in chapter 18 of Raymer [4]. The DAPCA (Development and Procurement Costs of Aircraft) cost model was developed by the RAND corporation to estimate costs for the engineering, tooling, manufacturing, quality control, development support, and flight testing aspects of the aircraft development and production process. The DAPCA model estimates the duration (in hours) of each stage of the process using values of empty weight, maximum velocity, and 5-year production quantity of the concept aircraft. The cost estimates produced from the DAPCA method were adjusted for inflation to represent cost in terms of 2017 dollars. The estimates were made for 5-year production quantities of 240, 360, 480, and 600 aircraft which corresponds to the production of 4, 6, 8, and 10 aircraft per month respectively. The lowest price required to gain 15% profit for each aircraft was found at maximum production quantity to be \$3.74 and \$4.22 million for the HT-LIT and HT-LITTLE aircraft respectively.

11.1.1 Implication of Family Aircraft Development Cost

The DAPCA IV model used to estimated the costs of the HT-LITTLE aircraft had to be adjusted for use with the HT-LIT aircraft to account for the cost reduction effect of commonality between the family of aircraft. The HT-LIT aircraft

featured identical components and component integration in all aspects except for the fuselage (same wing design, same horizontal and vertical stabilizers, etc...). The fuselage of the HT family aircraft was broken down into forward, mid, and aft sections, of which the HT-LIT and HT-LITTLE aircraft shared identical forward and aft components. The HT-LITTLE featured a 5.5 ft shorter mid fuselage component. Aspects of the cost model that were affected by commonality between aircraft include engineering labor, tooling labor, and development support cost. Tooling costs for the HT-LIT aircraft only corresponded to the 1 of 3 fuselage moldings that needed to be modified from the HT-LITTLE production. Conservatively approximating a 50% contribution of fuselage tooling towards tooling of all aircraft components lead to an approximation of a modified tooling cost for the HT-LIT aircraft of 16.5% of the DAPCA IV estimated value. This approximation was used to evaluate the engineering labor costs and development support costs as well. These approximations were very conservative and require development of a more accurate modified cost model to account for the cost implication of family aircraft production.

11.1.2 Research, Development, Testing, & Evaluation Costs

The wrap rates provided by Raymer [4] reflect direct employee salaries, benefits, overhead, and administrative costs. The wrap rates along with the inflation-adjusted values are shown in Table 11.1

Table 11.1: Wrap rates adjusted for inflation

Labor Area	2012 Dollars per Hour	2017 Dollars per Hour
Engineering	\$115	\$125
Tooling	\$118	\$128
Quality Control	\$108	\$118
Manufacturing	\$98	\$107

The DAPCA model estimates for labor costs were found by simply multiplying the aforementioned wrap rates by the estimated number of hours for each field of labor. These estimates were evaluated for varying quantities of 5-year aircraft production and adjusted for inflation as shown in Table 11.2.

Table 11.2: DAPCA estimates for labor costs for HT-LIT and HT-LITTLE (in millions of dollars)

5-year Aircraft Production Quantity	240 LIT	240 LITTLE	360 LIT	360 LITTLE	480 LIT	480 LITTLE	600 LIT	600 LITTLE
Engineering Cost	\$29.2	\$171	\$31.2	\$182	\$32.7	\$191	\$33.9	\$198
Tooling Cost	\$20.6	\$119	\$22.9	\$133	\$24.7	\$143	\$26.2	\$152
Manufacturing Cost	\$523	\$501	\$679	\$650	\$817	\$782	\$942	\$902
Quality Control Cost	\$76.8	\$73.4	\$99.5	\$95.3	\$120	\$115	\$138	\$132
Total Labor Cost	\$645	\$860	\$825	\$1,053	\$985	\$1,222	\$1,130	\$1,374

The DAPCA model also allowed for the estimation of flight testing and development-support costs. These costs,

estimated with the assumption of two flight-test aircraft being used for flight test, were constant for varying quantities of five-year aircraft production, and are shown in Table 11.3 along with the total RDT&E costs.

Table 11.3: DAPCA estimates for RDT&E costs for HT-LIT and HT-LITTLE(in millions of dollars)

5-year Aircraft Production Quantity	240 LIT	240 LITTLE	360 LIT	360 LITTLE	480 LIT	480 LITTLE	600 LIT	600 LITTLE
Development- Support Cost	\$5.29	\$31.5	-	-	-	-	-	-
Flight-Testing Cost	\$10.1	\$10.1	-	-	-	-	-	-
Total RDT&E Cost	\$141	\$405	\$168	\$451	\$191	\$490	\$212	\$523

Fixed production costs not accounted for by the DAPCA model include cost of the engines, batteries, motors, avionics, interior passenger components (seats, insulation, storage, lavatories, ceilings, flooring, walls, etc.), and initial spares. It was suggested in Chapter 18 of Raymer [4] that the cost per aircraft be increased by \$925 (\$850 before inflation) per passenger to account for the interior component costs of a general aviation aircraft. The engine cost was estimated using existing data for a purchase order of 3 M250-variant turboprop engines with comparable specifications to the M250-B17F for \$500,000 in the year 2000 [23]. After adjusting for inflation, the cost per engine of the M250-B17F was determined to be \$244,000 in terms of 2017 dollars. The cost of the Hartzell HC-B3TF-7A propeller system was found using data given by the manufacturer to be \$59,700 per system (including blade costs, assembly costs, etc...) after accounting for inflation [11]. Battery costs were estimated based on the projected price rate of \$200 per kWh for lithium ion batteries in the year 2020 [24] and the 80 kWh output of the batteries selected for the aircrafts electric propulsion components, resulting in a battery cost of \$16,000 per aircraft. The electric motor cost estimate was not able to be made accurately, as the electric motor chosen for the concept aircraft design is currently in production and there is no available data on its possible cost range. A cost was estimated as \$10,000 per motor using data on the most comparable electric motor with price data available (a 200 kW Siemens motor) [25]. The avionics cost was estimated by evaluating avionics costs for comparable aircraft. The cost of individual avionics components of the HT-LIT and HT-LITTLE aircraft is shown in Table 11.4

Table 11.4: Avionics components cost per aircraft (in thousands of dollars)

Avionics Component	Model	Unit Cost
Surveillance	Garmin GTX 330	\$3.50
Nav/Com	Garmin GTN 750	\$17.2
Audio Panel	Garmin GMA 340	\$1.80
Flight Deck Display	Garmin G500	\$16.0
Autopilot	Garmin G600	\$20.0
Weather	GDL 69 SXM	\$3.88
Active Traffic System	GTS 800 TAS	\$10.0
Total Avionics Cost	per aircraft	\$72.4

11.1.3 Flyaway Cost

The total flyaway cost of the aircraft covers the manufacturing labor, materials cost, avionics costs, and the propulsion system costs. The aircraft flyaway cost estimated for varying production quantities using DAPCA model estimates in conjunction with known costs (engines, avionics, etc.) can be seen in Table 11.5.

Table 11.5: Flyaway cost estimates for varying production quantities of 6-seater and 4-seater Aircraft (in millions of dollars)

5-year Aircraft Production Quantity	240 LIT	240 LITTLE	360 LIT	360 LITTLE	480 LIT	480 LITTLE	600 LIT	600 LITTLE
Manufacturing Materials Cost	\$181	\$112	\$250	\$155	\$314	\$195	\$376	\$233
Engine Cost	\$117	\$117	\$175	\$175	\$234	\$234	\$292	\$292
Battery Cost	\$3.84	\$3.84	\$5.76	\$5.76	\$7.68	\$7.68	\$9.60	\$9.60
Electric Motor Cost	\$4.80	\$4.80	\$7.20	\$7.20	\$9.60	\$9.60	\$12.0	\$12.0
Propeller System Cost	\$28.6	\$28.6	\$43.0	\$43.0	\$57.3	\$57.3	\$71.6	\$71.6
Avionics Cost	\$17.4	\$17.4	\$26.0	\$26.0	\$34.7	\$34.7	\$43.4	\$43.4
Interior Cost	\$1.33	\$0.888	\$2.00	\$1.33	\$2.66	\$1.78	\$3.33	\$2.22
Project Flyaway Cost	\$877	\$846	\$1,188	\$1,147	\$1,477	\$1,427	\$1,750	\$1,692
Flyaway Cost per Aircraft	\$3.65	\$3.52	\$3.30	\$3.19	\$3.07	\$2.97	\$2.92	\$2.82

11.1.4 Sell Price for 15% Profit

The aircraft price set to recover at least 15% profit must recover the cost of the RDT&E cost as well as the flyaway cost per aircraft. As would be expected, the lowest price per aircraft to recover the desired profit margin occurs at the maximum monthly production rate of the aircraft. The \$3.74 million price (HT-LIT) and \$4.22 million price (HT-LITTLE) for 15% profit at a production rate of 10 aircraft per month is competitive with comparable general aviation and small business jet aircraft such as the Cessna Citation M2 costing \$4.5 million and the Embraer Phenom 100 costing \$4.2 million. The concept aircraft also features comparable performance parameters to the aforementioned aircraft, indicating the viability of the concept aircraft program to be profitable in the general aviation and very light business jet market. The price for 15% profit at each production quantity for the HT-LIT and HT-LITTLE aircraft are shown in Table 11.6.

Table 11.6: Aircraft price to make 15% profit for 6-seater Aircraft (in millions of dollars)

5-year Aircraft Production Quantity	240 LIT	240 LITTLE	360 LIT	360 LITTLE	480 LIT	480 LITTLE	600 LIT	600 LITTLE
Flyaway Cost per Aircraft	\$3.65	\$3.52	\$3.30	\$3.19	\$3.07	\$2.97	\$2.92	\$2.82
RDT&E Cost per A/C	\$0.588	\$1.69	\$0.467	\$1.26	\$0.398	\$1.02	\$0.354	\$0.872
15% Profit Price per A/C	\$4.84	\$5.96	\$4.30	\$5.08	\$3.97	\$4.56	\$3.74	\$4.22

Purchase prices for new similar aircraft are shown for comparison in Table 11.7 along with the 15% profit price of the HT-LIT and HT-LITTLE at maximum production rate.

Table 11.7: Cost comparisons for similar aircraft (in millions of dollars)

Aircraft Model	Purchase Price in USD
HT-LTE	\$3.74
HT-LITTLE	\$4.22
Citation M2	\$4.50
King Air C90GTI	\$3.90
Phenom 100	\$4.20

11.2 Operations & Maintenance Cost Considerations

11.2.1 Fuel & Oil Costs

The fuel specifications of the M250-B17F require the use of Jet A fuel. The average cost per gallon of Jet A fuel was estimated to be \$5.41 per gallon, based on averaging sample data collected by Aviation Research [26] and accounting for inflation. The fuel used to complete the design mission was estimated in the Performance section to be 1,179.2 lb for the HT-LIT and 1,339.6 lb for the HT-LITTLE. The fuel consumption rate per hour was the same for both aircraft, as both used the same turboprop engines. The fuel price per mission flight hour was calculated from the aforementioned variables to be \$186 per flight hour.

11.2.2 Crew Salaries

The crew salary was estimated using the equation provided in Chapter 18 of Raymer [4] (derived using data provided by Boeing) relating the cost per flight hour of a two-man crew to the cruise velocity and gross takeoff weight of the aircraft. The estimation was then halved to account for the single pilot crew as requested in the RFI [3]. The single crew member cost per flight hour was found after inflation to be \$131.

11.2.3 Maintenance Expenses

From Raymer [4] the ratio of MMH/FH was assumed to be between 0.25 a 1 for light aircraft. Considering the added complexity in design due to the composite materials and the turboprop engines, the MMH/FH ratio was taken to be

its maximum typical value for light aircraft of 1. In the absence of significant comparable data, the maintenance labor cost was taken to be equivalent to the manufacturing labor wrap rate evaluated previously in the cost analysis. Maintenance cost per flight hour was then taken to be MMF/FH ratio multiplied by the approximated maintenance labor rate.

11.2.4 Yearly Maintenance & Operation Costs

The yearly maintenance and operations costs were evaluated by multiplying the cost per flight hour values found in the previous sections by 500 and 1,000 flight hours per year, the typical range for light aircraft provided by Raymer [4]. These values can be seen in Table 11.8.

Table 11.8: Maintenance & operations cost per year and per flight hour (in thousands of dollars)

Cost per Year	500 FH/yr	1000 FH/yr	Cost per Flight Hour
Fuel Costs	\$93.1	\$186	\$0.186
Crew Costs	\$65.6	\$131	\$0.131
Maintenance Costs	\$53.3	\$107	\$0.107
Total Maintenance and Operations Cost	\$199	\$398	\$0.398

11.3 Cost Saving Options

The DAPCA IV model used to estimate the production cost of the HT-LIT and HT-LITTLE aircraft is a parametric cost model based on the empty weight, maximum velocity, and production quantity of the aircraft as primary inputs. Costs of the avionics and powerplant components were determined directly from manufacturer data. As such, the only way to decrease the cost of propulsion and avionics components would correlate to a compromise of quality and performance of the aircraft by seeking lower cost options.

11.3.1 Maximum Production Quantity

Increasing the production quantity of the aircraft yields a significant reduction in production costs as a result of the "learning curve effect." The most obvious option for cost reduction is therefore maximizing the production quantity of the aircraft. The maximum production rates and quantities are limited, however, by the state of the market demands. Cost analysis was performed for reasonable production quantities varying from 4 to 10 aircraft per month. The production costs per aircraft were minimized at the production rate of 10 aircraft per month. Further increasing the production rates would yield lower cost, but the viability and feasibility of such production rates would need to be explored and justified.

11.3.2 Alternate Manufacturing Materials

The largest contributing cost components during production were found to be the manufacturing labor as well as the cost of manufacturing materials. The choice of composite materials resulted in a direct increase in manufacturing costs (approximated as 20% by the method illustrated in Raymer[4]), and as such the choice of a different structural material would yield an immediate cost reduction. However, composite materials lead to a marked decrease in the empty weight of the aircraft. The implications of composite materials on the production and lifetime operating cost of the aircraft was explored in the trade study in section 9.8.2. The relatively nominal increase in production cost per aircraft was found to be overcome by fuel cost savings in the first 10 years of the life cycle of the aircraft.

11.3.3 Weight and Speed Reduction

The two largest contributors to the cost of the aircraft found using the DAPCA model were the maximum speed of the aircraft as well as its empty weight. As both the HT-LIT and HT-LITTLE were designed to be manufactured completely out of composite materials, the only way to reduce the empty weight of both aircraft would be to reduce their size. The maximum speed of both aircraft could be reduced by the use of engines providing less power. This would require the switch from turboprop to piston engine, however, and would complicate the design of key auxiliary systems of the aircraft that feed of the bleed air and power generated from the turboprop.

11.4 Model Uncertainties and Inaccuracies

The DAPCA IV model used for cost estimation of most of the components of the HT-LIT and HT-LITTLE aircraft was developed by the RAND corporation almost entirely using data from military aircraft. This has a direct implication of significant inaccuracy in the cost estimation of general aviation aircraft and business jets. Using a strictly weight based cost estimation of \$200 per pound for general aviation aircraft, as given by Raymer [4], the approximate cost of the HT-LIT and HT-LITTLE aircraft were found to be \$0.941 and \$0.881 million respectively. This is significantly lower than the cost approximations found by the DAPCA IV model. The cost per pound estimation for business jet aircraft of \$800 per pound yielded cost estimations much closer (but still significantly lower) to the DAPCA estimates, \$3.76 and \$3.52 million for the HT-LIT and HT-LITTLE respectively.

12 CONCLUSIONS

With the advancement of hybrid-electric technologies a new market in aviation is emerging and at the forefront of that market is Team Hotel Inc. The HT-series provides a glimpse into the practicality and opportunities which this technology is sure to bring in the near future. With an unparalleled passenger experience whilst remaining an environmentally conscious option the HT-series has established a strong footing in this unexplored sector of aviation.

Both aircraft in the HT family close on all of the requirements in the RFI[3]. The HT-LIT and HT-LITTLE aircraft have cruise speeds of 270 knots and 260 knots, respectively, and each exceeds the climb requirement of 1300 feet/minute. Each aircraft meets the required takeoff and landing field lengths of 1800 feet and 1500 feet, respectively, while additionally being able to clear a 50-foot obstacle at sea level. Both aircraft meet the required ranges: 750 nautical miles for the HT-LIT and 1000 nautical miles for the HT-LITTLE. The aircraft family can accommodate the required minimum cargo capacity for both the passengers and pilot. The aircraft family has the required autopilot capabilities and deicing systems, and both aircraft meet the one engine inoperative requirement from the 14 CFR 23.67.

As for future work, there is to be verification work done more precise calculation in area such as aerodynamic using CFD methods. If possible, wind tunnel testing to verify the performance of the wing geometry. Another one is to design an autopilot for rudder roll stabilization to keep the course of aircraft and reducing roll during flight. Finally in order to create a luxurious environment for the passengers, more addition of amenities to increase the comfort and enjoyment for during their flight.

The composite mixed airframe as well as the hybrid electric twin turboprop propulsion system allow for an in-air experience like no other. With a luxurious interior outfitted with leather upholstery, high end finishes, and modern amenities the HT-series stakes it's claim as not just a capable aircraft but a desirable aircraft offering lavish transportation for the discerning customer.

References

- [1] Nelson, R. C., *Flight Stability and Automated Control*, 2nd ed.
- [2] “Rolls Royce M250 Turboprop Brochure,” 2009.
- [3] D’Urso, S. and Tran, H., “Request for Information,” *AE 443: Aerospace Systems Design*.
- [4] Raymer, D. P., *Aircraft Design: A Conceptual Approach*, AIAA, 5th ed., 2006.
- [5] Anderson, J. D., *Aircraft Performance and Design*, McGraw-Hill, 2010.
- [6] Yechout, T. and Morris, S., *Introduction to Aircraft Flight Mechanics: Performance, Static Stability, Dynamic Stability, and Classical Feedback Control*, American Institute of Aeronautics and Astronautics, 2003.
- [7] Roskam, J. and Lan, C. E., *Airplane Aerodynamics and Performance*, DARcorporation, 1997.
- [8] McCormick, B. W., *Aerodynamics, Aeronautics, and Flight Mechanics*, John Wiley and Sons, 1994.
- [9] Sadraey, M. H., *Aircraft Design: A systems Engineering Approach*, John Wiley and Sons, Ltd, 2012.
- [10] Daly, M. and Gunston, B., *Jane’s Aero Engines*, IHS, 2014.
- [11] “Hartzell Propeller: 2013 Price List,” 2013.
- [12] Wall, T. J. and Meyer, R. T., “Hybrid-Electric Propulsion for Aircraft,” *AIAA Propulsion and Energy Forum*.
- [13] Robertson, P. A. and Friedrich, C., “A Survey of Hybrid Electric Propulsion for Aircraft,” *Journal of Aircraft*.
- [14] National Academies of Sciences, E. and Medicine, “Electric Propulsion,” *Commercial Aircraft Propulsion and Energy Systems Research: Reducing Global Carbon Emissions*.
- [15] Duffy, K. P., “Electric Motor Considerations for Non-Cryogenic Hybrid Electric and Turboelectric Propulsion,” *AIAA Propulsion and Energy Forum*.
- [16] Department of Defense, *Composite Materials Handbook*, Vol. 2, June 2002.
- [17] Roskam, J., *Airplane Design Part III: Layout Design of Cockpit, Fuselage, Wing and Empennage*, Roskam Corporation, 1989.
- [18] Leland M. Nicolai, G. E. C., *Fundamentals of Aircraft and Airship Design*, AIAA Education Series.
- [19] Anonymous, “Aircraft Tire Data,” .
- [20] “Goodyear Tire Care and Maintenance Manual,” 2017.
- [21] Roskam, J., *Airplane Design Part V: Component Weight Estimation*, Roskam Corporation, 1989.
- [22] Moir, I. and Seabridge, A., *Design and Development of Aircraft Systems*, John Wiley and Sons, Ltd, 2013.
- [23] Daly, M., *IHS Jane’s Aero-Engines*, Jane’s Information Group, 2014.
- [24] Russell Hensley, J. N. and Rogers, M., “Battery technology charges ahead,” *McKinsey Quarterly*.
- [25] “EV West Vendor Catalog: 200kw Siemens AC Motor,” 2014.
- [26] “Aviation Research Group Survey: Jet-A and Avgas Fuel Prices,” August 2015.